THE INFLUENCE OF THE INCLINATION ANGLE ON VOID FRACTION AND HEAT TRANSFER DURING CONDENSATION INSIDE A SMOOTH TUBE

STEPHANUS PETRUS OLIVIER

SUBMITTED IN PARTIAL FULFILMENT OF THE REQUIREMENTS FOR THE DEGREE MASTER OF ENGINEERING (MECHANICAL ENGINEERING) IN THE DEPARTMENT OF MECHANICAL AND AERONAUTICAL ENGINEERING

UNIVERSITY OF PRETORIA

JUNE 2015

SUPERVISOR: PROF J.P. MEYER

UNIVERSITEIT VAN PRETORIA
UNIVERSITY OF PRETORIA
YUNIBESITHI YA PRETORIA

Abstract

Title: The influence of the inclination angle on void fraction and heat transfer during condensation inside a smooth tube

Author: Mr Stephanus Petrus Olivier

Supervisor: Prof J.P. Meyer

Department: Mechanical and Aeronautical Engineering

Degree: Master of Engineering (Mechanical Engineering)

The void fraction of condensation flow is an important parameter in determining the heat transfer and pressure drop characteristics of two-phase flow. In the past, studies involving void fraction, as well as heat transfer, have focused on horizontal and vertical flows. The current study measured void fractions during condensation and determined heat transfer coefficients for a full range of tube inclinations ranging from vertical downwards to vertical upwards at a condensation temperature of 40 °C. The void fractions were measured using capacitive void fraction sensors. The measurements were taken on an 8.38 mm inner diameter smooth tube with 200 W of induced condensation heat transfer at mass fluxes ranging from 100 – 400 kg/m^2.s and vapour qualities ranging from 10 – 90%. Alongside the void fractions, heat transfer measurements were also obtained for the full range of tube inclinations and compared with the void fraction measurements. The experimental data set generated consisted of 340 data points. At each data point, void fraction and heat transfer coefficients were measured. It was found that at combinations of low mass fluxes and vapour qualities, the void fraction and heat transfer coefficients were significantly affected by changes in inclination angle. Maximum values of heat transfer tended to coincide with downward inclinations where void fraction values decreased at low mass fluxes. Minimum heat transfer values tended to coincide with minimum void fraction measurements at upward inclinations for low mass fluxes. Predictions with established heat transfer, void fraction and flow pattern methods were also considered. For inclinations other than horizontal, the results were predicted less satisfactorily for low mass flux and vapour quality conditions. At high mass flux and vapour quality conditions, the void fraction and heat transfer coefficients tended to be independent of the inclination angle. At some intermediate mass flux and vapour quality conditions, the void fraction and heat transfer coefficients were observed to be independent of the inclination angle despite significant changes in the prevailing flow patterns. A sensitivity analysis revealed that the void fraction measurements needed to be very accurate to enable their use for heat transfer prediction purposes.

Keywords: Void fraction; two-phase flow; capacitance; flow pattern; condensation; inclination angle; heat transfer coefficient.

Acknowledgements

First and foremost I would like to thank my Heavenly Father for blessing me with the opportunities and talents required to complete this study. I would also like to extend my gratitude to my family and friends for their undying support throughout the study.

I would also like to thank the following people for their valuable contributions to the successful completion of this study:

Professor Josua Meyer ;

Professor Michel de Paepe ;

Danie Gouws ;

Louw Coetzee ;

Koos Mthombeni ;

Kunle Adelaja ;

Etienne Pienaar ;

Kathleen de Kerpel.

The guidance and assistance provided by the aforementioned people during the current study is greatly appreciated.

The funding obtained from the NRF, TESP, University of Stellenbosch/ University of Pretoria, SANERI/SANEDI, CSIR, EEDSM Hub and NAC is acknowledged and duly appreciated. The University of Ghent is thanked for providing two void fraction sensors.

Table of contents

Nomenclature

A	Area	[m^2]
C_o	Distribution parameter	[ ]
c_o	Parameter in Rouhani and Axelsson (1970) correlation	[ ]
c_p	Constant pressure specific heat	[J/kg.K]
D	Distance function	[ ]
d	Diameter	[m]
EB	Energy balance	[%]
F	Arbitrary quantity	[ ]
G	Mass flux	[$kg/m^2.s$]
g	Gravitational acceleration	[m^2/s]
h	Constant in Cioncolini and Thome (2012)	[ ]
	Specific enthalpy	[J/kg]
j	Superficial velocity	[m/s]
K	Volumetric quality	[ ]
	Empirical factor	
k	Thermal conductivity	[W/m.K]
L	Length	[m]
$\dot{m}$	Mass flow rate	[kg/s]
n	Constant in Cioncolini and Thome (2012)	[ ]
$\dot{Q}$	Heat transfer rate	[W]
R	Thermal resistance	[m.K/W]
S	Slip ratio	[ ]
T	Temperature	[°C]
u	Actual phase velocity	[m/s]
V	Voltage	[Volts]
$\dot{V}$	Volumetric flow rate	[m^3/s]
x	Vapour quality	[ ]
z	Axial tube dimension	[m]

Greek symbols

α	Heat transfer coefficient	[W/m^2.s]
β	Homogeneous void fraction	[ ]
ε	Void fraction	[ ]
θ	Tube inclination angle	[°]
v	Specific volume	[m^3/kg]
ρ	Density	[kg/m^3]
σ	Surface tension	[N/m]
φ	Coefficients in curve-fit polynomial	[ ]

Subscripts

atm	Atmospheric
Cu	Copper
f	Saturated liquid state
g	Saturated vapour state
H	Homogeneous
H_2O	Water side
i	Inner/inside Counter for curve-fit method
j	Centre of mass velocity Counter index
L	Liquid
Lj	Liquid drift velocity
$Norm$	Normalised
o	Outlet
$PreCond$	Pre-condenser
V	Vapour
Vj	Vapour drift velocity
VL	Drift flux
R	Refrigerant side
sat	Saturation state
$Test$	Test section
$System$	System conditions
w	Tube wall

Other

$\bar{}$	Weighted value
$\langle\,\rangle$	Averaged value

List of figures

List of tables

1. Introduction

1.1 Background

Convective condensation heat transfer is used in a wide range of power generation and industrial applications where large amounts of heat need to be removed. In most fossil fuel, nuclear and concentrated solar power plants, steam needs to be condensed to water for reuse by rejecting latent heat in cooling towers. These cooling towers are usually very big in size and therefore require large amounts of capital to construct. However, the efficiency of cooling towers directly influences the efficiency and/or power being generated by electricity-generating power plants.

On a smaller scale, many systems in the industrial, heating, ventilation and air-conditioning (HVAC) as well as refrigeration industries where cooling and/or heating is required make use of vapour-compression cycle systems. The condenser in the vapour compression system also needs to reject heat by condensing the refrigerant from a gas to a liquid. The condensation process happens in a heat exchanger which may be a cooling tower, but in many cases the heat exchanger is of the shell-and-tube type using water or air as the cooling medium.

On an even smaller, miniature scale, a considerable amount of work has recently been done on the cooling of electronic components (Winkler *et al.*, 2012). The physical scale is, however, not important. Condensation is a very complicated and important process and consequently much work has been done to improve the body of knowledge. Condensation has a direct impact on heat being rejected to the environment and/or energy consumption or -generation and for this reason engineers and designers need to understand it very well. Accurate equations should also be available for sizing and optimisation purposes.

Some of the most seminal work on condensation heat transfer over the past 30 years has been conducted by two groups consisting of Prof John Thome at the École Polytechnique Fédérale De Lausanne and Prof Alberto Cavallini at the University of Padova. Some of their recent work can be found in: Thome *et al*. (2013), Nebuloni and Thome (2013), Doretti *et al*. (2013) and Da Riva *et al*. (2012).

Their work present the importance of the identification of the prevailing flow pattern as it was used in the development of equations that estimate the local and average heat transfer and pressure drop coefficients during condensation.

Recently, Lips and Meyer (2011) conducted a review of the state of the art in condensation flow and they concluded that the majority of work was done for condensation in horizontal tubes and a limited amount in vertical tubes. However, very little work was done for condensation in inclined tubes. Most condensers in the industry operate in a horizontal configuration, but there are examples to the contrary. Examples of condensation flows at inclined orientations include aeroplanes during take-off, landing and banking. In the automotive industry, most air-conditioning condensers rarely operate in a fixed orientation. In many cases, the condenser will be inclined according to the orientation of the vehicle, which is dependent on the driving conditions.

Due to the fact that no data was available on condensation flow in inclination tubes, Professor Meyer and co-workers at the University of Pretoria produced a seminal body of work on this topic. They found that downward inclination angles could have significant advantages since gravity assisted in thinning the liquid layer inside the tube and reduce the thermal resistance to heat transfer. The aforementioned phenomenon presents a possible avenue for optimisation of heat transfer systems.

In the work of Lips and Meyer (2012b), a strong effect of inclination angle on liquid distribution, i.e. flow pattern and heat transfer, was observed. An increase in heat transfer of up to 20% at an inclination of -15° (downward flow) was observed for combinations of low mass flux and vapour quality. The heat transfer decreased with upward flow inclinations. At higher mass flux and vapour quality conditions, shear forces were dominant, which meant that the flow patterns tended to remain annular with the heat transfer coefficients exhibiting independence of the tube inclination angle. Also, the observed flow patterns did not correlate well with the considered models for inclined flow.

From the work of Lips and Meyer (2012c) for horizontal pressure drops, the model of Moreno Quibén and Thome (2007) along with the El Hajal *et al*. (2003) flow pattern map best represented the experimental results. Void fraction models were chosen in order to use pressure drop correlations for comparison with experimental results. The considered void fraction correlations led to good correlation between predictions and experimental results for upward flows. The correlations failed to predict pressure drops for downward flows. The apparent gravitational pressure drop was used to estimate the apparent void fraction. From the results, it appeared that the void fraction remained constant for upward flows. For downward flows, the apparent void fraction could not be considered to represent the actual void fraction since the frictional pressure drop was dependent on the inclination angle.

At lower mass fluxes (i.e. 100–200 kg/m^2.s), the heat transfer coefficients were observed by Meyer *et al*. (2014) to exhibit a maximum in the region of -30° to -15° (downward flow) due to gravity thinning of the stratified liquid layer, which led to less thermal resistance. The heat transfer coefficients were observed to reduce with increased saturation temperature for all inclination angles and mass fluxes. The reason provided was that the thermal conductivity of the particular refrigerant (R134a) decreased with increasing temperature meaning a reduction in heat transfer coefficient.

Adelaja *et al*. (2014) analytically studied the effects of two-dimensional wall conduction and fluid axial conduction for laminar flow in thick-walled tubes subject to convective boundary conditions. Parameters included in the investigation were tube wall thickness, Biot number and tube wall to fluid thermal conductivity ratio. It was found that the bulk fluid and wall temperatures decreased with decreasing tube wall thickness, increasing Biot number and increasing tube wall to fluid thermal conductivity ratio. It was also noted that an increase in tube wall thickness led to a reduction in convective heat losses while an increase in Biot number and tube wall to fluid ratio increased convective heat losses. Increasing the tube wall thickness led to an increase in the thermal entrance length. The thermal entrance length was seen to decrease with increased Biot number and tube wall to fluid conductivity ratio.

However, what has not yet been researched is the determination of the void fractions and their influence on heat transfer coefficients in tubes at different inclination angles. The knowledge of the void fractions is important in the developing of accurate heat transfer coefficient equations, which has also not yet been done in inclined tubes.

1.2 Problem statement

The heat transfer and pressure drop during condensation in a tube are directly related to the temporal and spatial distribution of the liquid and vapour phases. These phases are directly related to the void fraction and a considerable number of measurements have been taken to relate the void fraction to heat transfer and pressure drop equations during condensation. However, no work has been done to determine the void fraction and its influence on heat transfer coefficients during condensation in inclined tubes. In addition, no work has been done on the development of new and/or revision of existing equations, which takes into consideration the changes that occur in void fraction as a function of the inclination angle.

1.3 Purpose of the study

The purpose of the study was to measure void fractions, capture prevailing flow patterns visually and measure the heat transfer coefficients over a wide range of inclination angles during condensation in a smooth tube. The effect of the void fractions on the flow patterns and heat transfer coefficients was also investigated qualitatively.

1.4 Scope

An existing experimental set-up, which was used for several previous studies on condensation flow, was available (Canière *et al*. 2007; Van Rooyen and Christians 2007; Suliman *et al*. 2009; Van Rooyen *et al*. 2010; Lips and Meyer 2012a; Lips and Meyer 2012b; Lips and Meyer 2012c).

Lips and Meyer (Lips and Meyer 2012a; Lips and Meyer 2012b; Lips and Meyer 2012c) also used this set-up with a test section consisting of a smooth tube with an internal diameter of 8.38 mm using R134a as a condensing fluid. Due to the availability of the experimental set-up and previous data, which could be used for comparison purposes, the same experimental set-up and condensing fluid (R134a) were used. The void fraction measurements on the test section were taken with a newly developed capacitive-type sensor developed by Ghent University under the supervision of Prof Michelle de Paepe and co-workers (Canière *et al*., 2007, 2008, 2009, 2010).

To accommodate the measurements of the void fraction measurements, it was necessary to modify the test section that was used for previous work. The modification results showed that the measured heat transfer coefficients were not identical to previously published work of Lips and Meyer (2012b) as well as that of Lips and Meyer (2012c). This can be expected as the original test section was built and calibrated differently and measurements were taken about three years after the data capturing of Lips and Meyer (2012b) and Lips and Meyer (2012c) had been completed. Although the heat transfer coefficients reported in this paper are thus not original, they are very specifically linked to the void fraction measurements and captured flow regimes of this study. The additional advantage of the publication of the heat transfer coefficients of Lips and Meyer (2012b) and Lips and Meyer (2012c) in this study is an independent verification of their results.

1.5 Significance of the study

The insignificant amount of work and the importance of inclination on condensation were discussed in Section 1.1. Therefore, in the design of heat transfer systems where convective condensation takes place in tubes at inclinations other than vertical upward and horizontal or vertical downward

flow, the existing correlations developed in literature will be used outside their specified conditions of validity. Therefore, the result will most probably be inaccurate predictions for heat transfer behaviour. Although existing equipment such as dry cooling was designed and built before, no information on condensation of steam as a function of the inclination angle is available in the open literature. The work of this study and the previous work of Lips and Meyer (2012b) and Lips and Meyer (2012c) should therefore be repeated for steam, although the results of this study could be useful and could be used as a guideline from a qualitative point of view.

The current study aimed to broaden the experimental database for convective condensation of refrigerants as well as improving the general understanding of the effect of different tube inclinations on the void fraction of the flow. Being able to accurately predict the heat transfer and pressure drop characteristics of convective condensation in inclined tubes could enable future designers to use the tube inclination angle to optimise heat transfer and pressure drop behaviour in convective condensing flows.

1.6 Organisation of the study

Chapter 2 contains a literature review to acquaint the reader with selected pertinent void fraction models and correlations. Several methods of void fraction measurements are also discussed with a focus on capacitive measurement techniques because the current study used such a device.

The experimental system for the measurement of the void fractions, heat transfer coefficients and capturing of the photos of flow patterns is presented in Chapter 3. Chapter 4 explains the processes involved in the validation and calibration of the experimental set-up as well as the acquisition of the data. The process of data reduction is also presented.

The presentation and discussion of the experimental results are given in Chapter 5 along with the comparisons of the experimental data with correlations in literature. The study is concluded with Chapter 6.

2. Literature review

2.1 Introduction

The purpose of this chapter is to give an overview of the literature related to this study. Several salient void fraction models and/or correlations are also chronologically presented to illustrate the evolution of the field of void fraction study. Several void fraction measurement techniques are presented along with selected advantages and disadvantages after which the capacitive void fraction sensors used in the current study are briefly discussed. Finally, a brief overview of past work concerning heat transfer in inclined tubes is presented because it pertains to the current study.

2.2 Flow patterns for condensation flows

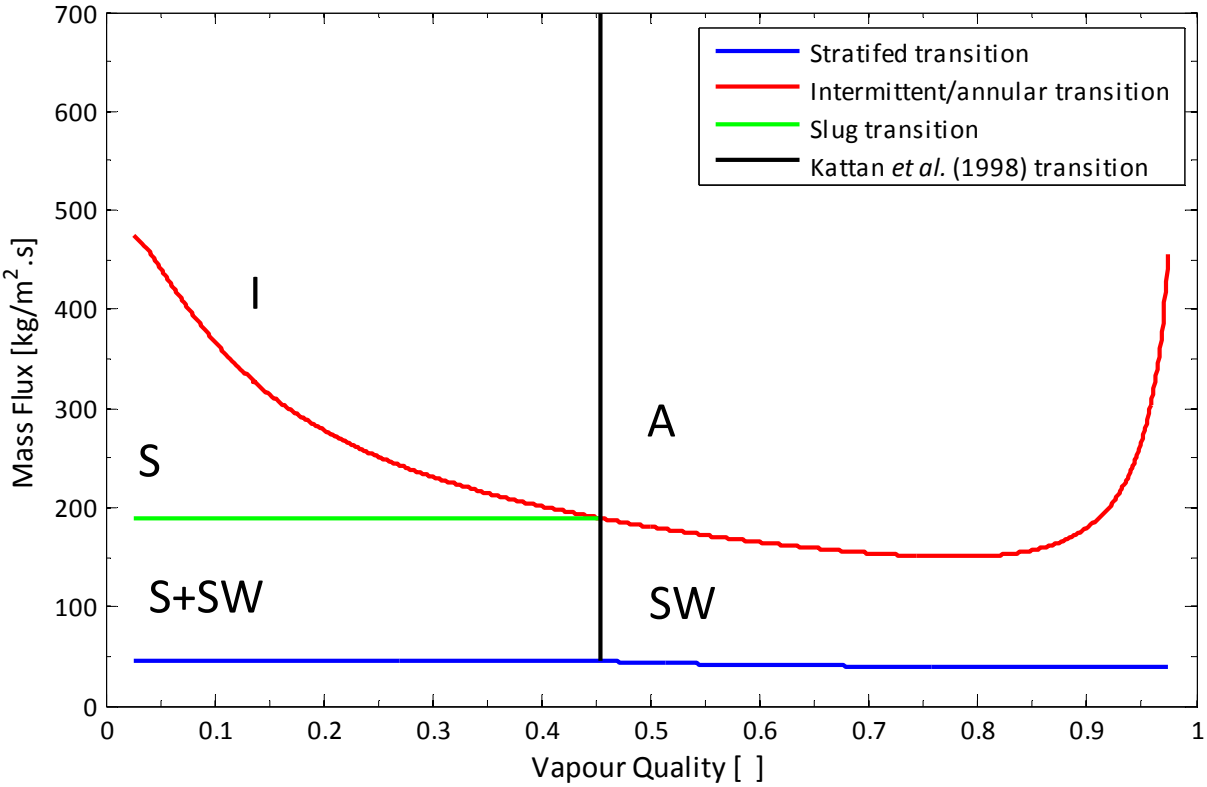

Figure 2.1: Representative Wojtan *et al.* (2005) flow pattern map for a mass flux of 300 kg/m^2.s illustrating flow pattern transition lines for annular (A), intermittent (I), stratified-wavy (SW) and slug (S) flows

The dependence of two-phase heat transfer coefficients during condensation on the prevailing flow patterns was discussed by Thome (2006a). The statement that only correlations which consider the prevailing flow pattern are fit for general use was made by Wojtan *et al.* (2005). The flow pattern characterisation for the current study was based on the flow map of Wojtan *et al.* (2005). The exclusive use of this flow pattern map is justified since the current study is a follow-up to the void

fraction sensor calibration work carried out by De Kerpel *et al.* (2013), in which the aforementioned flow pattern map was used.

The Wojtan *et al.* (2005) flow pattern map was developed as an improvement on the work of Kattan *et al.* (1998) after observations of dynamic void fractions were made. The conclusion was to subdivide the stratified-wavy region of the Kattan *et al.* (1998) flow map into the following flow patterns: (a) slug flow, (b) slug/stratified-wavy flow, and (c) stratified-wavy flow. In Figure 2.1 a representative flow pattern map is provided to illustrate its general appearance.

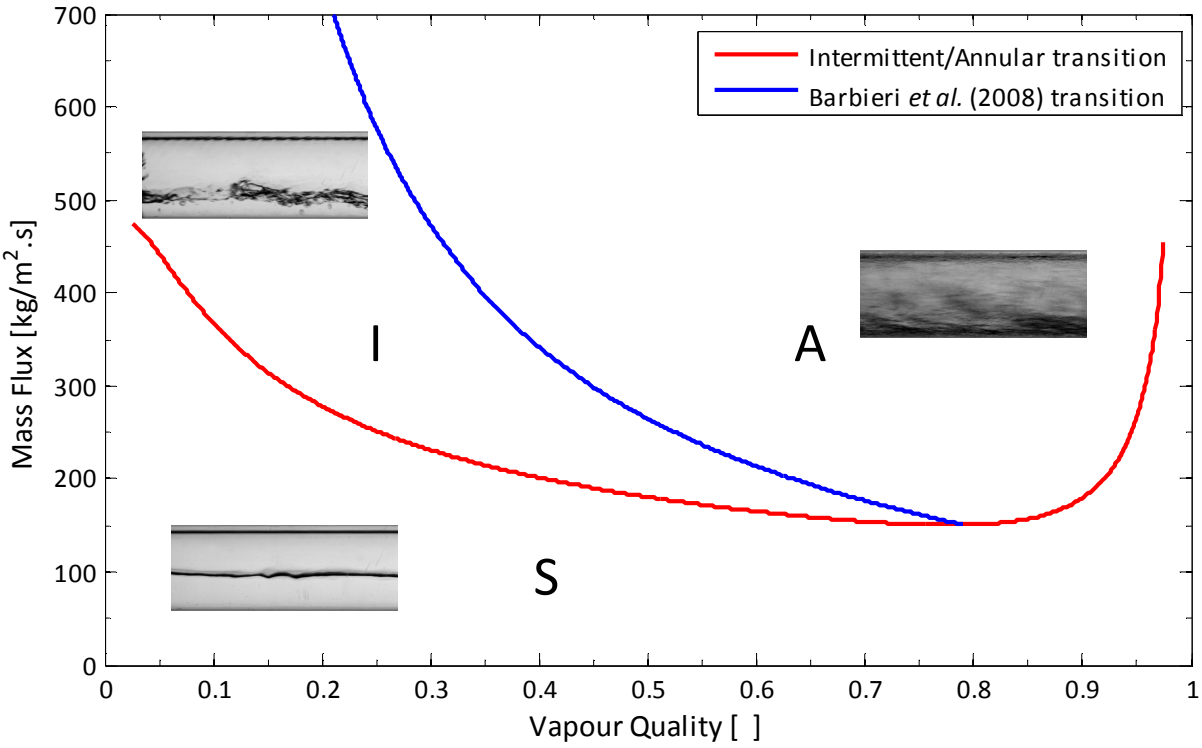

Figure 2.2: The flow pattern map which was used for the flow characterisation of the current study for a representative mass flux indicating annular (A), intermittent (I) and slug (S) flow transitions with photographic examples

In accordance with the work of De Kerpel *et al.* (2013, 2014), the aforementioned slug, slug/stratified-wavy and stratified-wavy flow regimes were all grouped together under "slug" flow for use in the void fraction calibration system. Also, the Kattan *et al.* (1998) transition between intermittent and annular flow was substituted for the Barbieri *et al.* (2008) transition criteria. The effective flow pattern map used for the flow characterisation in terms of the void fraction calibration scheme is provided in Figure 2.2 along with photographic examples of each flow pattern.

For visual flow classification, the flow pattern map of Wojtan *et al.* (2005) was modified by replacing the Kattan *et al.* (1998) transition line with that of Barbieri *et al.* (2008) to reflect the flow

classification used by De Kerpel *et al*. (2013, 2014). An example of the aforementioned modified Wojtan *et al*. (2005) flow pattern map is presented in Chapter 3.

2.3 Void fraction models and correlations

2.3.1 Homogeneous void fraction model

The homogeneous void fraction model (Thome, 2006b) is a simple tool to estimate the void fraction present in two-phase flow; it can be considered as a special case of a slip ratio-based correlation. It allows the liquid vapour mixture to be treated as single fluid with mean representative thermophysical properties.

The term slip ratio for two-phase flow is defined as the ratio of the actual vapour velocity to the actual liquid velocity; the slip ratio is defined as follows (Winkler *et al*., 2012):

$$S = \frac{u_V}{u_L} = \frac{j_V}{j_L}\frac{1-\varepsilon}{\varepsilon} \tag{2.1}$$

Substituting the relevant parameters equation (2.1) can be rearranged as follows:

$$\varepsilon = \left[1 + S\left(\frac{1-x}{x}\right)\frac{\rho_V}{\rho_L}\right]^{-1} \tag{2.2}$$

When the slip ratio is set to one, the actual liquid and vapour velocities are equal; the slip between the phases is thus disregarded. This leads to the equation for the homogeneous void fraction as follows:

$$\beta = \left[1 + \left(\frac{1-x}{x}\right)\frac{\rho_V}{\rho_L}\right]^{-1} \tag{2.3}$$

The core assumption of neglecting interfacial shear effects between the liquid and vapour phases is also the greatest limitation of the homogeneous void fraction model. Normally, the vapour velocity in two-phase flow is greater than the liquid velocity, which means that the slip ratio is usually greater than one. As a result, the homogeneous void fraction model does tend to over-predict the actual void fraction. This model is considered to represent the upper limit for possible values of void fraction at the prevailing flow conditions due to the aforementioned slip ratio assumptions.

2.3.2 Momentum flux model

The premise of an analytical method to describe the void fraction in two-phase flow is to minimise some quantity of interest, e.g. momentum or kinetic energy (Thome, 2006b). The assumption is implicitly made that the flow will tend to the minimum of the chosen quantity.

The momentum flux of a homogeneous fluid is given by:

$$Momentum\ flux = G^2 v_H \tag{2.4}$$

Where according to the homogeneous fluid assumption, the specific volume is defined as follows:

$$v_H = v_V x + v_L(1 - x) \tag{2.5}$$

However, if separated flow is considered, i.e. liquid and vapour phases are considered to flow individually, the momentum flux is expressed as follows:

$$Momentum\ flux = G^2 \left[\frac{x^2 v_V}{\varepsilon} + \frac{(1-x)^2 v_L}{1-\varepsilon}\right] \tag{2.6}$$

If it is assumed that the void fraction is obtained by minimising the momentum flux as given in equation (2.6), the relation can be differentiated with regard to the void fraction and set to zero. When the minimised relation is compared with the void fraction relation given in equation (2.2), the slip ratio can be expressed as follows:

$$S = \left(\frac{\rho_L}{\rho_V}\right)^{1/2} \tag{2.7}$$

2.3.3 Drift-flux model

The original derivation of the drift flux model was done by Zuber and Findlay (1965), but other workers in the field have attempted to improve or refine the model. The Rouhani and Axelsson (1970) correlation, which is a variation of the original drift-flux model, is considered to predict void fractions with good accuracy De Kerpel *et al*. (2013, 2014). The information used for the current explanation was sourced from the works of Hibiki and Ishii (2003a) and Thome (2006b).

Two-phase flow can be described using a dual-fluid model or a drift-flux model. A dual-fluid model considers the two fluid phases separately in terms of conservation equations of mass, momentum and energy. This description of the two-phase flow, although accurate, leads to considerable

problems with closing relations for the various conservation equations and defining what happens at the interface between the respective phases (Chexal *et al*., 1992).

The drift-flux model serves as a simplified method; it is effectively a hybrid between considering the two fluid phases completely separately and considering one homogeneous phase. As a concept, it is characterised by considering the two-phase flow with mass, momentum and energy conservation equations for the liquid-vapour mixture as a whole instead of the two phases separately. The relative motions between the liquid and vapour phases are taken into account with kinematic constitutive relations; the model therefore does not oversimplify the two-phase flow by neglecting phase slip, but simplifies the two-phase flow characteristics enough to be considered without the aforementioned theoretical problems with closing relations and interfacial effects.

The drift-flux model is most applicable when there is a strong coupling of the motion of both phases, e.g. dispersed flows where one phase is continuous and the other discontinuous. (Hibiki and Ishii 2003a).

The core assumption of the drift-flux model is that the dynamic behaviour of the discrete liquid and vapour phases could be adequately expressed by the conservation equations for the mixture as a whole; the interfacial constitutive relations are also considered for the liquid-vapour mixture as a whole.

The velocity fields for the drift-flux model are described in terms of the velocity of the centre of mass of the mixture and the drift velocity, which is defined as the vapour velocity relative to the velocity of the volume centre of the mixture.

A considerable thermal non-equilibrium exists during the two-phase flow. This was accounted for in the drift-flux model by phase-change constitutive equations which specify the rate of mass transfer per unit volume. The rates of interfacial mass and momentum transfer strongly depend on the prevailing flow pattern. This made the constitutive equations for vapour generation and drift velocity dependent on the flow pattern (Hibiki and Ishii, 2003b).

The derivation of the simplified one-dimensional drift velocity constitutive equations assumed that the average drift velocity due to local slip could be predicted by the same expression as the local constitutive equations provided that the local void fraction and differences in the stress gradients were replaced by average values.

The definition of drift flux was briefly mentioned earlier in this section; a more elaborate definition of the drift flux is provided by Thome (2006b) as follows: “The drift flux represents the volumetric

rate at which vapour is passing forwards or backwards through a unit plane normal to the channel axis that is itself travelling with the flow."

The velocity with which the aforementioned normal plane was travelling with the flow was presented as j, which was defined in terms of the superficial velocities of the liquid and vapour phases as follows:

$$j = j_V + j_L \tag{2.8}$$

The liquid and vapour superficial velocities were defined in terms of the local phase velocities and void fraction follows:

$$j_V = u_V \varepsilon$$
$$j_L = u_L (1 - \varepsilon) \tag{2.9}$$

The drift velocity of the liquid and vapour phases, which were merely the differences in velocities of the phases relative to the centre of mass velocity j, is expressed as follows:

$$j_{Vj} = u_V - j$$
$$j_{Lj} = u_L - j \tag{2.10}$$

The procedure continued as a one-dimensional consideration and the aforementioned parameters were taken as local in their respective cross-sectional profiles. For the next part in the explanation of the drift-flux model, the cross-sectional average of an arbitrary quantity F is denoted with brackets ($\langle\ \rangle$) and defined as follows:

$$\langle F \rangle = \frac{\int_A F dA}{A} \tag{2.11}$$

It should be noted that the current section will make use of brackets ($\langle\ \rangle$) to illustrate the use of the average cross-sectional void fraction; the same brackets will be used to describe other cross-sectional average parameters as well.

With equation (2.11) in mind and using equations (2.10), the mean actual vapour velocity could be written as follows:

$$\langle u_V \rangle = \langle j \rangle + \langle j_{Vj} \rangle = \langle j_V / \varepsilon \rangle \tag{2.12}$$

The following relations are presented due to their use in the next step of the drift-flux model development:

$$\langle j_V \rangle = \langle j_V \varepsilon \rangle \tag{2.13}$$

$$\langle j_V \rangle = \frac{\dot{V}_V}{A} \tag{2.14}$$

$$\langle j_L \rangle = \frac{\dot{V}_L}{A} \tag{2.15}$$

The actual vapour velocity could be weighted according to the void fraction. The result is presented below along with the definition of the vapour drift velocity and cross-sectional average of the local void fraction as follows:

$$\bar{u}_V = \frac{\langle u_V \varepsilon \rangle}{\langle \varepsilon \rangle} = \frac{\langle j_V \rangle}{\langle \varepsilon \rangle} = \frac{\langle j \varepsilon \rangle}{\langle \varepsilon \rangle} + \frac{\langle j_{Vj} \varepsilon \rangle}{\langle \varepsilon \rangle} \tag{2.16}$$

The drift flux is the result of the product between the local drift velocity (equation (2.10)) and local void fraction:

$$j_{VL} = \varepsilon j_{Vj} \tag{2.17}$$

Equation (2.17) for the drift flux can be modified by using the definitions of superficial phase velocity (equation (2.9)) and drift velocity (equation (2.10)). Upon substitution and simplification the following expression for the drift flux is obtained:

$$j_{VL} = (1 - \varepsilon) j_V - \varepsilon j_L \tag{2.18}$$

To account for the mathematical difference in averaging the void fraction and channel axis normal plane velocity as a product rather than separately, the following distribution parameter is introduced:

$$C_o = \frac{\langle \varepsilon j \rangle}{\langle \varepsilon \rangle \langle j \rangle} \tag{2.19}$$

To further aid the explanation of the drift-flux model, the weighted mean drift velocity is defined as follows:

$$\bar{j}_{Vj} = \frac{\langle j_{VL} \rangle}{\langle \varepsilon \rangle} \tag{2.20}$$

Using the definition in equation (2.20) along with equation (2.16), the following expression could be obtained for the weighted actual vapour velocity:

$$\bar{u}_V = \frac{\langle j_V \rangle}{\langle \varepsilon \rangle} = C_o \langle j \rangle + \bar{j}_{Vj} \tag{2.21}$$

Dividing by the average central axis normal plane velocity $\langle j \rangle$ the following is obtained:

$$\frac{\langle j_V \rangle}{\langle j \rangle \langle \varepsilon \rangle} = C_o + \frac{\bar{j}_{Vj}}{\langle j \rangle} \tag{2.22}$$

Next, a volumetric quality is defined according to the form of equation (2.22) as follows:

$$\langle K \rangle = \frac{\langle j_V \rangle}{\langle j \rangle} = \frac{\langle j_V \rangle}{\langle j_V \rangle + \langle j_L \rangle} = \frac{\dot{V}_V}{\dot{V}_V + \dot{V}_L} \tag{2.23}$$

Making use of the newly-defined volumetric quality in equation (2.23), equation (2.22) could be rewritten in the following manner, which provides the average void fraction explicitly:

$$\langle \varepsilon \rangle = \frac{\langle K \rangle}{C_o + \frac{\bar{j}_{Vj}}{\langle j \rangle}} \tag{2.24}$$

Inspection of the form of equation (2.24) reveals that for the case where there is no relative motion between the phases, i.e. the vapour-phase drift velocity is zero $\left(j_{Vj} = 0\right)$, the following relation for the average void fraction results:

$$\langle \varepsilon \rangle = \frac{\langle K \rangle}{C_o} \tag{2.25}$$

From equation (2.25) the distribution parameter C_o is merely a correction factor which relates to the one-dimensional homogeneous flow theory to separated flows by taking into account that the void fraction and velocity profiles could vary independently across the channel. This means that for truly homogeneous flow, the distribution parameter equals one and the void fraction is given by:

$$\langle \varepsilon \rangle = \langle K \rangle = \langle \beta \rangle \tag{2.26}$$

The final term of equation (2.26) is the average homogeneous void fraction and is added after observing that the definition of the parameter $\langle K \rangle$ relates to the volumetric vapour flow rate to the total volumetric flow rate without accounting for slip between the phases; this definition coincides with that of the homogeneous void fraction.

The focus is shifted to the last term of equation (2.23), which could be rewritten in terms of the specific volumes of the liquid and vapour phases as follows:

$$\langle K \rangle = \frac{x v_V}{x v_V + (1-x) v_V} \tag{2.27}$$

Expressing the two-phase density as the inverse of the two-phase specific volume, the following is obtained:

$$\rho = \frac{1}{v} = \frac{1}{\frac{x}{\rho_V} + \frac{(1-x)}{\rho_V}} \tag{2.28}$$

The mass flux of the flow could be written as follows:

$$G = \rho \langle j \rangle \tag{2.29}$$

Using the aforementioned relations to modify the average void fraction equation (equation (2.24)), the following is achieved upon simplification:

$$\langle \varepsilon \rangle = \frac{x}{\rho_V} \left[C_o \left(\frac{x}{\rho_V} + \frac{1-x}{\rho_L} \right) + \frac{\bar{j}_{Vj}}{G} \right]^{-1} \tag{2.30}$$

The relation in equation (2.30) clearly illustrates the fact that void fraction is dependent on the mass flux; this is not captured by all void fraction models in literature and represents a significant improvement.

The drift-flux model has been shown to be effective only when the drift velocity is significantly bigger than the total volumetric flux. The drift-flux model presented in equation (2.30) reduces to the homogeneous void fraction for the following cases:

- When the distribution parameter is set to one ($C_o = 1$), and
- When the drift velocity is zero $\left(\bar{j}_{Vj} = 0\right)$ or very high mass flux occurs.

2.3.4 Rouhani and Axelsson

Rouhani and Axelsson (1970) developed correlations for the vapour drift velocity in an attempt to improve the accuracy of the drift-flux model. For tubes in a vertical orientation, the vapour drift velocity was correlated as follows:

$$j_{Vj} = 1.18\left[\frac{g\sigma(\rho_L - \rho_V)}{{\rho_L}^2}\right]^{1/4} \tag{2.31}$$

A correlation for the distribution parameter over a wide range of mass fluxes was developed by Rouhani and Axelsson (1970) as follows:

$$C_o = 1 + 0.2(1 - x)\left(\frac{g d_i {\rho_L}^2}{G^2}\right)^{1/4} \tag{2.32}$$

Otherwise, the recommended values for the distribution parameter C_o were given as $C_o = 1.1$ for mass fluxes greater than 200 kg/m^2.s, and $C_o = 1.54$ for mass fluxes less than 200 kg/m^2.s

The expression given for the distribution parameter (equation (2.32)) was valid for void fractions bigger than 0.1.

For horizontal tubes, the Steiner (1993) version of the Rouhani and Axelsson (1970) correlation is generally accepted as accurate due to its good agreement with experimental data; the modified version also has the desirable characteristic of tending to the correct void fraction limits. The distribution parameter was given as:

$$C_o = 1 + c_o(1 - x) \tag{2.33}$$

The parameter c_o was set at a value of 0.12 as it correlated satisfactorily with the horizontal data.

The term $(1 - x)$ was added to the drift velocity correlation as provided in equation (2.31) to obtain the following slightly modified drift velocity correlation for horizontally inclined tubes:

$$j_{Vj} = 1.18(1 - x)\left[\frac{g\sigma(\rho_l - \rho_l)}{{\rho_l}^2}\right]^{1/4} \tag{2.34}$$

By virtue of its association with the drift-flux model, the Rouhani and Axelsson (1970) correlation took the effect of mass flux on void fraction into account. According to Wojtan *et al.* (2004), among

several others who will not be mentioned here, the Rouhani and Axelsson (1970) correlation produced commendable performance for void fraction predictions.

2.3.5 Thome *et al.*

While developing their flow pattern maps and subsequent flow regime-dependent heat transfer model, Thome *et al.* (2003) noticed that their heat transfer results tended to be segregated with regard to saturation pressure. They noticed that their heat transfer model, which used the Steiner (1993) version of the Rouhani and Axelsson (1970) void fraction model, over-predicted the measured heat transfer coefficients. The over-prediction rose with an increase in the saturation temperature/pressure.

They tried to resolve the over-prediction by using the homogeneous void fraction model and modifying coefficients within their heat transfer model; the homogeneous void fraction model represented the theoretical maximum value for the void fraction at the particular flow conditions. After incorporating these factors into their heat transfer model, they noted that the phenomenon they aimed to resolve had been reversed; their model over-predicted the heat transfer with decreasing saturation pressure.

It was concluded that neither of the aforementioned void fraction models correctly captured the effect of saturation pressure on the heat transfer results. In their attempt to develop a void fraction model which would be valid over the entire range of saturation pressures, they decided to use a logarithmic mean void fraction which is defined as follows:

$$\varepsilon = \frac{\varepsilon_{Homogenous} - \varepsilon_{Rouhani}}{ln\left(\frac{\varepsilon_{Homogenous}}{\varepsilon_{Rouhani}}\right)} \tag{2.35}$$

After implementing the logarithmic mean void fraction, Thome *et al.* (2003) observed an improvement in their heat transfer model's ability to predict the heat transfer results correctly over a spectrum of saturation pressures. They concluded that their recently defined logarithmic mean void fraction correctly captured the void fraction phenomena for saturation pressures varying from low pressures up to values close to the critical point.

2.3.6 Woldesemayat and Ghajar

A comprehensive literature survey was conducted by Woldesemayat and Ghajar (2007). Different void fraction correlations and experimental data were collected from various laboratories. This resulted in comparing the performance of 68 different void fraction correlations based on an

unbiased data set, which covered a wide range of experimental parameters. Making use of a wide range of experimental data minimised the systemic error which might have been present in each institution's results. Of particular relevance to the current study is that several studies of inclined-tubes were included in their literature and data search.

Woldesemayat and Ghajar (2007) observed that most of the void fraction correlations they found were very restricted in terms of their applicability; they were mostly only valid for the experimental conditions under which they were developed.

Based on their observations of the various void fraction correlations under consideration, an improved correlation was suggested based on the best-performing correlation according to their study. The Dix correlation (Coddington and Macian 2002) exhibited good consistency in predicting the void fraction over a wide range of cases. The aforementioned correlation also had the best performance in terms of predicting the most experimental data points within a 5% error band. They also observed that if only vertical and inclined tube orientations were considered, the Toshiba correlation (Coddington and Macian 2002) successfully predicted the experimental data. The Dix correlation (Coddington and Macian 2002) was, however, identified as the overall best candidate for further improvement.

Correction factors were introduced to the Dix correlation (Coddington and Macian 2002) to resolve the issue of under-prediction for several of the experimental data points considered. Zuber and Findlay (1965) made the statement that the drift velocity was a function of the concentration profiles in the tube. They also stated that the drift velocity depended on the momentum transfer between the two-phase flow. The concentration profile over the cross-section of the tube for a given orientation was generally assumed to remain constant for cases where no mass transfer occurred along the length of the tube.

Integrating the aforementioned observations regarding the flow and noting that their effect was in a normal direction relative to the tube inclination, the following correction factor was introduced:

$$[1 + cos\theta]^{0.25} \tag{2.36}$$

To capture the dependency of the drift velocity on momentum transfer between phases as mentioned earlier, the assumption of one-dimensional force interaction was employed. A further assumption was made that this force interaction would be a maximum for flows at high inclination angles operating near atmospheric pressure. The correction factor resulting from these considerations was given as follows:

$$[1 + sin\theta]^{\frac{P_{atm}}{P_{system}}} \tag{2.37}$$

Introducing these corrections into the Dix correlation (Coddington and Macian 2002) resulted in the following modified void fraction correlation:

$$\varepsilon = \frac{j_V}{j_V\left(1 + \left(\frac{j_L}{j_V}\right)^{\left(\frac{\rho_V}{\rho_L}\right)^{0.1}}\right) + 2.9\left[\frac{gd\sigma(1+\cos\theta)(\rho_L - \rho_V)}{\rho_L^2}\right]^{0.25}(1.22 + 1.22\sin\theta)^{\frac{P_{atm}}{P_{system}}}} \tag{2.38}$$

Woldesemayat and Ghajar (2007) noted a substantial improvement in their modified correlation on that of the Dix correlation (Coddington and Macian 2002) on which it was based.

2.3.7 Cioncolini and Thome

Cioncolini and Thome (2012) proposed a method for predicting the void fractions in annular two-phase flow using a large collection of data points originating from different studies. They did not use the drift-flux model as a basis for their new proposed method; the explanation they provided was: "Drift-flux models, in fact, are designed to handle distributed and unseparated two-phase flows where one phase is continuous, the other phase is dispersed and the dominant relative motion between the two phases is caused by an external force field such as gravity. As such, drift-flux models are most useful in the analysis of two-phase flows where the relative motion is primarily controlled by buoyancy" (Cioncolini and Thome 2012).

From the aforementioned statement when the relative motion between the liquid and vapour phases is dominated by the pressure and velocity gradients existing in the two phases, the drift-flux model cannot effectively predict the physics of the two-phase flow.

The correlation developed by Cioncolini and Thome (2012) was described by the authors as a "minimal model". This could be explained as the simplest possible model which still managed to capture the essential physics of the annular two-phase flow. They did this by disregarding all parameters which influenced the void fraction for annular flow barring the density ratio (ρ_V/ρ_L) and vapour quality (x).

The resulting correlation is provided in equation (2.39) along with the constants required in the void fraction formulation as follows:

$$\varepsilon = \frac{hx^n}{1 + (h-1)x^n}$$

$$h = -2.129 + 3.129\left(\frac{\rho_V}{\rho_L}\right)^{-0.2186} \qquad (2.39)$$

$$n = 0.3487 + 0.6513\left(\frac{\rho_V}{\rho_L}\right)^{0.5150}$$

The correlation provided in equation (2.39) was only valid for shear-driven annular flow; the effect of gravity on the two-phase flow had to be negligible. The authors did consider adding additional parameters to the "minimal model" described above, but upon comparison with other void fraction predictions they deduced that their correlation exhibited satisfactory performance. Cioncolini and Thome (2012) also noted that the drift-flux model based correlation of Woldesemayat and Ghajar (2007) performed well; this proved that drift-flux based models could and do in fact predict annular flows well. However, it seemed that the drift-flux based models used more parameters that appear secondary in nature as they did not perform significantly better than the "minimal model" proposed by Cioncolini and Thome (2012).

2.4 Void fraction measurement techniques

2.4.1 Shut-off valves

A physical technique for measuring the volumetric void fraction is to use inline shut-off valves which close simultaneously to capture the liquid-vapour mixture at the prevailing flow conditions. The captured mixture is then collected and accurately weighed to determine the void fraction which was present at the flow conditions.

An advantage of this technique is the ease with which the measured sample could be related to void fraction. A disadvantage is the difficulty in accurately measuring the void fractions for high and low void fraction flows due to uncertainties in obtaining the exact quantity of remaining liquid in the test section. A highly volatile solvent can be used to clean out valves and ensure that the minimum amount of liquid in the acquired sample is left behind as was done by Lockhart and Martinelli (1949). This technique is highly intrusive as the flow is completely stopped to acquire a sample.

Examples of researchers using this void fraction measurement technique are Yashar *et al*. (2001) and Koyama *et al*. (2004).

2.4.2 Radiation attenuation

The mass attenuation effect of the liquid-vapour mixture, which varies with flow and density, can be used to quantify the void fraction present in a flow domain. A beam of radiation is passed through the flow while observing the reduction in the electromagnetic radiation intensity. The large differences between liquid- and vapour phase densities lead to significant variations in the radiation absorption characteristics of the flow with changes in void fraction.

Gamma as well as X-rays can be used for void fraction measurements with the radiation attenuation effect. Gamma rays are generally preferred to X-rays, because gamma radiation is more monochromatic in nature and, therefore, is simpler to relate the response from the scintillator to the actual void fraction (Bertola, 2003).

Some advantages of this technique are that the tube containing the liquid vapour mixture does not need to be transparent as with optical void fraction measurement techniques. On the other hand, serious cost and safety issues accompany the use of radiation, which have to be addressed and therefore limit the method's widespread use. Furthermore, depending on the material used to construct the tube through which the fluid flows and the thickness of the tube wall, radiation attenuation may not always be practical. An example of using radiation attenuation to measure void fraction can be found in the work of Jones and Zuber (1975).

2.4.3 Wire-mesh tomography

Wire-mesh tomography involves a grid of electrodes spanning the cross-section of the tube which captures the liquid vapour distribution by utilising the differences in electrical resistivity and/or permittivity between the liquid and vapour phases of the fluid flow. In general, an excitation signal is generated at one end of the electrodes and the subsequent response is monitored at the other end. Investigations into the flow structure of two-phase flows were carried out for both the electrical resistivity (Fuangworawong *et al*., 2007) and permittivity (Da Silva *et al*., 2010) techniques.

If the electrodes are adequately compacted, wire-mesh tomography provides good resolution information of the liquid-vapour distribution within the two-phase flow while being considerably less expensive than some other void fraction measurement techniques, i.e. radiation attenuation.

Because the electrodes are positioned in the flow, wire-mesh tomography is classified as an intrusive technique as it results in disturbance and deceleration of the flow.

2.4.4 Neutron radiography

Thermal neutrons have the desirable characteristics of being able to easily penetrate metals, as well as being attenuated well by fluids commonly used in two-phase flows. Neutron radiography is therefore well suited for measuring void fractions of two-phase flows in metal tubes. This technique is also non-intrusive, which is advantageous. However, as with radiation attenuation, serious safety and cost implications accompany the use of neutron radiography to measure void fractions.

Extensive research has been done using neutron radiography and the reader is referred to the work available in literature for more information (Mishima and Hibiki 1996; Mishima *et al*. 1997; Mishima and Hibiki 1998; Saito *et al*. 2005).

2.4.5 Visual methods

Void fraction has been measured in the past by taking videos/photographs of the flow and using image processing to extract the liquid-vapour distribution in the flow domain. Spatial information extracted through image processing techniques is almost exclusively in two dimensions. Extracting three-dimensional information on the two-phase flow distribution entails making assumptions regarding the liquid-vapour interface which may compromise the validity.

The quality of data from visual measurement techniques is sensitive to lighting conditions, optical reflections and the angle of observation. Reliability in quantifying the void fraction may therefore be an issue. Visual techniques do not lend themselves to quantifying flow patterns in which the liquid-vapour interface is not clearly defined, e.g. mist flow (Winkler *et al*., 2012). Visual techniques have, however, been used by researchers to determine the void fraction in two-phase flows (Ursenbacher, Wojtan and Thome, 2004), albeit for limited cases. Visually observing the two-phase flow has proved to complement other two-phase flow studies well in the past (Lips and Meyer 2012b; Van Rooyen *et al*. 2010).

Image-processing techniques become more suitable with decreasing channel diameters since for smaller diameters, the vapour-in-liquid-shapes are more symmetrical than for larger diameter tubes (Winkler *et al*., 2012). The requirement for visual void fraction measurements to have a transparent tube may be a disadvantage; the range of temperatures and pressures at which the system can be operated may be limited by the physical properties of the transparent material. An advantage of using visual methods is that there is no intrusion on the flow.

A few examples of past researchers using optical methods to quantify void fraction measurements are Kawahara *et al*. (2005), Rezkallah and Clarke (1995) and Ursenbacher *et al*. (2004).

2.4.6 Electrical impedance

Electrical impedance methods rely on the different electrical properties of the liquid and vapour phases. The specific parameter which is measured is usually the electrical conductance or the electrical capacitance of the two-phase flow. The void fraction is subsequently related to the electrical response in some manner.

For cases where fluid capacitance is measured, the process is usually considered as non-intrusive with similarities to neutron radiography and radiation attenuation. For conductance-type measurements, there is usually some flow disturbance since the sensor needs to be in physical contact with the fluid. Wire-mesh tomography is an example of conductance type measurements.

Different sensor designs have been considered in the past, but helically-wound and concave plate capacitance sensors have produced desirable results. Consequently, ring/half-ring sensors which sit flush with the inner surface of the channel are generally preferred (Bertola, 2003). Concave plate capacitance sensors have been observed to exhibit superior sensitivity and shielding characteristics. Keska *et al*. (1999) compared four different void fraction measurement techniques and concluded that capacitive and resistive measurements were effective in classifying two-phase fluid flow.

The capacitance of a specific fluid is less susceptible to temperature variations than the electrical conductance (Bertola, 2003), which presents an advantage in favour of capacitive measurements. In addition, from past work, it is clear that there are ways to compensate for the temperature variations in the capacitance of some fluids such as refrigerants (Dos Reis and Goldstein 2005). Disadvantages include that the measured capacitances tend to be very small, which makes them susceptible to stray capacitance and sensor inaccuracies; electrical shielding is therefore important to minimise stray capacitance. Capacitive sensors must be manufactured with small tolerances to maintain measurement accuracy.

Examples of work which incorporated electrical impedance measurements are those of Elkow and Rezkallah (1996), Canière *et al*. (2010), Demori *et al*. (2010) and De Kerpel *et al*. (2013, 2014).

2.4.7 Discrepancy between measurement techniques

Different void fraction measurement techniques applied to the same flow conditions could result in discrepancies in void fraction values. Ma *et al*. (1991) observed deviations of up to 20% in void

fraction measurements using electrical impedance and shutoff valve methods. Ali *et al*. (1993) observed a ±8% deviation in their void fraction measurements using electrical impedance methods and visual observations made using photographs of the flow. Rezkallah and Clarke (1995) compared results from image processing and capacitance measurements and found deviations in the void fraction of bubbly and slug flow in the order of 10% and about 17% for annular flow.

2.5 Void fraction sensors used in the current study

In this study, a capacitive void fraction sensor was used which was developed by the Department of Flow, Heat and Combustion Mechanics at the University of Ghent, Belgium (Canière *et al*., 2007, 2008, 2009, 2010; De Kerpel *et al*., 2013, 2014). This section provides a brief overview of the operation of the void fraction sensors in the context of the current study.

The operation of the void fraction sensors depended on two sets of three electrodes on either side of the flow; one set was connected to a 15 V block signal source, which served to charge the total capacitance of the fluid flow. The other set was used to capture the resulting discharge current from the fluid flow. Figure 2.3 provides an illustration of the electrode configuration inside the sensor. The electrodes were etched from flexible circuit material and fitted around a PVC tube with an internal diameter of 8 mm. The PVC tube provided the structural strength to be able to resist the internal pressure of the fluid and also served as a dielectric layer to separate the electrodes from the fluid flow.

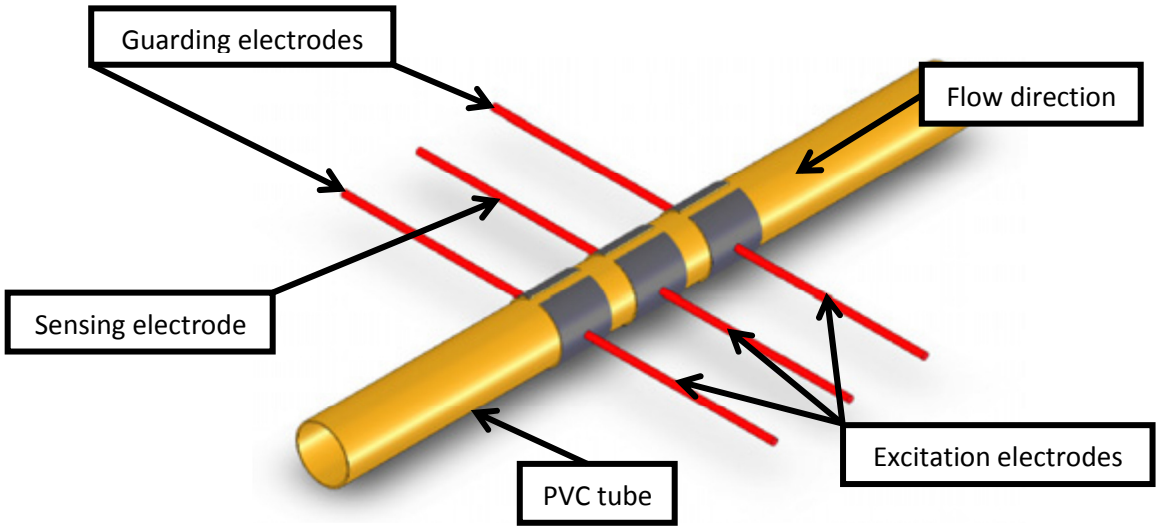

Figure 2.3: Graphic representation of electrode configuration within void fraction sensor (Canière *et al*., 2010)

The middle electrode pair was used to measure the capacitance of the fluid flow. The other electrode pairs only served to guard the electric field generated by the aforementioned electrodes.

The two sensing electrodes were constructed to have the same length in the flow direction as the internal diameter of the PVC tube. This arrangement was chosen as a compromise between the amount of fluid capacitance and the fact that semi-local measurements of void fraction were desirable.

The electrodes were designed with a large inscribed angle (β) of 160 degrees, which increased the measurable capacitance and thus the sensitivity of the sensors. The larger inscribed angle, however, resulted in a greater non-linear response between flow capacitance and sensor output as a result of the higher contributions at the electrode edges.

The entire ensemble described above was placed inside a cylindrical metal tube and the annular space was filled with a resin. To eliminate noise interference, the outer metal shell was also electrically grounded.

The electric field generated by the sensing electrodes is non-linear in nature; thus the sensor response to changes in void fraction is also non-linear. As a result, the relation between the measured fluid capacitance and actual void fraction depended on the spatial distribution of the liquid and vapour phases relative to each other in the tube. To address this, a calibration strategy was devised in which simplified flow structures were assumed to represent each separate flow regime De Kerpel *et al*. (2013, 2014).

Using the properties of the materials and fluids present in the void fraction sensors, finite element method (FEM) simulations were conducted to establish the normalised capacitance-void fraction relation for each specified fluid interface structure. From the calibration strategy developed by De Kerpel *et al*. (2013, 2014), the dielectric constants resulting from the FEM model correlated well with values available in literature for R134a.

To ensure that the original calibration curves could be considered for the current study, measurements were taken at ambient and 40 ^{o}C. The sensor outputs were sent to the Department of Flow, Heat and Combustion Mechanics at the University of Ghent to determine the dielectric constants of the liquid phases measured by each sensor. The values were found to be comparable with those obtained during the De Kerpel *et al*. (2013, 2014) study.

The original calibration curves were sixth-order polynomial curve fits to the normalised capacitance-void fraction relations. The coefficients to the calibration curves for both types of flows are provided in Table 2.1.

Table 2.1: Coefficients for void fraction calibration curves

$y = Ax^6 + Bx^5 + Cx^4 + Dx^3 + Ex^2 + Fx + G$							
	A	**B**	**C**	**D**	**E**	**F**	**G**
Slug flow	4,674907	-21,9445	33,8118	-19,6798	3,003132	-0,87448	1,005536
Annular flow	-2,2043	6,551456	-6,67354	3,029121	-1,17776	-0,52566	1,000481

The normalised sensor outputs were substituted into the calibration curves as provided in Table 2.1 according to the prevailing flow regime as described in De Kerpel *et al*. (2013, 2014).

2.6 Heat transfer coefficients for inclined flows

Numerous studies involving convective condensation heat transfer have been conducted, many of which were captured in the intensive literature survey on the topic produced by Dalkilic and Wongwises (2009). However, Lips and Meyer (2011) identified a relative lack of research which focused on condensation flows within inclined tubes. Some studies which considered condensation flow for inclined tubes were conducted for thermosyphons (Noie, Sarmasti Emami & Khoshnoodi, 2007), but observations made for thermosyphons and reflux condensers cannot be directly related to the case of convective condensation even though some similarities in the flow may be evident, e.g. liquid recirculation.

According to Lips and Meyer (2012b), Chato (1960) was the first to observe an inclination effect on the heat transfer coefficients. He observed increases in heat transfer coefficients with increasing downward inclination angle, which was put down to the decrease in the thickness of the liquid layer i.e. decreased thermal resistance.

Akhavan-Behabadi *et al*. (2007) performed condensation experiments using a similar diameter tube, albeit enhanced tube, and identical refrigerant on inclined tubes for a full range of inclination angles with intervals of 30°. The mass fluxes considered were quite low compared with those of the current study (54 kg/m^2.s - 107 kg/m^2.s). It was observed that the tube inclination affected the heat transfer coefficients with the greatest effect noted at combinations of lower vapour quality and mass flux. The maximum increase in heat transfer coefficients was observed for 30° upward flow, which contradicted the observations of past research (Chato 1960; Lips and Meyer 2012b).

From the work of Lips and Meyer (2012b), it was observed that the tube inclination had a substantial effect on the liquid-vapour distribution of the flow (i.e. flow patterns), which in turn affected the heat transfer coefficients. The heat transfer coefficients were observed to increase with downward

inclination angles with an optimal downward inclination angle observed in the region -15° to -30°. The heat transfer coefficients were also observed to decrease with upward inclinations, which contradicted the observations of Akhavan-Behabadi *et al*. (2007). At low vapour qualities, the lowest heat transfer coefficients for a particular set of flow conditions were observed in the region of 15° upward inclination.

2.7 Summary and conclusions

An overview was presented of void fraction correlations and/or models as they pertained to the current study. Modifications to the Wojtan *et al*. (2005) flow pattern map were also introduced in accordance with the work of De Kerpel *et al*. (2013, 2014). Another observation from the work of De Kerpel *et al*. (2013, 2014) was the good correlation between their adiabatic void fraction results with the predictions of the Rouhani and Axelsson (1970) correlation.

Literature has revealed several different techniques which can be employed to measure void fractions in multiphase flow with varying degrees of success and intrusiveness. The possibility of discrepancies in void fraction results obtained by different means was also pointed out.

The work of Cioncolini and Thome (2012) suggested that the drift-flux model was most useful for the case of flows where the relative movement between the respective phases was a result of buoyancy forces. The Rouhani and Axelsson (1970) correlation was based on the drift-flux model and was instrumental in the current study. They also proved that in some cases, additional parameters in a model did not significantly contribute to additional levels of accuracy.

A brief overview of selected past work conducted for convective condensation in inclined tubes was presented. The consensus is that heat transfer coefficients for condensation flows strongly depend on the liquid-vapour distribution (i.e. flow pattern) as this is directly linked to the thermal resistance to heat transfer. The tube inclination angle was observed to affect the prevailing flow patterns as well as heat transfer coefficients with increased heat transfer generally being observed for downward inclination angles and decreased heat transfer observed for upward inclination angles. The effect of tube inclination angle on the flow was observed to be more profound at combinations of low mass fluxes and vapour qualities. At combinations of higher mass fluxes and vapour qualities, the heat transfer coefficients tended towards an independence of tube inclination angle.

There has been very little research done for the case of condensing flows in inclined tubes, let alone void fraction measurements at inclined tubes. Therefore, the results of the current study should

contribute to the body of knowledge on the subject of void fraction measurements for condensing flows.

3. Experimental set-up

3.1 Introduction

This chapter discusses the experimental set-up used in the current study. The experimental system was inherited from past research projects performed by the Thermoflow Research Group at the University of Pretoria (Canière *et al*. 2007; Suliman *et al*. 2009; Van Rooyen *et al*. 2010; Lips and Meyer 2012a; Lips and Meyer 2012b; Lips and Meyer 2012c). The experimental set-up used a vapour-compression refrigeration cycle and a water cycle. Each cycle is presented briefly along with details of the test section and instrumentation. The procedures followed to calibrate the thermocouples and the void fraction sensors are also presented.

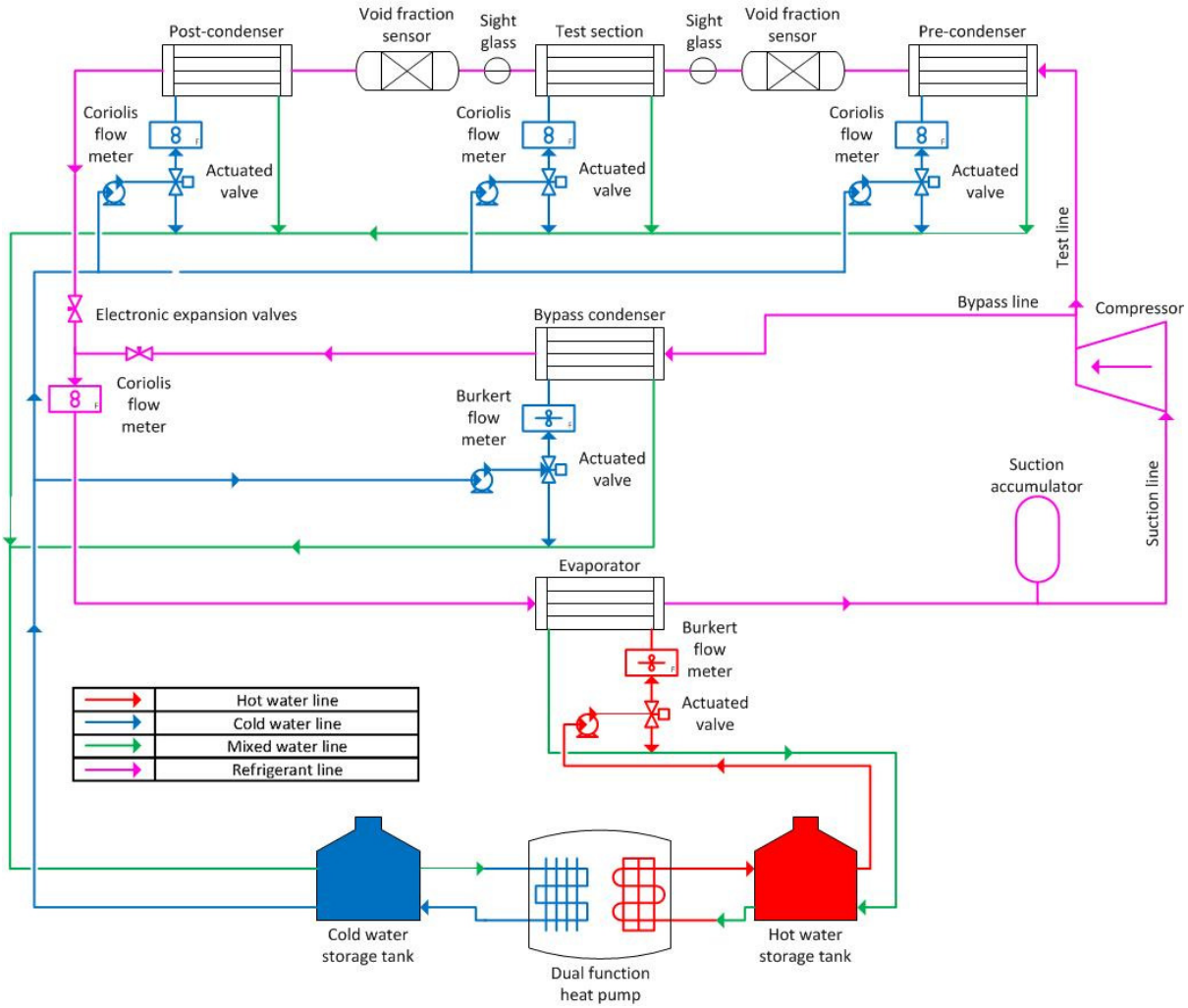

Figure 3.1: Schematic of the experimental set-up

3.2 Refrigerant and water cycles

The vapour-compression refrigeration cycle consisted of two high-pressure lines, i.e. the test line and bypass line, through which the condensing fluid was pumped (Figure 3.1). The flow of refrigerant through each respective line was controlled using a set of electronic expansion valves (EEVs), which could be selected depending on the desired flow rates. Before any testing commenced, the system was repeatedly flushed with high-purity nitrogen and evacuated to remove any traces of moisture and impurities which might affect the measurements negatively. The procedure which was followed is discussed in Appendix B.

Fluid flow was obtained using a hermetically sealed scroll compressor with a nominal cooling capacity of 10 kW. Using a scroll-type compressor had the advantage of requiring less lubricant than reciprocating-type compressors, which meant that less oil that could affect experimental results was circulated (Shao and Granryd 1995). The oil concentration within the system was measured for flow conditions conducive to oil circulation in the past and the oil concentration was found to be negligible (Van Rooyen and Christians 2007).

The test line was served by three respective condensers: the pre-condenser, the test condenser as well as the post-condenser. The pre-condenser was responsible for controlling the vapour quality at the inlet of the test condenser where temperature, pressure, flow pattern and void fraction measurements were taken, while the post-condenser ensured that the refrigerant reached the EEV in a fully liquid state and that the refrigerant mass flow rate could be accurately measured. The bypass condenser was used to control the mass flow rate, saturation temperature as well as saturation pressure of the refrigerant flowing through the test section. The bypass condenser was also adjusted to ensure a fully liquid state at the EEV. Downstream of the respective EEVs, the test and bypass lines merged into a single lower-pressure line, which led to the suction of the scroll compressor through an evaporator, which superheated the refrigerant. The degree of superheat was controlled to prevent damage to the compressor. A suction accumulator ensured that only vapour was available at the compressor suction.

Hot and cold water was supplied by a 50 kW heating and 70 kW cooling dual-function heat pump. Thermostat control was used to maintain the hot water between 25 °C and 30 °C and the cold water between 15 °C and 25 °C respectively in two tanks with a capacity of 5 000 litres each. From the tanks the water was supplied to the experimental setup. The hot water was used in the evaporator while the cold water was used in the various condensers situated in the experimental set-up. The

heat transfer of the respective heat exchangers was adjusted by altering the flow rate using actuated valves and bypass flow, which could be controlled from the data acquisition system.

3.3 Test section

The test condenser was constructed as a tube-in-tube counterflow heat exchanger with refrigerant flowing in the inner tube and water flowing in the annulus between the inner and outer tubes. The inner tube was constructed from 8.38 mm inner diameter (0.6 ± 0.002 mm wall thickness) smooth copper tube and the outer tube from 15.9 mm inner diameter smooth copper tube. A capillary tube of 2 mm diameter was wrapped around the outside of the inner tube at a constant pitch to improve fluid mixing within the annulus and prevent temperature stratification. The heat transfer length of the test section was 1.488 m. The refrigerant and water flows were directed to the inner tube and annulus respectively by using flexible rubber hoses to facilitate tilting of the test section. The entire test section was insulated with 60 mm thick insulation of thermal resistance 0.041 W/m.K to minimise heat losses. The inclination angle was measured using a digital inclinometer that was attached at the pivot point of the test section.

To ensure fully developed flow at the inlet to the test section an unheated, straight section of tube with a length of 260 mm was situated upstream of any measuring equipment to serve as a calming section. This translated to 31 tube diameters in length, which was less than the recommended 50 tube diameters (Lienhard & Lienhard, 2005) to ensure fully developed flow. Space limitations within the test facility prevented any further increase in length of the test section while still maintaining a full range of inclination angles.

Borosilicate sight glasses were installed at both the inlet and outlet of the test section, which enabled visual observation of the flow patterns. The sight glasses had the additional function of insulating the test section against any axial heat conduction due to their low thermal conductivity. A monochromatic high-speed camera set at roughly 200 frames per second was used at the outlet sight glass to capture the prevailing flow patterns within the test section. To improve the image quality of the flow pattern observations, a Phlox uniform light emitting diode (LED) backlight was used. The LED backlight was chosen with a low energy output so that it did not thermally affect the passing flow.

Three pressure measurement taps were installed at both the inlet and outlet of the test section respectively. Two of the aforementioned taps were connected to Sensotec FP 2000 ratiometric pressure transducers, which measured the prevailing absolute pressure at both the inlet and outlet respectively. The remaining pressure taps on the test section were available for measuring the

differential pressure between the inlet and outlet of the test section. Differential pressure measurements were, however, not considered for the purpose of the current study.

On the outer periphery of the inner tube, four countersunk indentations were drilled to enable the thermocouples to be affixed by soldering. The indentations were equally spaced around the periphery in such a way that two thermocouples could be located on a plane perpendicular to a stratified liquid interface and two in parallel to form a measuring station. There were seven equidistant measuring stations along the length of the test section, which meant that there were 28 thermocouples with which heat transfer measurements were taken. Three thermocouples were also installed upstream of the inlet sight glass and downstream of the outlet sight glass to determine the prevailing saturation temperature. The saturation temperature was also corroborated by the absolute pressure measurements and the REFPROP (2005) database. The differences in the measured saturation temperature and those determined from the database using absolute pressure measurements were less than 0.1 °C at high mass fluxes, i.e. 400 kg/m^2.s.

The fluid flow rates of the test section, pre-condenser, test condenser and post-condenser were measured using Coriolis mass flow meters with a factory-default uncertainty of 0.1% within the specified mass flow rate. The Coriolis mass flow meters responsible for measuring water flow rate were installed just upstream of each respective condenser. The Coriolis mass flow meter which measured the refrigerant mass flow rate through the test section was situated downstream of the post-condenser and upstream of the EEVs.

A computerised data acquisition (DAQ) system was used to gather the data from the thermocouples, pressure transducers, Coriolis flow meters as well as the void fraction sensors. The DAQ system consisted of a computer using LabVIEW software with which the measurements could be logged and control of the experimental system could be exercised. The data acquisition package used for the current study was the SCXI (Signal Conditioning Extensions for Instrumentation) range of products, which contained the necessary multiplexers, analogue-to-digital converters and terminal blocks to successfully log the data onto the computer.

3.4 Calibration procedures

3.4.1 Thermocouples

All thermocouples were constructed using T-type thermocouple wire with a 30-gauge thickness (0.1 mm). The thermocouples installed on the periphery of the test section were calibrated to within ±0.1 °C accuracy using an in-situ calibration method described in Appendix A. All other

thermocouples were calibrated by placing them in a temperature-controlled thermal bath along with a PT-100 resistance temperature detector (RTD) with an accuracy of ±0.1 °C and logging the measurements. The measurements were taken for temperatures ranging from 20 °C to 59 °C in increments of 3 °C. The thermocouple measurements were linearly curve-fitted to those of the PT-100 RTD to improve the measurement accuracy.

3.4.2 Void fraction sensors

Preliminary work with the capacitive void fraction sensors revealed unexpected discrepancies when compared with past results ((De Kerpel *et al*., 2013, 2014). The main challenge was that the inlet and outlet void fraction sensors did not produce the same void fraction results at adiabatic flow conditions. The void fractions should remain fairly constant between the inlet and outlet of the test section for adiabatic conditions. Furthermore, the results obtained by De Kerpel *et al*. (2013, 2014) correlated well with the predictions of the Rouhani and Axelsson (1970) void fraction correlation. The fact that neither of the sensors' adiabatic results correlated well with the predictions of the Rouhani and Axelsson (1970) correlation indicated a problem with the performance of the void fraction sensors. The aforementioned discrepancies are presented in Figure 3.2 for each respective mass flux.

Possible causes for the discrepancies were investigated, including the following:

- checking individual transducer performance with test capacitors;
- checking individual void fraction sensor performance with representative fluids;
- checking the electrical grounding of the test set-up;
- testing alternate void fraction sensor/transducer permutations;
- checking the void fraction sensor electrode alignment.

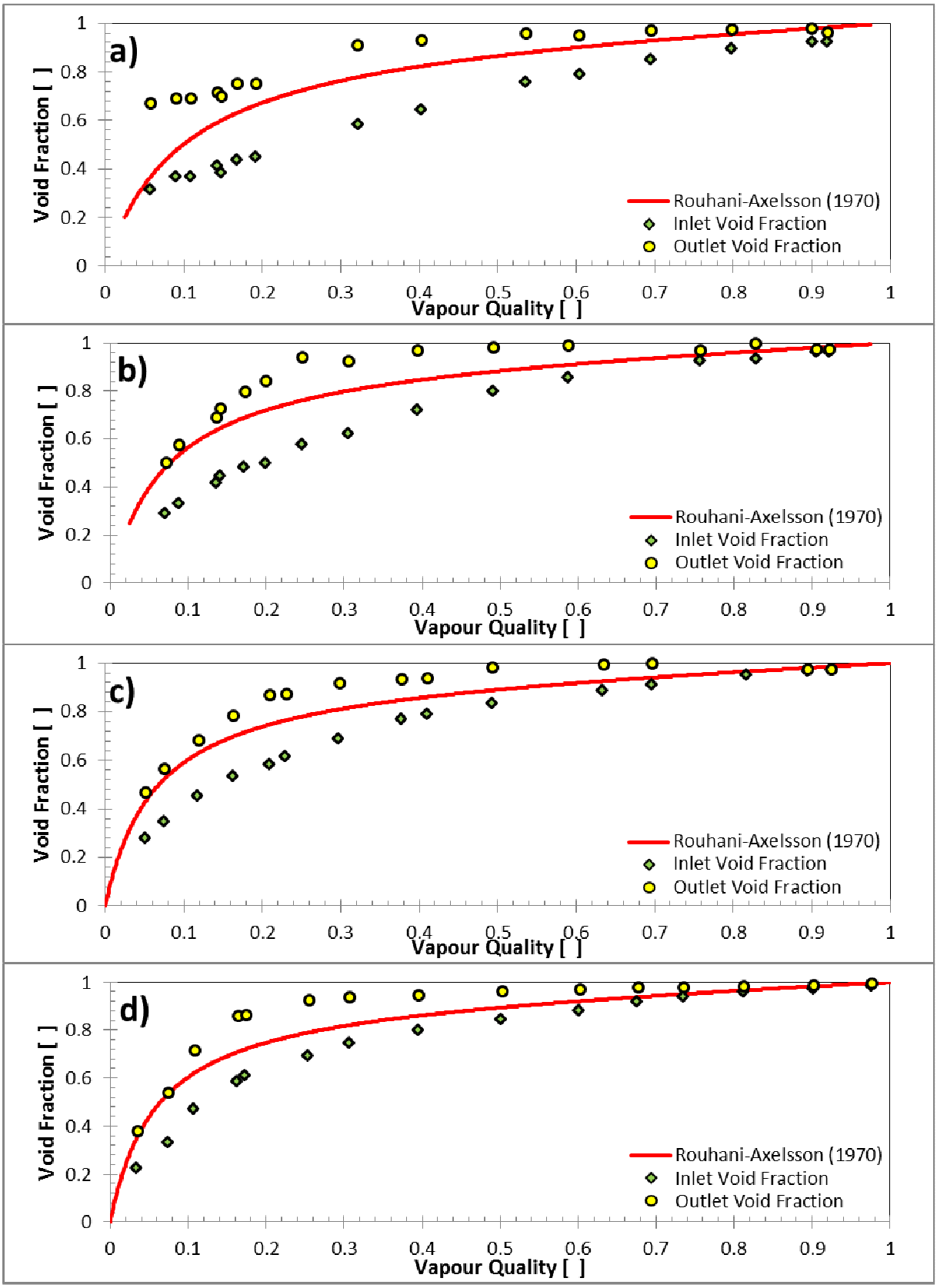

Figure 3.2: Uncalibrated void fraction results for adiabatic horizontal flow: a) G = 100 kg/m^2.s; b) G = 200 kg/m^2.s; c) G = 300 kg/m^2.s; d) G = 400 kg/m^2.s

None of the aforementioned made a significant difference to the results and the discrepancies could be isolated to the void fraction sensors themselves. The void fraction sensors were therefore re-calibrated to the predictions of the Rouhani and Axelsson (1970) correlation for the case of horizontal adiabatic flow because De Kerpel *et al*. (2013, 2014) observed good correlation for the aforementioned conditions. The calibration procedure for the void fraction sensors will now be discussed in more detail.

Let $y_{x_i}^{observed}$ be the originally measured void fraction at a vapour quality of x_i. The distance between the observed and predicted void fractions is given by the following expression:

$$D(x_i) = y_{x_i}^{observed} - \varepsilon_{Rouhani-Axelsson}(x_i) \tag{3.1}$$

A sixth order polynomial model was then fitted to the observed differences $D(x_i)$ with the following form:

$$f(x, \varphi) = \sum_{j=1}^{5} \varphi_j x_i^{j-1} \tag{3.2}$$

A sixth order polynomial was chosen since the original calibration of the void fraction sensors also used a sixth order polynomial (De Kerpel *et al*., 2013). Using a least squares optimisation[1] package, the values $\varphi = \{\varphi_1, \varphi_2, \dots, \varphi_5\}$ which minimised the error with which the fitted polynomial $f(x, \varphi)$ approximated the observed differences $D(x_i)$ were found as follows:

$$Polynomial = \sum_{i=1}^{N} \{f(x_i, \varphi) - D(x_i)\}^2 \tag{3.3}$$

The values for which equation (3.3) was minimised ($\hat{\varphi} = \{\varphi_1, \varphi_2, \dots, \varphi_5\}$) were substituted into equation (3.2), which approximated the observed differences between the actual measured void fractions and the values predicted by the Rouhani and Axelsson (1970) correlation. Using the aforementioned formulations, the calibrated void fraction values were determined as follows:

$$y_{x_i}^{corrected} = y_{x_i}^{observed} + f(x_i, \hat{\varphi}) \tag{3.4}$$

The calibration procedure was carried out for the inlet and outlet void fraction sensors separately at each respective mass flux which would be considered during the current study. The parameters

[1] The author is indebted to Etienne Pienaar for his valuable contribution in the least squares optimisation procedure and the explanation thereof.

$\hat{\varphi} = \{\varphi_1, \varphi_2, \dots, \varphi_5\}$, which were determined to minimise the error for $f(x, \varphi)$ in equation (3.2), are provided in Table 3.1 for each mass flux.

Table 3.1: Parameters to minimise error of calibration function

Inlet sensor					
G [kg/m^2.s]	$\boldsymbol{\varphi_1}$	$\boldsymbol{\varphi_2}$	$\boldsymbol{\varphi_3}$	$\boldsymbol{\varphi_4}$	$\boldsymbol{\varphi_5}$
100	0.0037	3.2022	-11.0868	13.5809	-5.7030
200	0.2111	1.1904	-5.7867	7.7186	-3.3388
300	0.1912	0.7804	-4.6077	6.8236	-3.2190
400	0.2062	-0.0401	-1.1872	1.8620	-0.8362
Outlet sensor					
G [kg/m^2.s]	$\boldsymbol{\varphi_1}$	$\boldsymbol{\varphi_2}$	$\boldsymbol{\varphi_3}$	$\boldsymbol{\varphi_4}$	$\boldsymbol{\varphi_5}$
100	-0.3582	3.8126	-13.7818	19.2087	-8.9811
200	0.2061	-2.3206	6.2339	-6.6122	2.5343
300	0.0982	-1.3664	4.2631	-5.5516	2.6433
400	0.1110	-1.9272	6.2724	-7.5804	3.1437

The results of the calibration procedure are presented graphically in Figure 3.3 and Figure 3.4 for the inlet and outlet sensors respectively for mass fluxes of 100, 200, 300 and 400 kg/m^2.s. From the graphs it was evident that the calibration strategy significantly reduced the discrepancy between the measured void fraction results and the Rouhani and Axelsson (1970) predictions.

The greatest deviations between the corrected void fractions and the predictions of the Rouhani and Axelsson (1970) correlation came at low vapour qualities, i.e. less than 10%. For the regions of interest (10 - 90% vapour quality), the predictions correlated with the corrected void fractions within ±20% for all mass fluxes. Again, the greatest deviations were observed at lower vapour qualities as expected; the Rouhani and Axelsson (1970) correlation had a very steep gradient at low vapour qualities making curve-fitting less accurate. From vapour qualities of 50% upwards, the corrected void fractions matched the Rouhani and Axelsson (1970) predictions within ±5%.

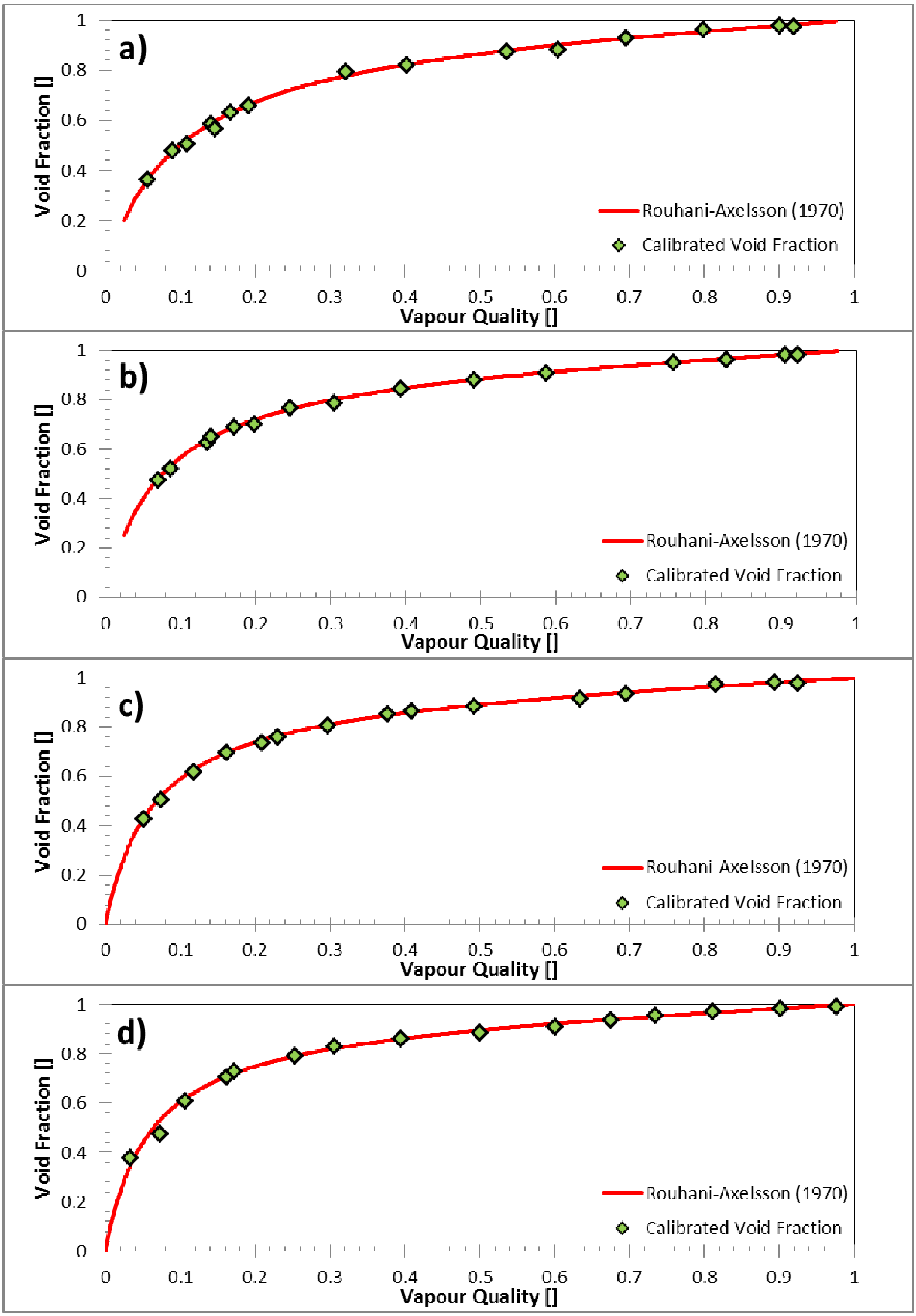

Figure 3.3: Calibration results of inlet void fraction sensor for mass fluxes of a) 100 kg/m^2.s; b) 200 kg/m^2.s; c) 300 kg/m^2.s; d) 400 kg/m^2.s

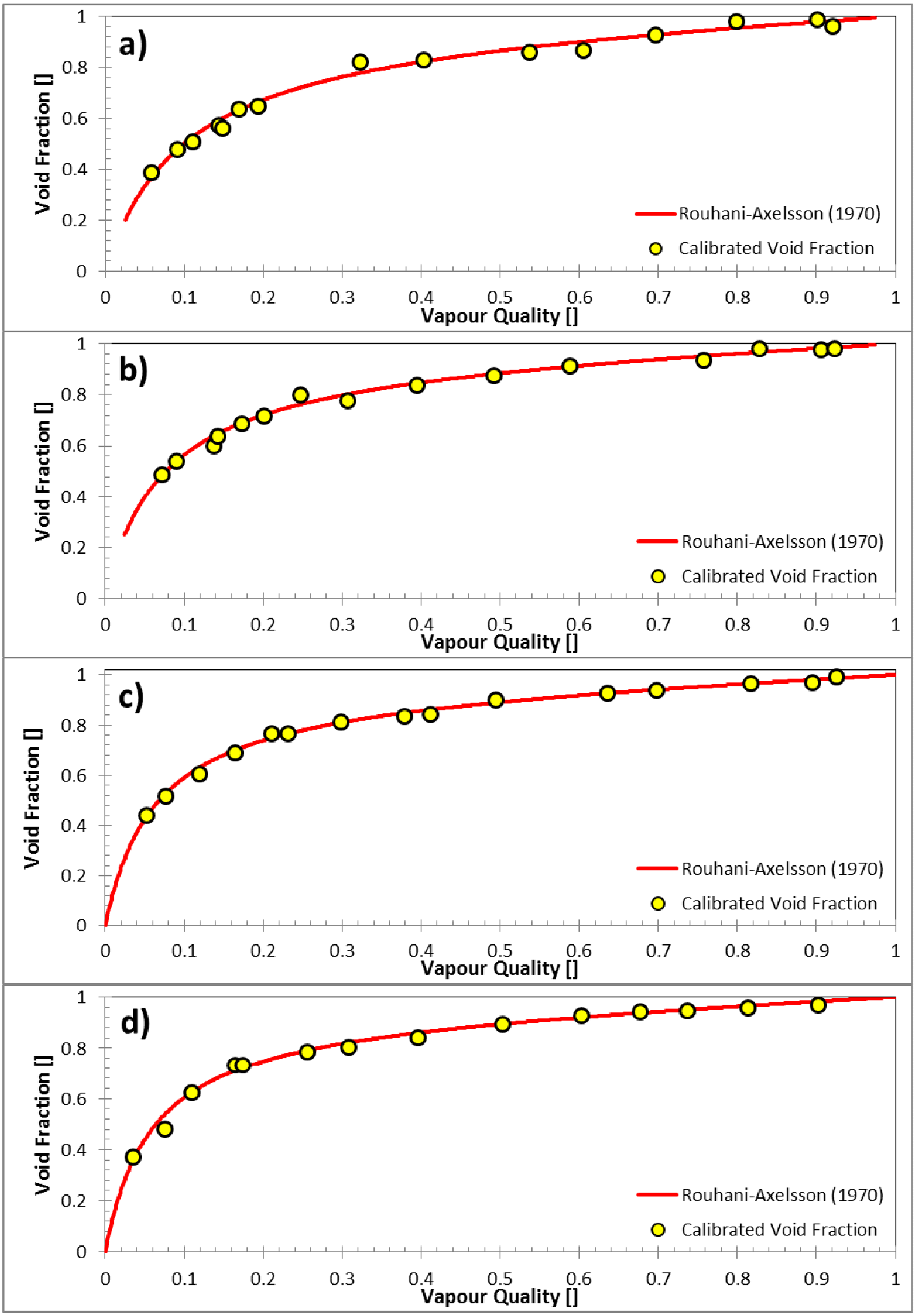

Figure 3.4: Calibration results of outlet void fraction sensor for mass fluxes of a) 100 kg/m^2.s; b) 200 kg/m^2.s; c) 300 kg/m^2.s; d) 400 kg/m^2.s

3.5 Population and sample

The current study is a follow-up to past work carried out by the Thermoflow Research Group of the Department of Mechanical Engineering at the University of Pretoria (Lips and Meyer 2012b; Lips and Meyer 2012c) and part of the data population was therefore similar. An exception to the data set of the previous study was the inclusion of a lower mass flux condition at the expense of a higher mass flux. This was done because the effect of inclination angle on two-phase flow was expected to be more profound at lower mass fluxes than at higher mass fluxes. The current study aimed to focus on the effect of the inclination angle on two-phase flow and the data set was therefore adjusted accordingly.

The experimental data set consisted of 360 data points in total and a summary of the data set is provided in Table 3.2. For the lowest mass flux (100 kg/m^2.s), the average vapour quality cases of 10% and 90% were not considered. They were omitted from the data set because the vapour quality drop across the test section was greater than 10%; thus either the inlet fluid state would be superheated or the outlet fluid state would be sub-cooled to obtain the required average vapour quality of 10%. The current study focused on the saturated state of the refrigerant, which automatically disqualified the aforementioned data points from the data set. The complete data set could be summarised on the Wojtan *et al*. (2005) flow map with the Barbieri *et al*. (2008) intermittent-annular transition line; this is presented in Figure 3.5.

Table 3.2: Experimental criteria

Parameter	Range	Deviations
Saturation temperature	40 °C	± 0.5°C
Mass fluxes	100–400 kg/m^2.s	± 5 kg/m^2.s
Vapour qualities	10–90%	± 1%
Heat flux	200 W	± 5 W

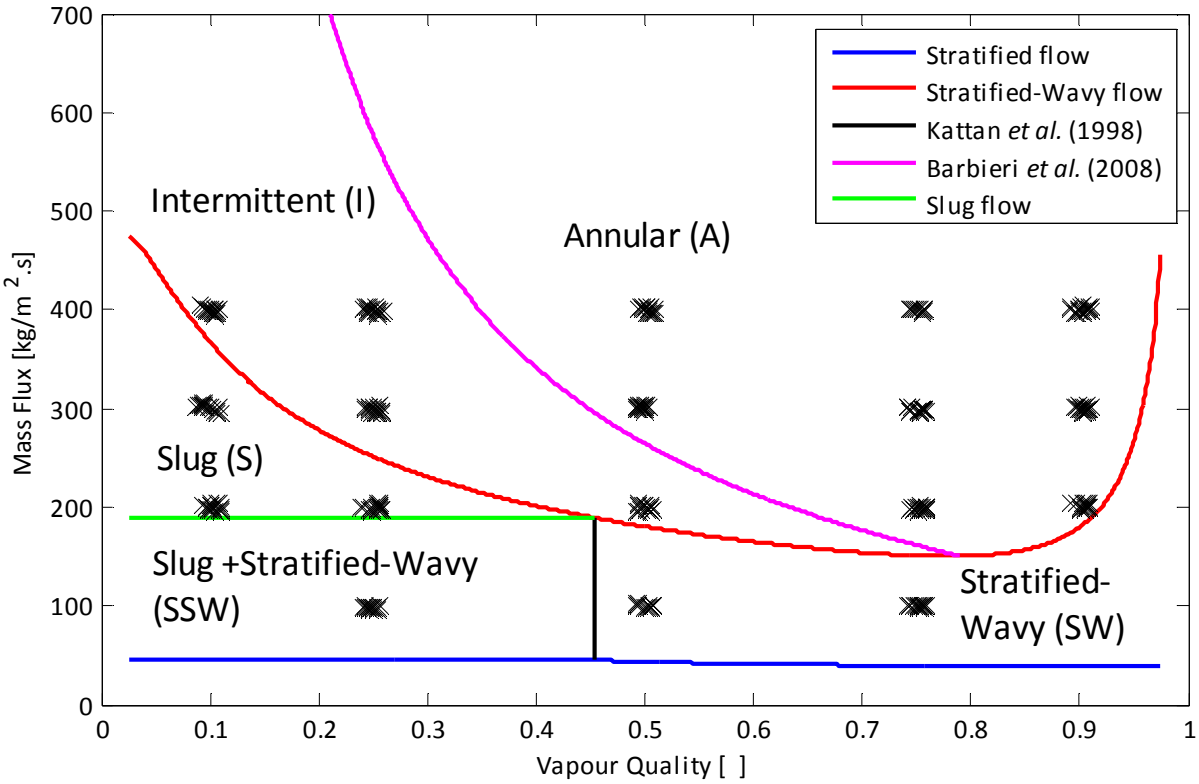

Figure 3.5: Summary of experimental data set for current study plotted on modified Wojtan *et al.* (2005) flow pattern map

The flow patterns were given abbreviations to simplify the presentation of the results which are listed in Table 3.3. The churn semi-annular flow pattern was included in the study after consulting the video gallery on the École Polytechnique Fédérale De Lausanne Heat and Mass Transfer Laboratory website[2]. This flow pattern best described some of the upward inclined flow patterns encountered.

Table 3.3: Abbreviations used for flow pattern classification purposes

Abbreviation	Flow pattern
A	Annular
I	Intermittent
SL	Slug
C	Churn
C/SA	Churn Semi-Annular
SW	Stratified Wavy

[2] www.ltcm.epfl.ch/cms/lang/en/pid/71947

Observations of the flow patterns were made using high-speed video footage. When the observed flow patterns were adjudged to be a combination of two distinct flow types, a system of naming the flow pattern using a backstroke and the abbreviations mentioned in Table 3.3 was adopted. The first abbreviation (before the backstroke) was considered the dominant flow pattern with the second abbreviation a significantly contributing secondary flow pattern.

Challenges were encountered with the heat transfer coefficients of the 90% vapour quality case for mass fluxes of 300 kg/m^2.s and 400 kg/m^2.s. The measured heat transfer coefficients were too high and were therefore eliminated from the heat transfer discussion. The reason for the deviations could be the result of the liquid film thickness becoming critically thin. The thin annular layer could result in the relative effect of systemic errors being amplified as a result of the high heat transfer conditions.

3.6 Summary and conclusions

The refrigerant and water flow loops used to obtain the desired flow conditions were presented and discussed along with the instrumentation used to capture the experimental results. The procedure which was followed to calibrate the various thermocouples was discussed. The calibration of the void fraction sensors was also presented along with a justification for doing the calibration. The data set, as well as the abbreviations used for the various flow patterns in the study, was also presented.

4. Data analysis and validation

4.1 Introduction

This chapter describes the methodology for determining the void fraction, vapour quality, heat transfer coefficient and energy balance used in the current study. The procedure followed to obtain experimental results is also discussed. Finally, the void fraction and heat transfer coefficients for the case of horizontal flow are compared with established correlations. The goal of comparing the results with well-known correlations is to establish whether the results emanating from the experimental set-up could be considered valid.

4.2 Data reduction

4.2.1 Void fraction

The void fraction results were obtained in a similar fashion to that of De Kerpel *et al*. (2013, 2014). The normalised voltage outputs of the capacitive sensors were calculated as follows:

$$V_{Norm} = \frac{V_{Measured} - V_V}{V_L - V_V} \tag{4.1}$$

Before any experiments were conducted, the voltage response of each void fraction sensor at the proposed saturation temperature of 40 °C was measured. This was to account for any potential effect of deviations to the dielectric constants from the conditions under which the sensors were developed, i.e. 15 °C. Liquid refrigerant was made to flow at a temperature of 40 °C through the test section and the voltage response for each void fraction sensor was noted. The dielectric constant of refrigerant vapour was shown to be temperature independent (Dos Reis and Goldstein 2005) and thus the vapour-only response of the sensors was obtained at ambient temperature only. Using the measured responses for the liquid-only and vapour-only cases, the denominator in equation (4.1) for the entire data set was determined. This value was assumed to remain constant for the duration of the current study since it was not practical to repeat the liquid-only measurements for each day of data capturing.

The numerator in equation (4.1) was determined using the raw sensor voltage outputs as well as an ambient vapour-only measurement, which was taken daily during the data capturing process before any measurements were taken. This would account for any drift in the void fraction sensors.

For each respective mass flux, vapour quality and inclination angle condition, the average void fraction over the sampling time was desired. To obtain the average void fraction, each normalised voltage data point was first converted to a void fraction value using the calibration equation developed in Chapter 3. An average void fraction for each sensor was calculated using a trapezoidal integration routine on the void fraction results for each data point. The average void fraction results were taken as the arithmetic mean between the trapezoidal integrated inlet and outlet void fraction values.

4.2.2 Vapour quality

To determine the vapour quality of the fluid at the inlet to the test section, the specific enthalpy at the outlet of the pre-condenser was calculated from the measured heat transfer rate and refrigerant mass flow rates:

$$h_{R,PreCond,o} = h_{R,Test,i} = h_{R,PreCond,i} - \left| \frac{\dot{Q}_{H_2O,PreCond}}{\dot{m}_R} \right| \tag{4.2}$$

The parameter $h_{R,PreCond}$ was the specific enthalpy of the refrigerant at the inlet and outlet of the pre-condenser (subscripts denote inlet or outlet position). Heat losses between the pre-condenser and test section were neglected; thus the specific enthalpy was assumed to stay constant from the pre-condenser outlet to the test section inlet. The heat transfer through the pre-condenser used in equation (4.2) was calculated using the measured water mass flow rate, specific heat capacity, and measured water inlet- and outlet temperatures:

$$\dot{Q}_{H_2O,PreCond} = \dot{m}_{H_2O,PreCond} c_p \left(T_{PreCond,i} - T_{PreCond,o} \right) \tag{4.3}$$

The temperature and pressure measurements at the inlet to the test section were used along with a refrigerant property database (REFPROP, 2005) to determine the saturated liquid and vapour specific enthalpies. The inlet vapour quality was determined as follows:

$$x_{Test,i} = \frac{h_{R,Test,i}}{h_{R,g} - h_{R,f}} \tag{4.4}$$

The specific enthalpy at the outlet of the test section was calculated using the inlet specific enthalpy and the heat transfer from the test section as follows:

$$h_{R,Test,o} = h_{R,Test,i} - \left|\frac{\dot{Q}_{H_2O,Test}}{\dot{m}_R}\right| \tag{4.5}$$

The heat transfer rate through the test condenser was obtained by substituting the parameters in equation (4.3) for those of the test condenser. The outlet vapour quality was then calculated in a similar fashion to equation (4.4) by substituting the outlet specific enthalpy calculated from equation (4.5). The average vapour quality was taken as the arithmetic mean between the calculated inlet and outlet values.

4.2.3 Heat transfer coefficient

The average heat transfer coefficient in the test section was determined from the tube wall, water and saturation temperature measurements. The water heat transfer rate $\left(\dot{Q}_{H_2O,Test}\right)$ was used and not the refrigerant heat transfer rate as the water side was considered to be the more accurate of the two flows to measure.

Assuming a constant heat transfer coefficient across the length of the test section, the average heat transfer of the test section was determined as follows:

$$\alpha_{Test} = \left|\frac{\dot{Q}_{H_2O,Test}}{A\left(\overline{T_{w,i}} - T_{sat}\right)}\right| \tag{4.6}$$

In equation (4.6) A is the inner surface area of the test section for the heat transfer length and T_{sat} is the saturation temperature calculated as the arithmetic mean between the thermocouple measurements at the inlet and outlet of the test section (it was also checked against the saturation pressure measurements). $\overline{T_{w,i}}$ is the mean inner-wall temperature of the test section and is related to the mean outer-wall temperature $\overline{T_{w,o}}$ by the thermal resistance of the tube wall R_w as presented in the following equation:

$$\overline{T_{w,i}} = \overline{T_{w,o}} + \left|\dot{Q}_{H_2O,Test} R_w\right| \tag{4.7}$$

The thermal resistance of the tube wall was calculated as follows:

$$R_w = \frac{\ln\left(\frac{d_o}{d_i}\right)}{2\pi k_{Cu} L} \tag{4.8}$$

The thermal resistance of the tube wall was found to be negligible and therefore it was assumed that the average wall temperature on the outside of the test section was equal to the average wall

temperature on the inside of the test section. The mean outer-wall temperature $\left(\overline{T_{w,o}}\right)$ was calculated by averaging the measurements from each of the seven measurement stations along the test section using a trapezoidal integration routine as follows:

$$\overline{T_{w,o}} = \frac{1}{L}\sum_{j=1}^{6}\left[\left(\frac{T_{w,o}^{j} + T_{w,o}^{j+1}}{2}\right)\left(z_{j+1} - z_{j}\right)\right] \tag{4.9}$$

In equation (4.9) z_j is the jth temperature measurement station on the test section.

4.2.4 Energy balance

The energy balance was determined by comparing the heat transferred to the water cycle of the experimental set-up with the heat transferred from the refrigerant cycle. The latent heat of condensation flow meant that the refrigerant heat transfer needed to be considered from the inlet of the pre-condenser (superheated state) to the outlet of the post-condenser (sub-cooled state). This heat transfer was compared with the total heat transfer across the pre-condenser, test-condenser and post-condenser. The energy balance formula was used as follows:

$$EB_{System} = \left|\frac{\dot{Q}_R - \dot{Q}_{H_2O}}{\left(\dot{Q}_R + \dot{Q}_{H_2O}\right)/2}\right| \times 100 \tag{4.10}$$

4.3 Uncertainty summary

This section serves as a brief summary of the accuracy of the experimental measurements and proves the quality of the data obtained during the current study. Table 4.1 presents the average, maximum, minimum and standard deviations of the measured experimental parameters at all flow conditions considered during the study. From the table, the saturation conditions were well controlled with standard deviations of 0.31 °C and 9.67 kPa for saturation temperature and saturation pressure respectively. The average measured values (39.70 °C and 1 044.36 kPa) also correlated well with the desired values (40 °C and 1 017 kPa). The energy balance was controlled within a 1% standard deviation with an average value of -2.65% for all experimental conditions; the negative sign was expected since it denoted heat loss to the atmosphere. The largest deviation (6% heat loss to ambient atmosphere) was observed at the lowest mass flux and vapour quality combinations.

Table 4.1: Summary of statistics for experimental parameters at all flow conditions

Parameter	Average	Minimum	Maximum	Standard deviation
Saturation temperature	39.70 °C	39.00 °C	40.41 °C	0.31 °C
Saturation pressure	1044.36 kPa	1029.12 kPa	1073.32 kPa	9.67 kPa
Energy balance	-2.65%	-6.08%	0.46%	1.07%

The agreement between the desired and experimentally obtained mass fluxes is summarised in Table 4.2. From the table, it is evident that all the experimentally measured mass fluxes were well controlled since the averages for each respective mass flux differed with less than 1 kg/m^2.s from the desired value. This corresponds to a maximum absolute deviation of about 1% for the 100 kg/m^2.s mass flux case. The standard deviations calculated from the measurements for all data points at each respective mass flux were also observed to be 1% or less of desired value.

Table 4.2: Comparison between measured mass fluxes and desired mass fluxes

Desired mass flux	Mean measured mass flux	Standard deviation
100 kg/m^2.s	99.38 kg/m^2.s	1.38 kg/m^2.s
200 kg/m^2.s	199.73 kg/m^2.s	2.20 kg/m^2.s
300 kg/m^2.s	299.84 kg/m^2.s	2.60 kg/m^2.s
400 kg/m^2.s	399.78 kg/m^2.s	2.21 kg/m^2.s

As a final note, it is mentioned that the Coriolis mass flow meters used in the experimental measurements had an uncertainty of 0.1% of the nominal reading and the pressure sensors used to measure the saturation pressure had an uncertainty of 0.1% relative to its full scale of 3447 kPa, i.e. they were accurate to within 3.45 kPa. The thermocouples were calibrated to within 0.1 °C; the procedure used to do the calibration is discussed in Appendix A. No conclusions could be made regarding the uncertainties of the void fraction sensors as they were the product of past research by another institution in which no attempt was made to quantify the accuracy of the measurements.

4.4 Experimental procedure

After start-up, the experimental set-up was adjusted until the mass flux, vapour quality, test section heat transfer rate and saturation temperature of the test section were in the vicinity of the desired values. Thereafter, the system was adjusted incrementally depending on the parameters that needed to change. Once the desired flow conditions were obtained, the system was allowed to

stabilise until all measurements were visually observed to remain constant and the energy balance across the test section was less than 5%. Steady-state conditions were then assumed. At the lowest mass flux (100 kg/m^2.s), the energy balances could not always be maintained below 5% and values of up to 6% were reached. The average energy balance of all the other measurements (mass fluxes greater than 100 kg/m^2.s) was 2.6%. The amount of time required for steady-state operation depended on the prevailing mass flux conditions but varied between 10 and 30 minutes. As expected, higher mass flux conditions led to quicker steady-state conditions than lower mass flux conditions.

Data capturing of the heat transfer coefficients and the void fraction results was done individually and, in turn, with the capturing of the heat transfer coefficients preceding the capturing of the void fraction results for each data point. The heat transfer coefficients were captured at a frequency of 1 Hz over a 120-second time span for each data point, after which the void fraction results were immediately acquired at a frequency of 1 000 Hz for a time span of 120 seconds. Therefore, each void fraction data point was determined from a data set containing 120 000 data points. The sampling frequency was sufficient as most two-phase flow phenomena occur at a frequency of 100 Hz (Canière *et al*., 2007). The Nyquist criterion for sampling was thus satisfied and aliasing of the observed void fraction signals was therefore not an issue.

4.5 Validation of experimental set-up

The void fraction and heat transfer coefficients were validated by taking measurements for the case of horizontal flow with 200 W of condensation heat transfer and comparing the results with literature.

4.5.1 Void fraction

Figure 4.1 presents the measured void fractions for horizontal flow plotted against vapour quality at mass fluxes of 100, 200, 300 and 400 kg/m^2.s. Additionally, the predictions of the Rouhani and Axelsson (1970) correlation as well as the prevailing observed flow patterns are also presented. The flow patterns are compared with the flow pattern map of Figure 3.5.

For mass fluxes of 100 kg/m^2.s and 200 kg/m^2.s, only slug flows were observed. At the lowest vapour quality conditions for the aforementioned mass fluxes, as well as the 300 kg/m^2.s case, the two data points taken for the same vapour quality conditions were observed to deviate from each other to a small degree. This may be due to the physical nature of slug flow; the instantaneous liquid-vapour distribution changed chaotically, which made deviations in the results more likely. For the case of

300 kg/m^2.s mass flux, annular flow was observed at the 75% and 90% vapour quality conditions; at the other vapour quality conditions (10%, 25% and 50%), slug flow was observed. As with the aforementioned case, the 400 kg/m^2.s mass flux produced annular flow at the higher vapour quality conditions, specifically at 50%, 75% and 90%. However, at the lower vapour qualities (10% and 25%) the flow pattern was observed to exhibit intermittent characteristics, i.e. flashing between annular- and slug-type flows. Five observed data points out of a total of 18 data points did not match the predictions of the Wojtan *et al*. (2005) flow pattern map, which was modified with the Barbieri *et al*. (2008) intermittent-annular transition line; thus 72% of the horizontal flow regimes were correctly predicted by the modified Wojtan *et al*. (2005) flow map. The aforementioned exceptions could be isolated to the predictions of intermittent flow, which were difficult to classify using subjective visual means.

It can, therefore, be concluded that the predictions of the Rouhani and Axelsson (1970) correlation tracked the void fraction results quite well, especially at higher vapour quality conditions. Excluding the 100 kg/m^2.s mass flux case, the degree of correlation between void fraction predictions and measurements declined with a decrease in vapour quality; the degree of correlation is presented in Figure 4.2. The Rouhani and Axelsson (1970) void fraction correlation as a function of vapour quality predicted all flow conditions within a ±5% error band.

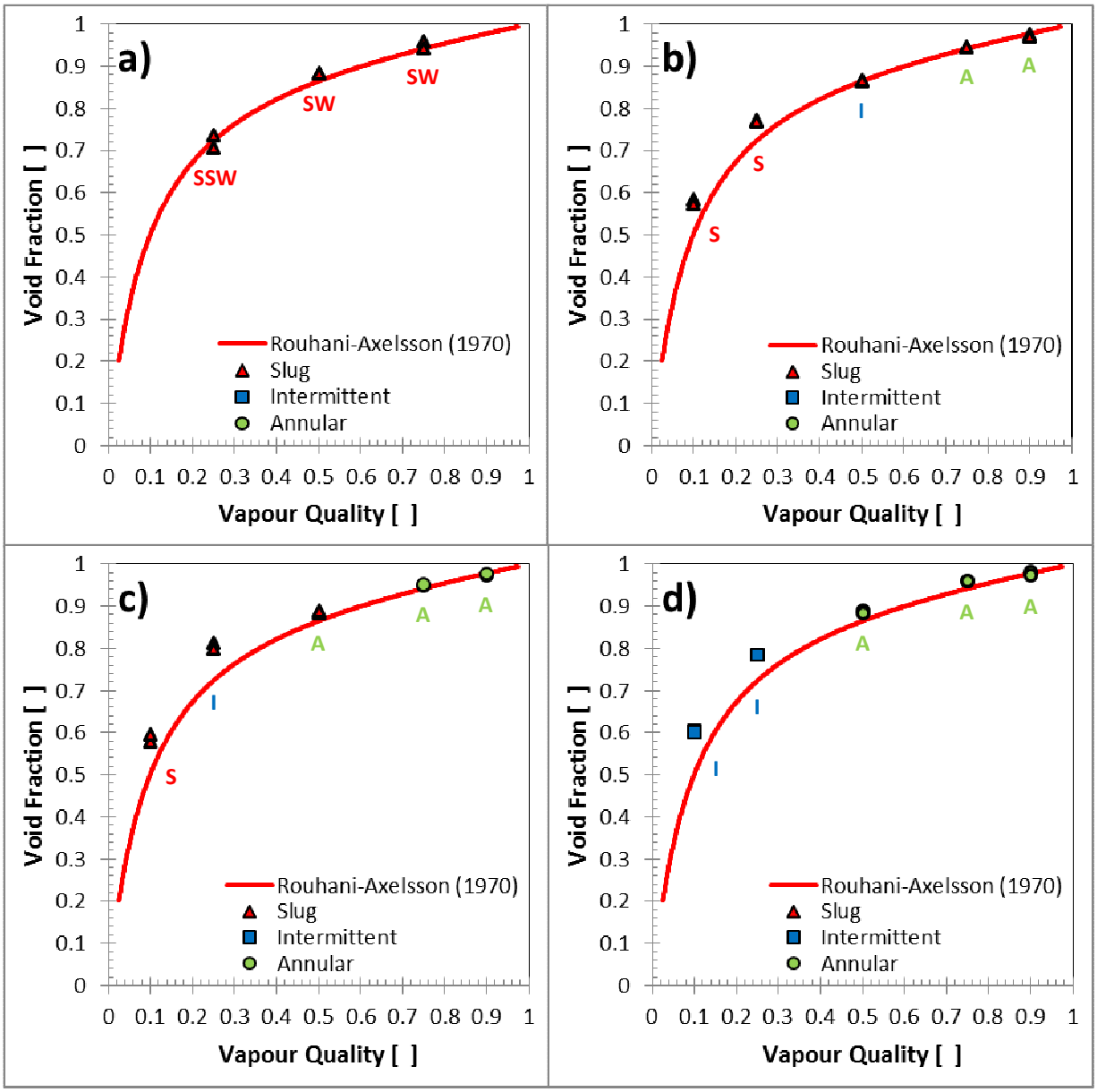

Figure 4.1: Experimental void fraction measurements as a function of average vapour quality compared with the predictions of the Rouhani and Axelsson (1970) void fraction correlation for the case of a horizontal tube for mass fluxes of a) 100 kg/m^2.s, b) 200 kg/m^2.s, c) 300 kg/m^2.s and d) 400 kg/m^2.s. The prevailing flow pattern as observed is indicated by the symbols in the legend. At each data point, the flow pattern predicted by the modified Wojtan *et al.* (2005) flow pattern map is indicated using the following abbreviations: Slug (S), stratified-wavy (SW), slug and stratified-Wavy (SSW), intermittent (I) and annular (A). The colour-coding of the abbreviations also correlates with the flow classification of De Kerpel *et al.* (2013) in the legend.

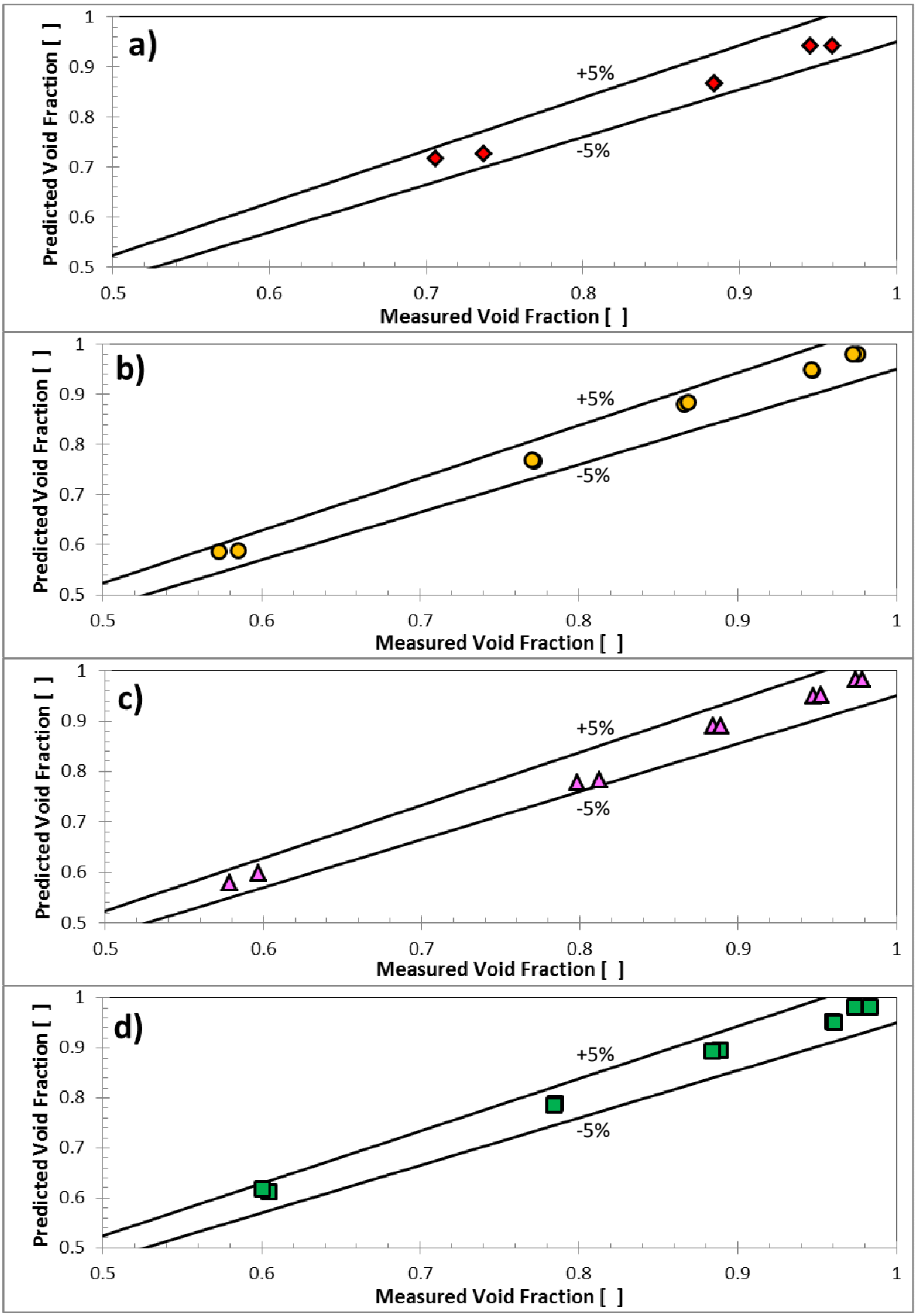

Figure 4.2: Comparison between predictions of the Rouhani and Axelsson (1970) correlation and measured void fraction results for horizontal flow at a) G = 100 kg/m^2.s; b) G = 200 kg/m^2.s; c) G = 300 kg/m^2.s; d) 400 kg/m^2.s

4.5.2 Heat transfer coefficient

In Figure 4.3, the measured heat transfer coefficients are compared with predictions. The comparisons were made using the Thome *et al*. (2003) heat transfer correlation using their prescribed logarithmic mean void fraction model as well as the experimentally measured void fractions of this study. Comparisons were also made with the Thome *et al*. (2003) correlation making use of the Woldesemayat and Ghajar (2007) void fraction predictions and the Cavallini *et al*. (2006) heat transfer correlation.

For horizontal flows, 67% of the heat transfer coefficients were predicted within a ±10% error by the Thome *et al*. (2003) correlation. At low-heat transfer conditions, i.e. low mass flux and vapour quality, the Thome *et al*. (2003) correlation over-predicted the experimental results by about 20–30%. The heat transfer predictions exhibited scatter; this could be the result of the Thome *et al*. (2003) correlation's dependence on the void fraction, which varied with the flow configuration.

The substitution of the void fraction parameter with the experimental void fractions deteriorated the prediction accuracy of the Thome *et al*. (2003) correlation. The general trend was that the data points were under-predicted using this method; a number of data points were under-predicted by more than 20%. A similar trend was observed when the void fraction parameter was substituted for the predictions of the Woldesemayat and Ghajar (2007) void fraction correlation. Subsequently, this method did not produce acceptable heat transfer predictions as many data points were not predicted within a ±30% error band.

The Cavallini *et al*. (2006) heat transfer correlation correlated the results well with the majority of the data points predicted within a ±10% error. At the higher heat transfer conditions, i.e. higher mass flux and vapour quality, the results were under-predicted, but still fell within a ±20% error band. The heat transfer predictions of the Cavallini *et al*. (2006) correlation did not exhibit as much scatter throughout the data set. This may be a result of the Cavallini *et al*. (2006) correlation's independence of the void fraction.

The measured heat transfer coefficients were also compared with the measured heat transfer coefficients of Lips and Meyer (2012b) who used the same experimental set-up. However, for this study, the test section was modified and a more rigorous in-situ thermocouple calibration was used. It was found that the general behaviour of the heat transfer coefficients with changes in inclination angle was very similar to the observations made in the study of Lips and Meyer (2012b) with minimums and maximums observed at broadly similar inclination angles. However, the absolute values of the heat transfer coefficients for the current study were greater than those found in the

study of Lips and Meyer (2012b). For the reference case of 300 kg/m^2.s mass flux, the measured heat transfer coefficients were an average of 17% greater than those of Lips and Meyer (2012b) with the discrepancies increasing with increased vapour quality (32% maximum deviation observed at 75% vapour quality). Similarly, for the case of varying mass flux (200 kg/m^2.s to 400 kg/m^2.s) at a constant vapour quality of 50%, the measured heat transfer coefficients were an average of 26% greater than those obtained during the study of Lips and Meyer (2012b) with a maximum deviation of 39% observed at 400 kg/m^2.s mass flux. The discrepancies were observed to increase with increasing mass flux. The deviations in heat transfer coefficient relative to those of the Lips and Meyer (2012b) study were relatively constant for each mass flux and vapour quality combination for all inclination angles, which seemed to indicate that the deviations could be purely a result of the more rigorous in-situ thermocouple calibration technique which was employed for the current study. The aforementioned calibration technique is discussed in Appendix A.

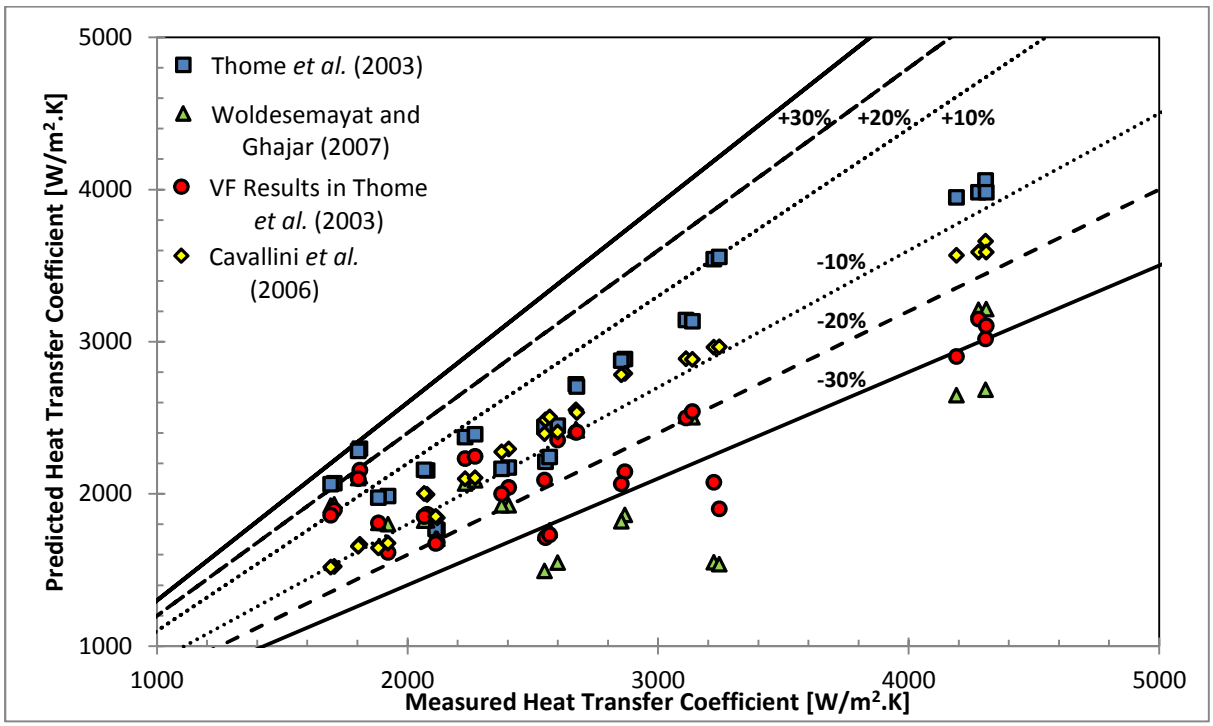

Figure 4.3: Experimental heat transfer coefficients for the case of horizontal flow compared with the correlations of Thome *et al.* (2003) and Cavallini *et al.* (2006). Also included are the comparisons with the Thome *et al.* (2003) heat transfer correlation with the void fraction (VF) model replaced with the correlation of Woldesemayat and Ghajar (2007) and the experimentally measured void fraction results.

It should be noted from Figure 4.3 and the observations made during the study of Lips and Meyer (2012b) that the heat transfer coefficients for horizontal flow of the current study were correlated more closely by the Thome *et al.* (2003) as well as the Cavallini *et al.* (2006) heat transfer

correlations. This may indicate that the in-situ thermocouple calibration technique improved the accuracy of the heat transfer coefficients.

4.6 Summary and conclusions

The measured void fraction results were observed to correlate well with the predictions of literature for all mass fluxes with all horizontal flow cases within ±5%. The calibration procedure described in Chapter 3 was therefore deemed successful. At low vapour qualities, the successive (i.e. identical flow conditions, but different instance) void fraction results deviated to a small degree. This was probably due to the greater degree of fluctuation in liquid-vapour distribution observed for low vapour quality conditions, i.e. slug-type flows.

In general, the observed flow patterns also correlated well with literature. However, the intermittent flow patterns were not predicted accurately during the experiments. It should be taken into account that the subjective nature of the visual observations might lead to discrepancies in identifying the intermittent flow pattern.

The heat transfer coefficients exhibited good correlation with predictions found in literature with the bulk of the results predicted within a ±20% error band. Some over-predictions of heat transfer coefficients were observed at the lower heat transfer conditions (i.e. low vapour quality and mass flux), but the over-predictions were limited within a ±30% error band. Substituting the measured void fractions into the models found in literature did not improve their heat transfer prediction performance.

The heat transfer coefficients were also compared with those of the Lips and Meyer (2012b) study, which used the same experimental set-up to obtain their results. It was found that the behaviour of the heat transfer coefficients with changing inclination angle was very similar. However, the absolute values of the heat transfer coefficients obtained for the current study were greater than those of Lips and Meyer (2012b). The deviations could be put down to the more rigorous in-situ thermocouple calibration procedure used for the current study. The horizontal flow results were correlated more closely by the Thome *et al*. (2003) and Cavallini *et al*. (2006) heat transfer correlations than was the case for the Lips and Meyer (2012b) study, which may indicate an improvement brought about by the in-situ thermocouple calibration technique.

The good correlation of the void fraction and heat transfer coefficients for horizontal flow with established models provided confidence that the experimental set-up could yield agreeable results.

5. Results

5.1 Introduction

This chapter first discusses the void fraction and heat transfer coefficient measurements for condensing vertical upward and downward flow at a saturation temperature of 40 °C. The observations made in terms of the flow patterns are also presented. Secondly, the heat transfer coefficient and void fraction results for the full range of tube inclinations are presented, also with flow pattern observation incorporated into the analysis. High-speed photographic evidence of the prevailing flow patterns for selected flow conditions is also included in the discussion. Finally, a sensitivity analysis is conducted to determine the possible effect of errors in the void fraction measurements on the heat transfer coefficient predictions.

5.2 Vertical flows

5.2.1 Vertical upward flow

Figure 5.1 presents the void fraction results for vertical upward flow compared with the predictions of the Rouhani and Axelsson (1970) correlation. The results are presented in four separate figures for mass fluxes of 100, 200, 300 and 400 kg/m^2.s respectively (Figure 5.1a, Figure 5.1b, Figure 5.1c and Figure 5.1d). The prevailing observed flow patterns are also noted and compared with the predictions of the modified Wojtan *et al*. (2005) flow pattern map as presented in Chapter 3.

For the 100 kg/ m^2.s case, only slug flow was observed during the measurements. The observed flow patterns for the 200 kg/m^2.s and 400 kg/m^2.s mass flux cases were in general very similar. The vapour qualities of 10% and 25% resulted in slug flows while vapour qualities of 50%, 75% and 90% resulted in annular flow at the prevailing mass fluxes. For the case of 300 kg/m^2.s mass flux, slug flow was only observed at the 10% vapour quality condition; for all other considered vapour qualities, the flow was observed to be annular. No intermittent-type flow was observed for vertical upward flow inclinations. At higher vapour qualities, i.e. 50%, 75% and 90%, the observed flow patterns correlated well with the predictions of the modified Wojtan *et al*. (2005) flow pattern map for all mass fluxes barring the 100 kg/m^2.s case where a churn-type flow with liquid recirculation was observed in lieu of the predicted stratified-wavy flow. At lower vapour qualities, i.e. 10% and 25%, the flow patterns did not correlate with the predictions with churn-type flows dominating in lieu of stratified-type flows for all mass fluxes. However, it should be noted that according to the void

fraction calibration scheme of De Kerpel *et al*. (2013, 2014), no distinction is made between stratified-type and churn-type flows; both are considered slug-type flows.

From Figure 5.2, it was evident that all the void fraction measurements for vertical upward flow at the higher vapour quality conditions, i.e. 50%, 75% and 90%, were predicted within a ±5% error band of the Rouhani and Axelsson (1970) predictions. Tilting the tube to the vertically-upward inclination did therefore not affect the void fraction significantly compared with the case of horizontal flow for these flow conditions. At the 25% vapour quality condition for a mass flux of 100 kg/m^2.s, the over-prediction of the Rouhani and Axelsson (1970) fell outside the ±5% error band, but was still within 25%. For the other mass fluxes, the 25% vapour quality void fraction results were under-predicted by the correlation, barring the 100 kg/m^2.s and 300 kg/m^2.s mass flux case, all the 25% vapour quality results for vertical upward flow were still predicted within a ±5% error band. For the 10% vapour quality cases, the Rouhani and Axelsson (1970) correlation tended to over-predict the void fraction results. The predictions were, however, seen to improve with an increase in the mass flux.

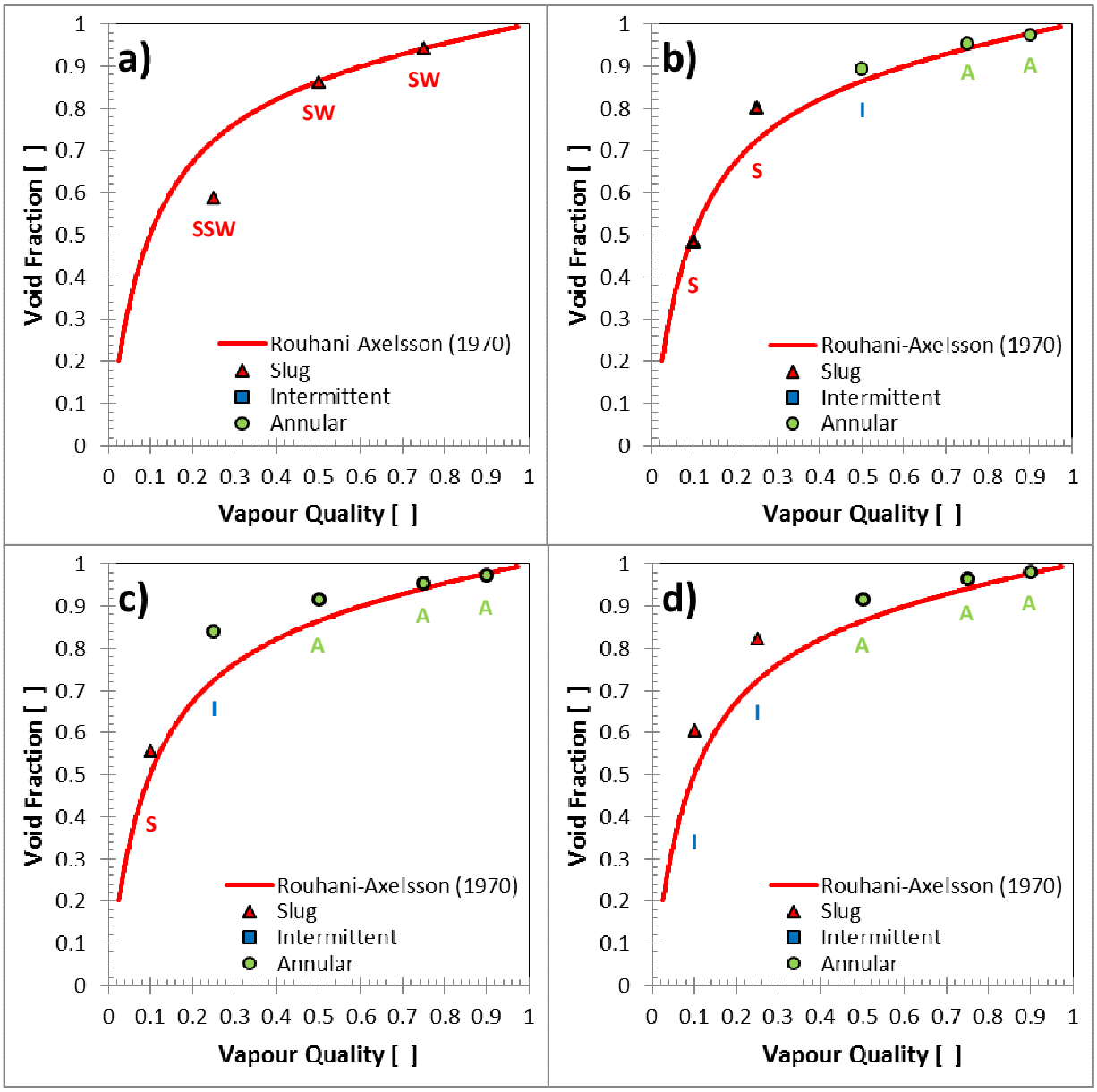

Figure 5.1: Experimental void fraction measurements as a function of average vapour quality compared with the predictions of the Rouhani and Axelsson (1970) void fraction correlation for the case of a vertical upward tube for mass fluxes of a) 100 kg/m^2.s, b) 200 kg/m^2.s, c) 300 kg/m^2.s and d) 400 kg/m^2.s. The prevailing flow pattern as observed is indicated by the symbols in the legend. At each data point, the flow pattern predicted by the modified Wojtan *et al.* (2005) flow pattern map is indicated using the following abbreviations: Slug (S), stratified-wavy (SW), slug and stratified-wavy (SSW), intermittent (I) and annular (A). The colour-coding of the abbreviations also correlates with the flow classification of De Kerpel *et al.* (2013) in the legend.

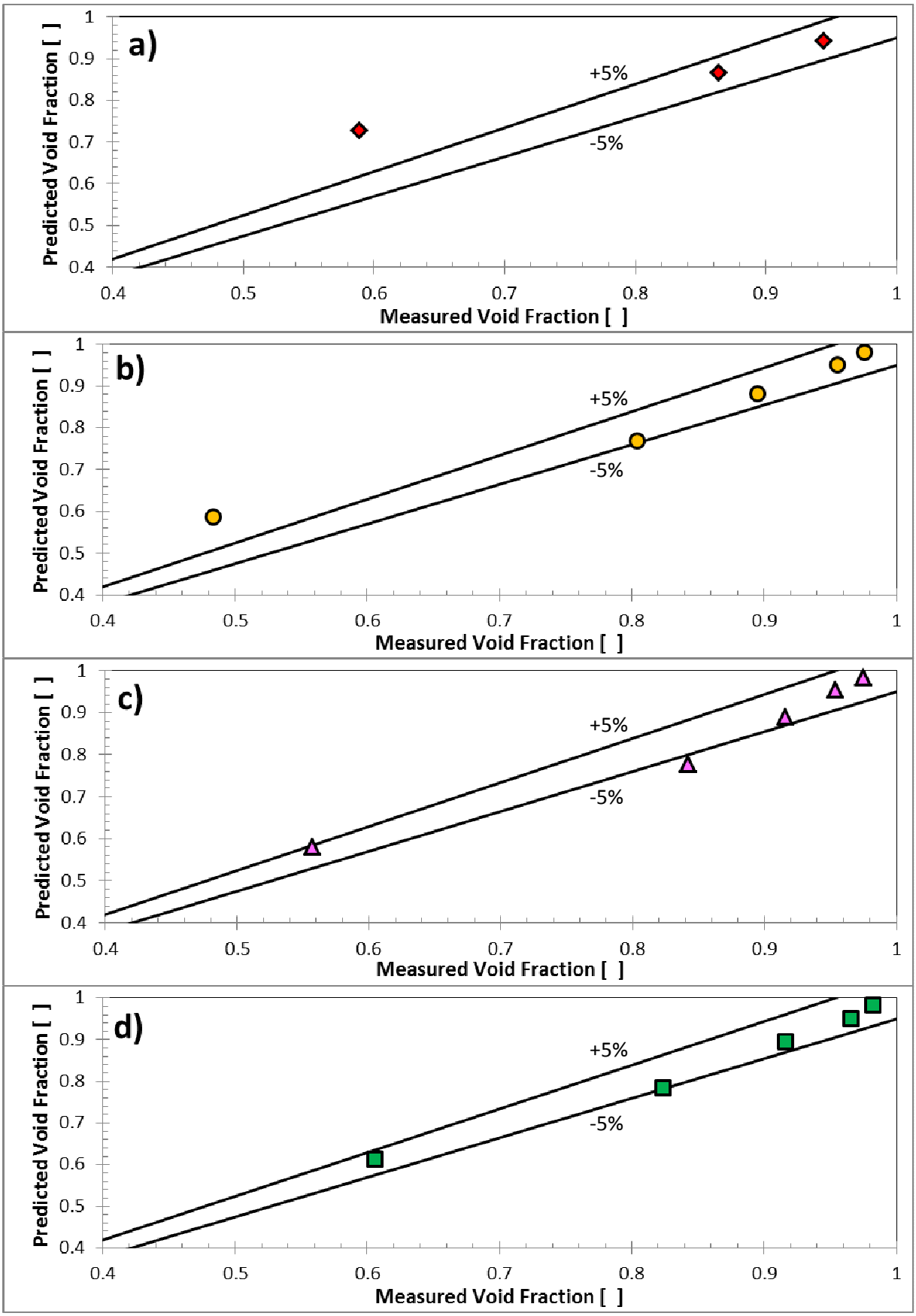

Figure 5.2: Comparison between predictions of the Rouhani and Axelsson (1970) correlation and measured void fraction results for vertical upward flow at a) G = 100 kg/m^2.s; b) G = 200 kg/m^2.s; c) G = 300 kg/m^2.s; d) 400 kg/m^2.s

The Thome *et al*. (2003) heat transfer correlation (Figure 5.3) predicted nearly all results for vertical upward flow within ±30%. Exceptions were observed at low heat transfer coefficient conditions where the results were over-predicted by more than 30%. Many of the data points were predicted within a ±20% error band; the prediction performance did, however, decline compared with the horizontal case. In general, the results at low heat transfer conditions were over-predicted and the results at higher heat transfer conditions were under-predicted by the correlation. A number of the lower heat transfer coefficients were observed to accumulate around the 2 000 $W/m^2.K$ value. The results exhibited a greater degree of scatter than observed for the horizontal flow orientation, which correlated with the more chaotic observed flow patterns.

Substituting the measured void fractions into the Thome *et al*. (2003) heat transfer correlation resulted in similar prediction behaviour than that of the original Thome *et al*. (2003) method. The heat transfer predictions were, however, observed to be consistently below those of the original Thome *et al*. (2003) method. This meant that the heat transfer predictions improved for the lower heat transfer coefficients. At higher heat transfer flow conditions, the predictions were observed to deteriorate when compared with the values predicted by the original Thome *et al*. (2003) method. The void fraction predictions of the Woldesemayat and Ghajar (2007) correlation were also substituted into the Thome *et al*. (2003) heat transfer correlation. These predictions were seen to under-predict most of the measured heat transfer coefficients and fell outside the ±30% prediction error band. The aforementioned predictions were consistently below those when using the measured void fractions in the Thome *et al*. (2003) heat transfer correlation.

The Cavallini *et al*. (2006) correlation again exhibited good prediction accuracy and the bulk of the predictions fell within a ±20% error band. However, at the highest heat transfer flow condition, the heat transfer was under-predicted by more than 30%. The degree of scatter in the Cavallini *et al*. (2006) predictions was also observed to be greater than for the case of horizontal flow.

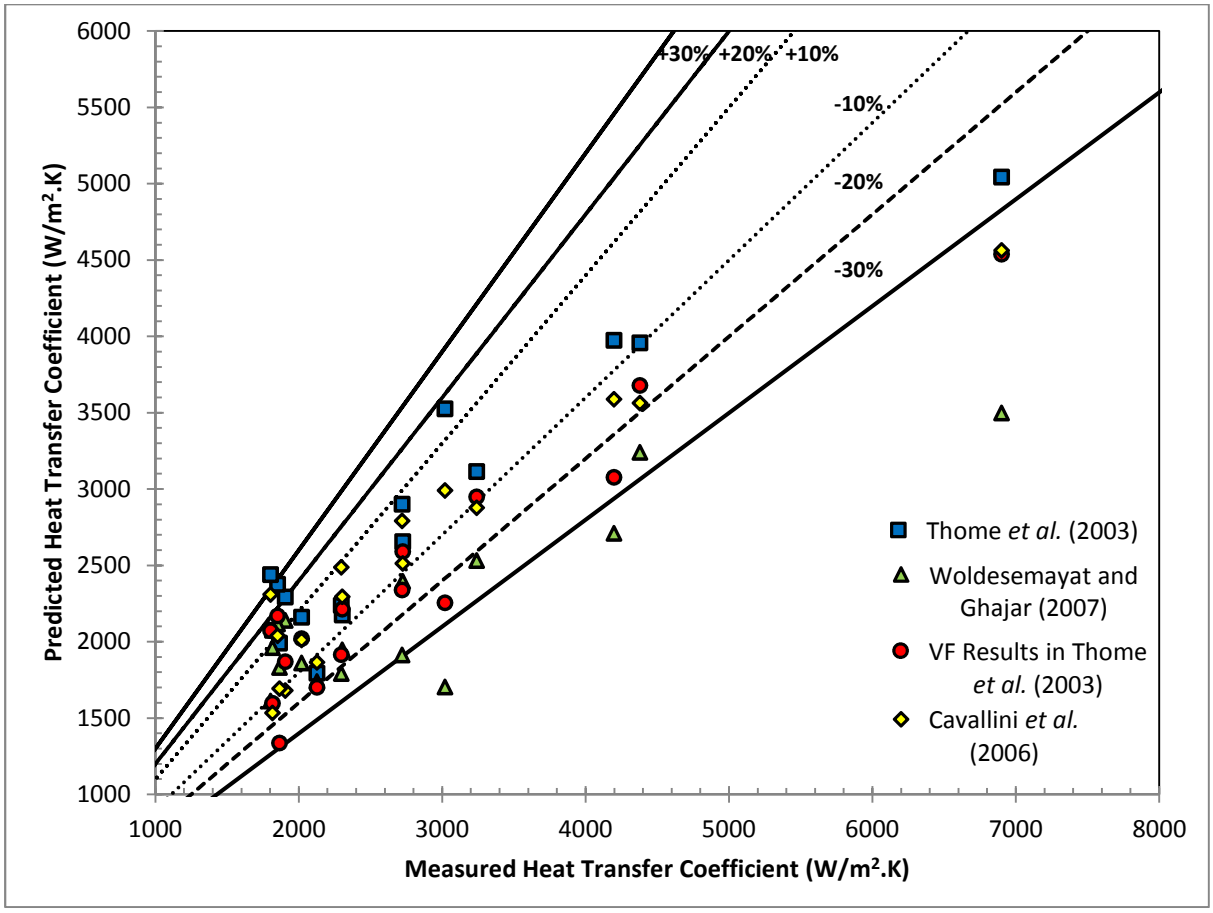

Figure 5.3: Experimental heat transfer coefficients for the case of vertical upward flow compared with the correlations of Thome *et al*. (2003) and Cavallini *et al*. (2006). Also included are the comparisons with the Thome *et al*. (2003) heat transfer correlation with the void fraction (VF) model replaced with the correlation of Woldesemayat and Ghajar (2007) and the experimentally measured void fraction results.

5.2.2 Vertical downward flow

For all mass flux and vapour quality conditions, annular-type flow patterns (Figure 5.4) were observed. This was a marked departure from the observations made for horizontal and vertical upward flows, as well as the predictions of the modified Wojtan *et al*. (2005) flow pattern map. This served as an indication of the significant effect of gravity on the flow. For all mass fluxes, the vapour qualities of 75% and 90% were predicted well by the Rouhani and Axelsson (1970) correlation; from Figure 5.5, the aforementioned predictions were within ±5% for the aforementioned conditions.

With further reductions in the vapour quality conditions, the Rouhani and Axelsson (1970) correlation under-predicted the measured void fraction results; the degree of under-prediction increased with decreasing vapour quality. Therefore, it seemed that the Rouhani and Axelsson (1970) model did not predict the liquid-vapour distribution induced by the tube inclination well. Barring the 100 kg/m^2.s mass flux case, all 50% vapour quality cases were still predicted within

a ±5% error band as evidenced by Figure 5.5. Further reduction of the vapour quality conditions (10% and 25%) resulted in the void fraction predictions falling outside a ±5% error band with the greatest deviation observed for the 200 kg/m^2.s mass flux case where an under-prediction of 29% was observed at 10% vapour quality. The under-prediction behaviour of the Rouhani and Axelsson (1970) correlation was observed to improve with an increased mass flux.

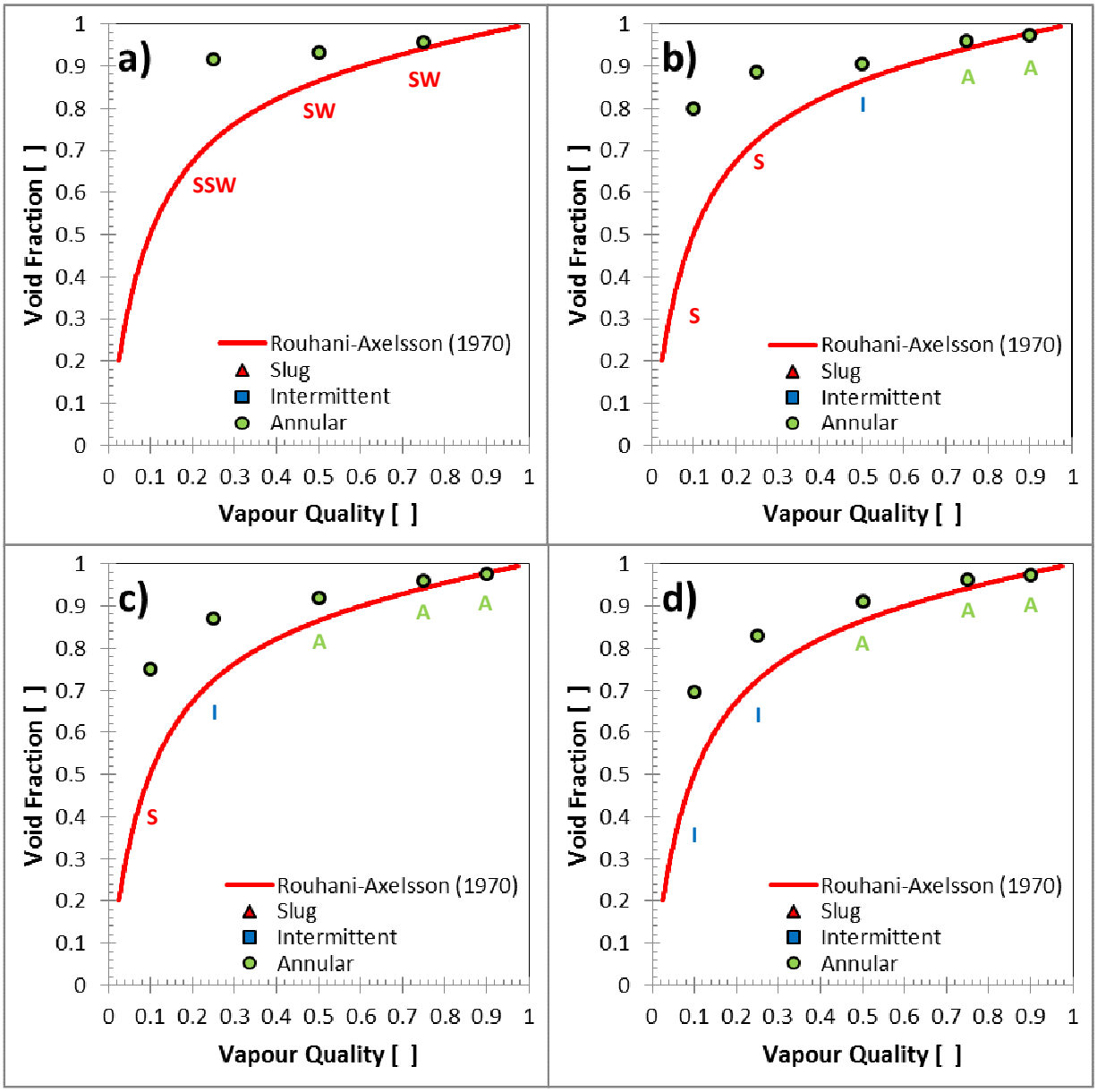

Figure 5.4: Experimental void fraction measurements as a function of average vapour quality compared with the predictions of the Rouhani and Axelsson (1970) void fraction correlation for the case of a vertical downward tube for mass fluxes of a) 100 kg/m^2.s, b) 200 kg/m^2.s, c) 300 kg/m^2.s and d) 400 kg/m^2.s. The prevailing flow pattern as observed is indicated by the symbols in the legend. At each data point, the flow pattern predicted by the modified Wojtan *et al.* (2005) flow pattern map is indicated using the following abbreviations: Slug (S), Stratified-Wavy (SW), Slug and Stratified-Wavy (SSW), Intermittent (I) and Annular (A). The colour-coding of the abbreviations also correlates with the flow classification of De Kerpel *et al.* (2013) in the legend.

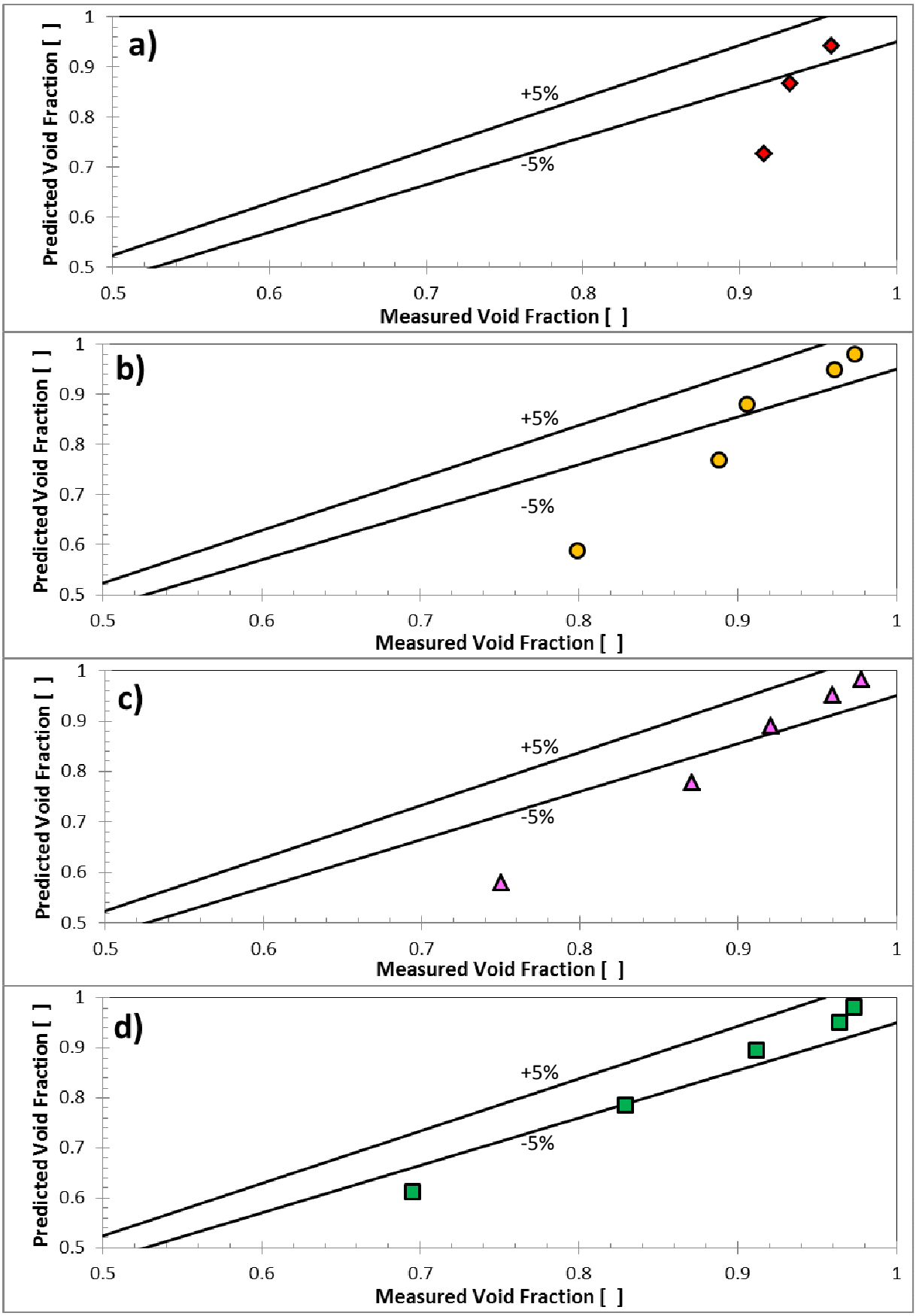

Figure 5.5: Comparison between predictions of the Rouhani and Axelsson (1970) correlation and measured void fraction results for vertical downward flow at a) G = 100 kg/m^2.s; b) G = 200 kg/m^2.s; c) G = 300 kg/m^2.s; d) 400 kg/m^2.s

The results presented in Figure 5.6 reveal the effect of vertical downward inclination on the heat transfer coefficients of the flow. The Thome *et al*. (2003) heat transfer correlation tended to over-predict the lower heat transfer coefficients; some of the predictions fell outside a ±30% error band. A number of Thome *et al*. (2003) heat transfer predictions were still within a ±20% error band. The highest measured heat transfer coefficient for vertical downward flow (6993 $W/m^2.s$ at 300 $kg/m^2.s$ and 90% vapour quality) was under-predicted by the Thome *et al*. (2003) correlation by 29%.

Substituting the measured void fractions for vertical downward flow did not improve the prediction ability of the Thome *et al*. (2003) heat transfer correlation; a number of the lower heat transfer coefficients were over-predicted by more than 30%. The higher heat transfer coefficients were predicted with better accuracy, but no improvement on the original Thome *et al*. (2003) correlation was observed. The heat transfer predictions with the Woldesemayat and Ghajar (2007) void fraction correlation tracked those of the original Thome *et al*. (2003) predictions quite closely at low heat transfer conditions. Similar to the case of using the measured void fractions, no improvement was observed when using the Woldesemayat and Ghajar (2007) void fraction predictions in the Thome *et al*. (2003) heat transfer correlation.

The predictions of the Cavallini *et al*. (2006) heat transfer correlation exhibited markedly more scatter at low heat transfer conditions than for the horizontal flow case. Even so, a number of the results were predicted within ±30% accuracy. The prediction of the highest vertical downward heat transfer data point was nearly identical to the Thome *et al*. (2003) value using the measured void fraction. In general, the prediction performance of the Cavallini *et al*. (2006) heat transfer correlation was comparable with that of the Thome *et al*. (2003) correlation.

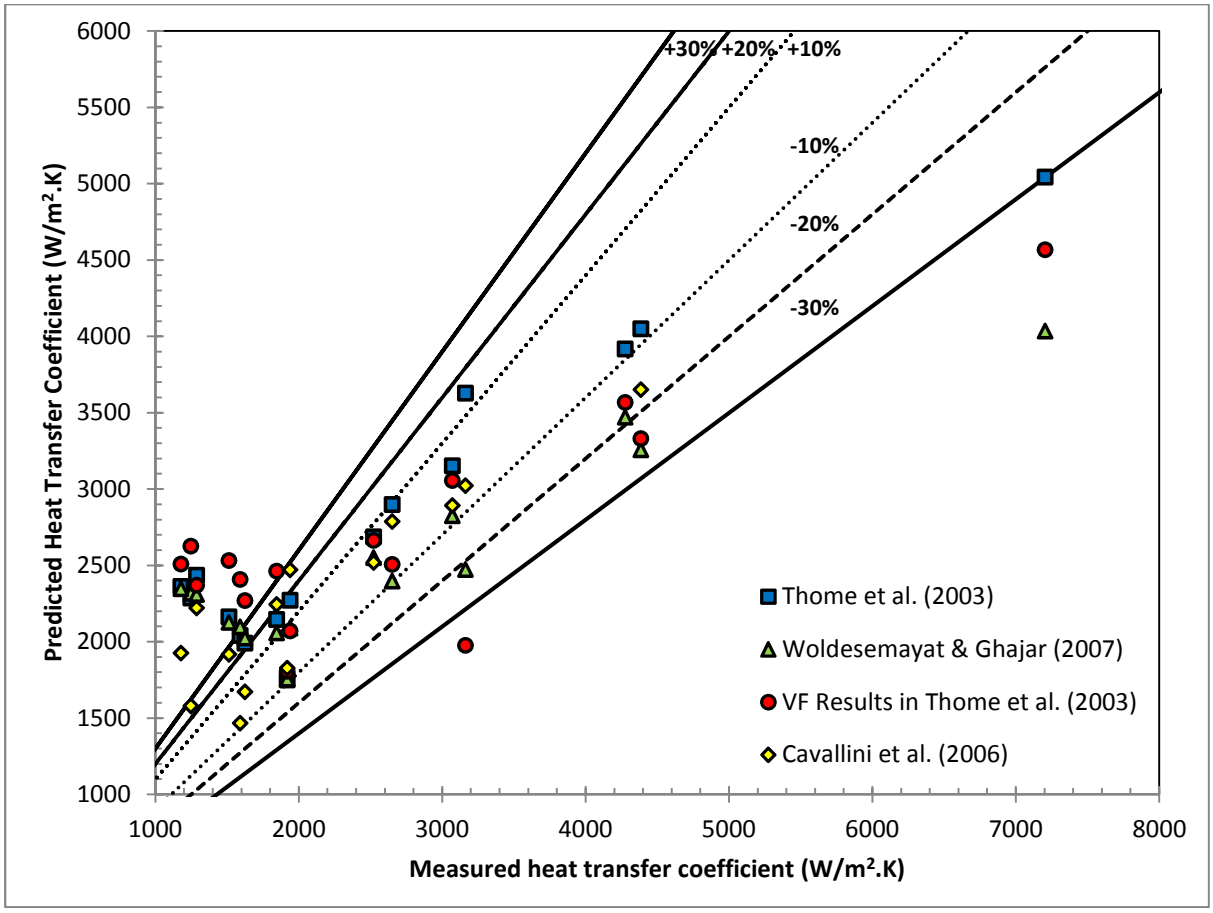

Figure 5.6: Experimental heat transfer coefficients for the case of vertical downward flow compared with the correlations of Thome *et al.* (2003) and Cavallini *et al.* (2006). Also included are the comparisons with the Thome *et al.* (2003) heat transfer correlation with the void fraction model (VF) replaced with the correlation of Woldesemayat and Ghajar (2007) and the experimentally measured void fraction results.

5.3 Inclined tube orientations

The effect of inclination angle on the void fractions and heat transfer coefficients is discussed as a function of mass flux in Sections 5.3.1 to 5.3.4 for mass fluxes of 100 kg/m^2.s, 200 kg/m^2.s, 300 kg/m^2.s and 400 kg/m^2.s respectively. The results for the aforementioned mass fluxes are presented in Figure 5.7 to Figure 5.18. For each mass flux, the measured void fractions are discussed, a comparison of the void fraction measurements are made with the predictions of the Rouhani and Axelsson (1970) correlation and the observed flow patterns are compared with the predictions of the modified Wojtan *et al*. (2005) flow pattern map. The accompanying heat transfer coefficients are also presented for each case. All the results are presented as a function of inclination angle. The discussion of the results for each respective mass flux is presented according to varying vapour quality to highlight the differences in the observed results.

5.3.1 Mass flux of 100 kg/m^2.s

Vapour quality of 25%

The measured void fractions for the 25% vapour quality case varied significantly from the horizontal flow case (0° inclination angle), even for small adjustments in the inclination angle as is evident from Figure 5.7. The measured void fractions were observed to increase by a maximum of 25% compared with horizontal flow with increasing downward inclination (negative inclination angles) up to -45° after which the void fraction remained relatively constant up to vertical downward flow. The increase in the measured void fraction could be explained by observing the prevalence of stratified-type flow with the characteristic thin liquid layer as a result of gravity-dominated flow, which reduced the cross-sectional area of the liquid phase, i.e. increased the void fraction.

The measured void fractions decreased by 35% compared with horizontal flow with increased upward inclinations (positive inclination angles) up to an inclination of 30° after which the void fractions were observed to increase again by 17% from the aforementioned minimum. The decrease in measured void fractions could be explained by observing the prevailing flow patterns, which changed from stratified- to churn-type flows wherein liquid slugs would tend to form and recirculate as a result of the vapour shear velocity being insufficient to carry the liquid slugs against gravity. Thus, liquid phases were present for a greater time fraction of the measurements when compared with downward flows, i.e. decreased void fraction. The greatest degree of recirculating flow corresponded to the minimum measured void fraction. Increasing the upward inclination angle past 30° resulted in a reduction in the degree of flow stratification and, in turn, the prevalence of recirculating liquid slugs; this was once again deduced from the flow pattern observations. The reduction of the degree of flow stratification could be explained by the more annular distribution of the liquid layer with increased upward inclination angle, which reduced the degree of liquid slug recirculation and, in turn, resulted in increased void fraction values being measured.

For the case of 25% vapour quality, the discrepancy between the measured void fraction values and the predictions of the Rouhani and Axelsson (1970) correlation was the greatest (Figure 5.8). For downward inclinations (-60° and -30°), the Rouhani and Axelsson (1970) correlation under-predicted the measured void fractions by 20% (Figure 5.8a and Figure 5.8b). The observed flow patterns correlated relatively well with the predictions of the modified Wojtan *et al*. (2005) flow pattern map even though slug-stratified-wavy-type flow was predicted while only stratified-wavy flow was observed. For upward flow inclinations (30° and 60°), the Rouhani and Axelsson (1970) correlation over-predicted experimental void fraction values by 50% (Figure 5.8c and Figure 5.8d).

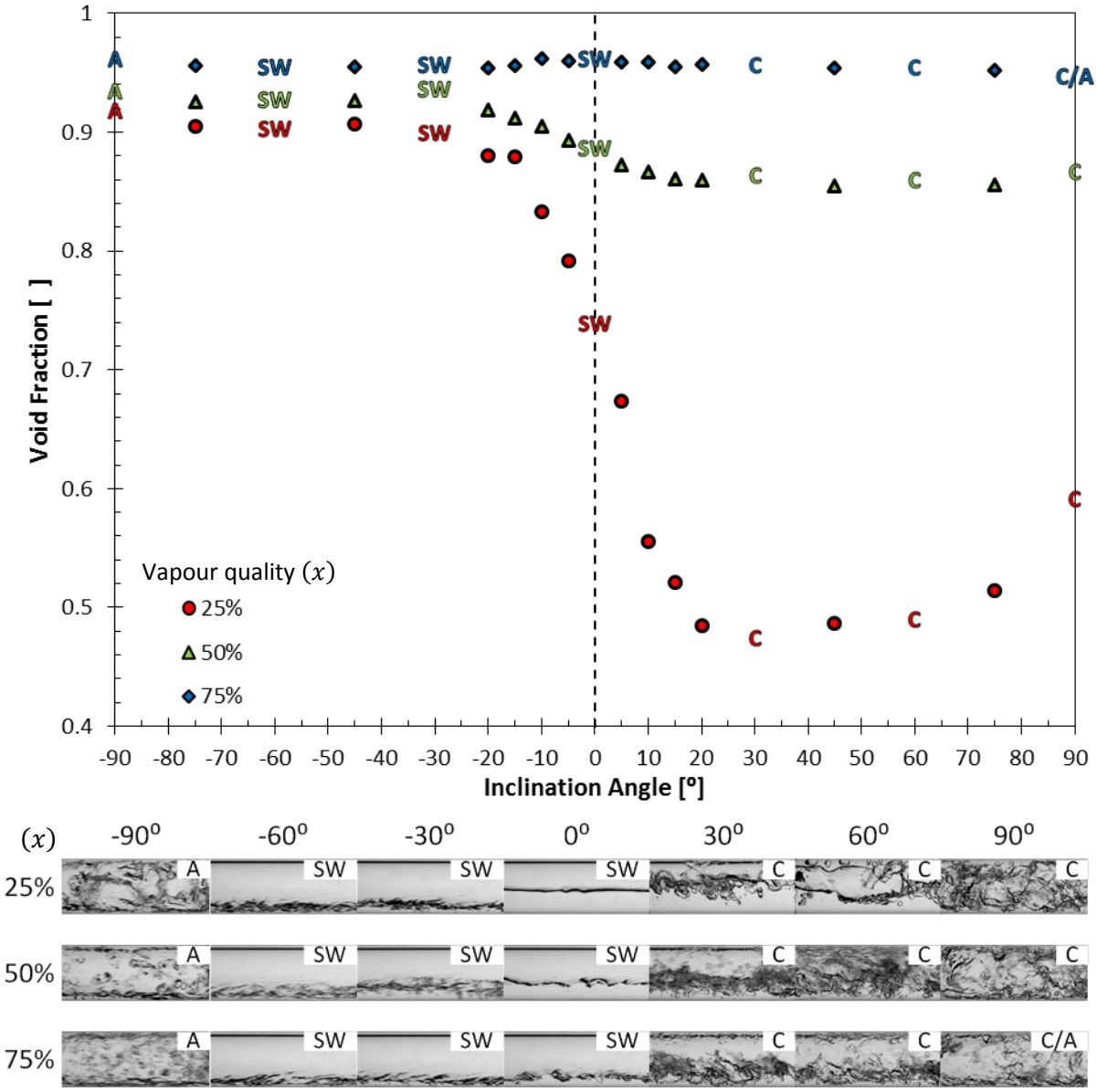

Figure 5.7: Void fractions as function of test section inclination angle for a mass flux of G = 100 kg/m^2.s and average vapour qualities of 25%, 50% and 75%. The flow pattern abbreviations are A=annular; SW=stratified-wavy; C=churn

The modified Wojtan *et al.* (2005) flow pattern map did not predict the flow patterns for upward flows correctly since the flow map did not account for recirculating, churn-type flows. In general, the void fractions and flow patterns were not predicted satisfactorily for the current case of low vapour quality and low mass flux flow conditions at upward inclinations.

The heat transfer coefficients (Figure 5.9) were observed to increase up to a maximum (38% increase relative to horizontal case) in the region of -20° to -15° downward inclination. The maximum heat transfer coefficient was observed at approximately the same downward inclination angle as the maximum void fraction. At this inclination angle, one could therefore deduce that the thermal

resistance was at a minimum, i.e. the liquid film thickness was at a minimum as a result of the liquid layer that not only flowed from the top of the tube radially downward, but also forward in the direction of the fluid flow. Further increases in the downward inclination of the flow resulted in reductions of the measured heat transfer coefficients. At vertical downward flow, the heat transfer coefficient was reduced by 30% compared with the case of horizontal flow. The aforementioned could be explained with reference to the flow pattern observations by noting that the flow transitioned from a stratified-wavy-type flow to a more annular-type flow with an irregular liquid film thickness. At the vertical downward flow inclination, the thermal resistance of the flow was increased by the change in flow pattern, i.e. the thermal resistance experienced a net increase as a result of the increased downward inclination and subsequent liquid-vapour redistribution.

Transitioning to upward inclinations, the heat transfer coefficients were observed to reduce to a minimum (4% reduction compared with the horizontal case) at 10° upward inclination. The reduction in heat transfer could be put down to an increase in thermal resistance resulting from the more substantial liquid layer thickness, which was also quite stagnant at the current flow conditions. The inclination angle at which a minimum was observed for the measured heat transfer coefficients coincided with that of the minimum void fraction measurements. Further increases in upward inclination angle actually increased the measured heat transfer coefficients by approximately 6% compared with those of horizontal flow; the increase in heat transfer corroborated with an increase in the measured void fractions for the same inclination angles. The aforementioned observation could be explained by noting that the physical liquid-vapour interactions (i.e. mixing) increased with increased upward inclination angle which, despite a similar liquid layer thickness at 30° of inclination angle, reduced the thermal resistance of the flow resulting in increased heat transfer.

Vapour qualities of 50% and 75%

With the case of 50% vapour quality, similar void fraction trends to those of the 25% vapour quality case were observed as is evident from Figure 5.7. The effect of the change in inclination angle on the absolute void fraction values was, however, not as profound. The 75% vapour quality case did not exhibit a strong dependence on the inclination angle. The reduction in the amount of liquid phase present compared with the 25% vapour quality case suppressed the effect of inclination angle as the relative effect of gravity was reduced. The maximum change in measured void fraction values resulting from changes to the inclination angle was in the order of 6% and 1% compared with the case of horizontal flow for 50% and 75% vapour quality conditions respectively. This could be compared with the case of 25% vapour quality where changes to the inclination angle resulted in void fraction measurements differing in the region of 30% compared with horizontal flow.

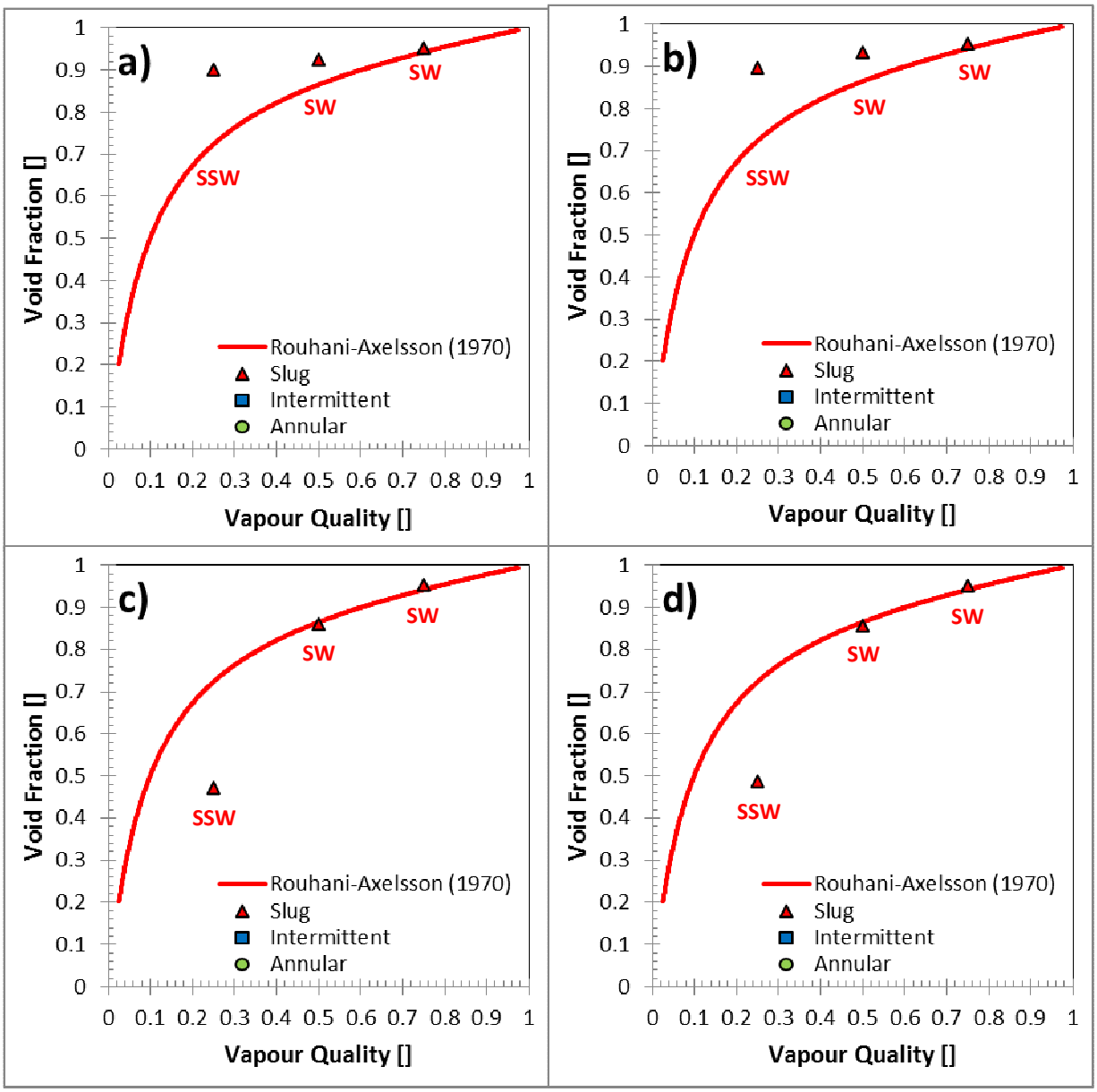

Figure 5.8: Experimental void fraction measurements as a function of average vapour quality compared with the predictions of the Rouhani and Axelsson (1970) void fraction correlation for the case of 100 kg/m^2.s mass flux and tube inclinations of a) -60°, b) -30°, c) 30° and d) 60°. The prevailing flow pattern as observed is indicated by the symbols in the legend. At each data point, the flow pattern predicted by the modified Wojtan *et al.* (2005) flow pattern map is indicated using the following abbreviations: Slug (S), stratified-wavy (SW), slug and stratified-wavy (SSW), intermittent (I) and annular (A). The colour-coding of the abbreviations also correlates with the flow classification of De Kerpel *et al.* (2013) in the legend.

For 75% vapour quality conditions, the liquid-vapour distribution and the accompanying flow patterns were observed to change with inclination angle, but the measured void fractions remained relatively unaffected. This could be a result of the vapour shear velocity at this combination of mass flux and vapour quality being just sufficient to redistribute the liquid phase to keep the void fraction present at a constant value.

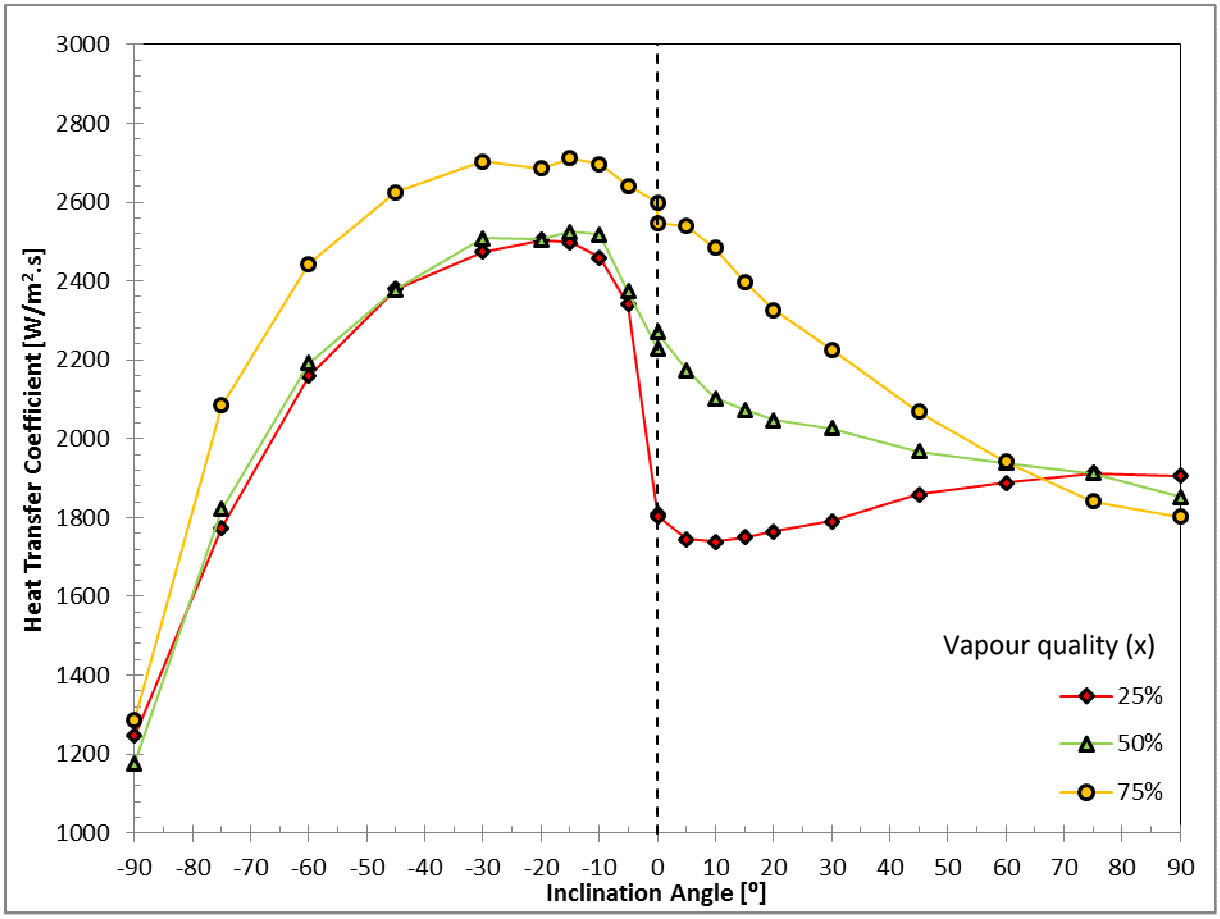

Figure 5.9: Heat transfer coefficients as a function of inclination angle for a mass flux of G = 100 kg/m^2.s and average vapour qualities of x = 25%, x = 50% and x = 75%

Figure 5.8 again presents the measured void fractions along with the observed flow patterns for downward (-60° and -30°) and upward (30° and 60°) flow inclinations compared with the predictions of the Rouhani and Axelsson (1970) correlation. The measured void fractions for the 50% vapour quality case at downward inclinations (Figure 5.8a and Figure 5.8b) were under-predicted by the correlation (7%) while the 75% vapour quality cases were closely predicted (less than 2% deviation). The downward flow patterns were predicted with similar accuracy to those of the 25% vapour quality case.

For all upward inclinations, both the 50% and 75% vapour quality cases, the measured void fractions were satisfactorily predicted (within ±2%). From the flow pattern observations (Figure 5.7), the similarities in all upward flows are evident. However, the flow patterns were not accurately predicted since the modified Wojtan *et al*. (2005) flow pattern map did not account for churn-type recirculating flows.

The heat transfer coefficients of the 50% and 75% vapour quality cases exhibited very similar behaviour to the 25% vapour quality case for downward inclinations; maximum heat transfer values

were also observed at -20° downward inclination. The heat transfer coefficients of the 25% and 50% vapour quality cases correlated closely with each other for downward flows. The relative increase in heat transfer for the 50% and 75% vapour quality cases compared with horizontal flow was reduced with a maximum increase of 12% and 5% respectively. This could be put down to the decreased influence of gravity on the flow at higher vapour qualities. The similarities in heat transfer behaviour for downward flows could be corroborated with the observed flow patterns; the flow patterns remained very similar for both current vapour qualities at downward flow inclinations. The measured heat transfer coefficients were observed to gradually decrease with increasing upward inclination angle with a minimum being reached at vertical upward flow for both 50% and 75% vapour quality cases. The measured heat transfer coefficients for the case of 60° upward inclinations were almost identical for both 50% and 75% vapour quality cases. This could be corroborated with the flow pattern observations, which revealed very similar flow behaviour for both vapour qualities. Interestingly, the heat transfer coefficients for the 75% vapour quality case decreased up to the point where the 50% vapour quality results were greater. A postulation for the aforementioned observation is that the mixing of the liquid phase at near-vertical upward flow increases the heat transfer, hence at lower vapour qualities, i.e. more liquid phase present, the heat transfer may be slightly improved compared with the higher vapour quality case.

5.3.2 Mass flux of 200 kg/m^2.s

Vapour qualities of 10% and 25%

The measured void fractions for both 10% and 25% vapour quality cases also varied significantly with changes in inclination angle from horizontal flow. The measured void fractions were observed to increase by a maximum of 39% compared with horizontal flow at a downward inclination angle of -45° for the case of 10% vapour quality. Similarly, a maximum increase of 15% relative to the horizontal case was observed for the 25% vapour quality case, but at a vertical downward inclination angle of -90°. The aforementioned observation deviated from the observations made for the 100 kg/m^2.s mass flux case. The relative effect of inclination angle on the void fraction values was observed to diminish for the 25% vapour quality case at a mass flux of 200 kg/m^2.s compared with the 100 kg/m^2.s mass flux case. As discussed previously, the increase in measured void fractions could be put down to the prevalence of stratified-type flows at downward inclinations.

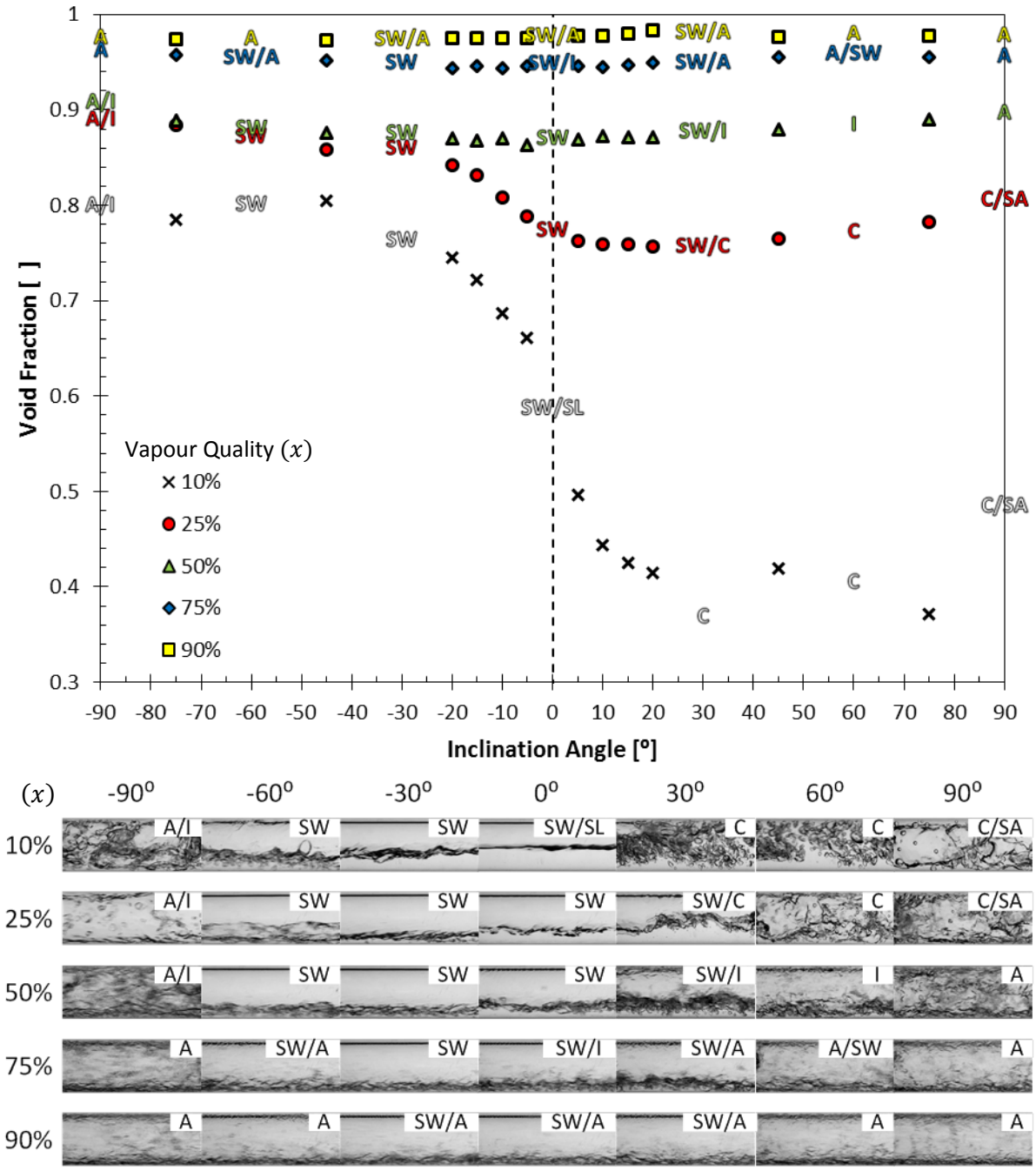

Figure 5.10: Void fractions as a function of test section inclination angle for a mass flux of G = 200 kg/m^2.s and average vapour qualities of 10%, 25%, 50%, 75% and 90%. The flow pattern abbreviations are A=annular; SW=stratified-wavy; C=churn; I=intermittent; SL=slug; SA=semi-annular

Similar to prior observations made in this chapter, the measured void fractions decreased with increasing upward inclination angles. For the 10% vapour quality case, the measured void fractions decreased to a minimum (37% decrease compared with the horizontal case) at an inclination angle of 30°, which correlated with the observation made for the case of 100 kg/m^2.s mass flux and 25% vapour quality. Further increases to the upward inclination angle led to some scatter, but ultimately

the void fraction values increased by 20% from the minimum value up to the case of vertical upward flow. The scatter in the results could be a result of the highly chaotic churn-type flow that prevailed. For the case of 25% vapour quality, the effect of increasing upward inclination angle was less profound than for the 10% vapour quality case with only a 2% decrease relative to the horizontal case. The aforementioned minimum was also observed at a 30° upward inclination angle. Again the reduction in measured void fractions for upward inclinations could be put down to the churn-type flows with liquid recirculation which prevailed. This led to liquid phase being present for a greater time fraction than for downward inclinations hence a reduction in the measured void fractions. The diminished influence of upward inclinations on the measured void fractions for the 25% vapour quality case compared with the 100 kg/m^2.s mass flux case could be due to the reduced degree of liquid recirculation at a higher mass flux of 200 kg/m^2.s with the vapour shear velocity being great enough to continuously propel the liquid phase against gravity.

Both the 10% and 25% vapour qualities exhibited significant discrepancies when compared with the Rouhani and Axelsson (1970) predictions (Figure 5.11) at downward inclinations (-60° and -30°). The void fraction measurements for the 10% vapour quality case were under-predicted by 29% and 26% for inclinations of -60° and -30° respectively (Figure 5.11a and Figure 5.11b). Similarly, for the 25% vapour quality case, the measurements were under-predicted by 12% and 11% for -60° and -30° inclinations respectively. The observed flow patterns (Figure 5.10) did not correlate well with the predictions of the modified Wojtan *et al*. (2005) flow pattern map. At both 10% and 25% vapour qualities as well as -60° and -30° inclinations, stratified-wavy-type flows were observed while slug flows were predicted.

For upward inclinations at a vapour quality of 10%, the Rouhani and Axelsson (1970) correlation over-predicted the measured void fractions by 54% and 40% at upward inclinations of 30° and 60° respectively (Figure 5.11a and Figure 5.11b). The diminished prediction accuracy could be a result of the chaotic nature of the flow at the aforementioned conditions. The non-linear nature of the Rouhani and Axelsson (1970) correlation, i.e. large gradient at lower vapour qualities, also meant that larger discrepancies could be expected. At a 25% vapour quality the Rouhani and Axelsson (1970) predictions resembled the measured void fraction values more closely with an over-prediction of 1.3% at 30° inclination and a 0.7% under-prediction at 60° inclination. The reduced degree of liquid recirculation for the 25% vapour quality could be the reason for the improved correlation between the observations and the predictions of void fractions. The observed flow patterns did not correlate well with the predictions of the modified Wojtan *et al*. (2005) flow pattern map since only churn-type flows with liquid recirculation were observed for both 10% and 25%

vapour qualities at upward inclinations while the modified Wojtan *et al*. (2005) flow pattern map predicted slug-type flows.

The heat transfer coefficients for the full range of tube inclinations at both 10% and 25% vapour qualities exhibited similar behaviour at both upward and downward inclinations (Figure 5.12). The heat transfer coefficients were observed to increase with increasing downward inclinations by a maximum of 44% and 18% compared with horizontal flow. Both maximums were observed at the same downward inclination of -20°, which correlated well with observations from the 100 kg/m^2.s mass flux case. The maximum heat transfer coefficient values (-20°) and the maximum measured void fractions (-45° and -90°) were not observed at the same downward inclinations for the flow conditions currently under consideration. Thus, the conditions for minimal thermal resistance did not correlate with the case of minimum liquid phase present, i.e. thin liquid layer. Therefore, there had to be other factors (e.g. improved liquid mixing) that dominate the maximum possible heat transfer at the current flow conditions in lieu of purely liquid film thickness. Further increases in downward inclination led to reductions in heat transfer coefficients for both 10% and 25% vapour qualities up to a minimum at vertical downward flow where reductions of 6% and 27% were observed compared with horizontal flow.

Similar trends were again observed for upward inclinations for 10% and 25% vapour qualities. Heat transfer coefficients were observed to decrease even at near-horizontal flow. For 10% vapour quality, a 4% reduction compared with horizontal flow was observed at 5° upward inclination angle while a 6% reduction was observed at 15° upward inclination angle for the case of 25% vapour quality. Further increases in upward inclination angle actually resulted in increased heat transfer coefficients relative to the minimum values. For 10% vapour quality, the heat transfer coefficients increased with inclination angle up to vertical upward flow where a 7% increase was observed relative to the horizontal flow case. The increase in heat transfer coefficients could be explained using the observed flow patterns. For increasing upward inclination angle above 15°, the flow patterns were observed to exhibit churn-type behaviour, but with the liquid layer distributed relatively thinly and evenly around the periphery of the tube, i.e. annular flow tendencies. The aforementioned phenomenon could account for the increased heat transfer coefficients because the net thermal resistance could be reduced as a result of the thinner liquid layer, as well as improved mixing of the liquid phase.

Vapour qualities of 50%, 75% and 90%

The void fraction results of the 50%, 75% and 90% vapour qualities exhibited similar behaviours with changes in inclination angle, albeit with different absolute values (Figure 5.10). The aforementioned vapour quality cases did not present the same degree of dependence on inclination angle as was the case with the 10% and 25% vapour qualities. A slight increase in the measured void fraction was observed for the 50% vapour quality case (4% compared with horizontal flow) at vertical downward flow. For 75% vapour quality, the maximum increase in measured void fraction was 1.4% compared with the horizontal case and also occurred at vertical downward flow. At 90% vapour quality, the variations in measured void fractions were less than 1% making them insignificant.

For all vapour qualities currently under consideration, the changes in the void fraction measurements for upward inclinations did not vary significantly. At 50% vapour quality, the measured void fraction actually increased slightly (3% compared with horizontal flow) at vertical upward flow. The aforementioned observation differed from earlier results where the measured void fraction declined with increased upward inclination angles. The variations in measured void fractions for both 75% and 90% vapour qualities were 1% or less compared with horizontal flow. The aforementioned flow conditions could therefore be considered independent of inclination angle.

The measured void fractions were predicted with greater accuracy by the Rouhani and Axelsson (1970) correlation than for the 10% and 25% vapour qualities (Figure 5.11). Both upward and downward inclination void fraction measurements were predicted within ±1.3%, which represented a significant improvement on the lower vapour quality cases (10% and 25%). The observed flow patterns were predicted well by the modified Wojtan *et al*. (2005) flow pattern map for the case of 60° upward inclination angle (Figure 5.11d). For the other inclinations (Figure 5.11a, Figure 5.11b and Figure 5.11c), the observed flow patterns were not predicted with quite as much accuracy; the majority of observed flow patterns tended to stratified-type flows despite the higher vapour quality conditions. However, the predicted flow patterns did not differ from the observed flow patterns to a large degree with most of the stratified-type flows exhibiting annular tendencies. The upward and downward inclinations were observed to supress the occurrence of intermittent-type flows.

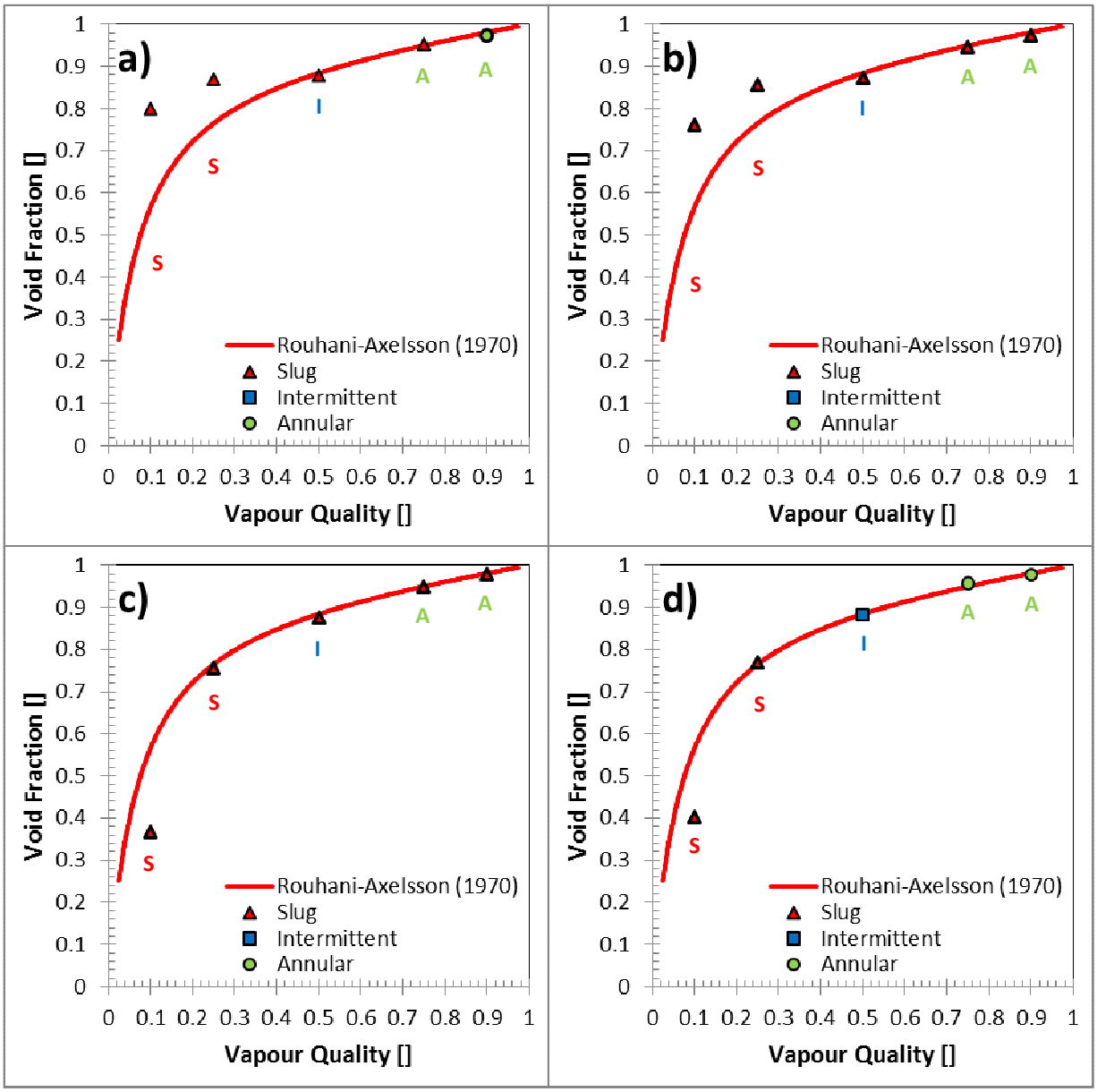

Figure 5.11: Experimental void fraction measurements as a function of average vapour quality compared with the predictions of the Rouhani and Axelsson (1970) void fraction correlation for the case of 200 kg/m^2.s mass flux and tube inclinations of a) -60°, b) -30°, c) 30° and d) 60°. The prevailing flow pattern as observed is indicated by the symbols in the legend. At each data point, the flow pattern predicted by the modified Wojtan *et al.* (2005) flow pattern map is indicated using the following abbreviations: Slug (S), stratified-wavy (SW), slug and stratified-wavy (SSW), intermittent (I) and annular (A). The colour-coding of the abbreviations also correlates with the flow classification of De Kerpel *et al.* (2013) in the legend.

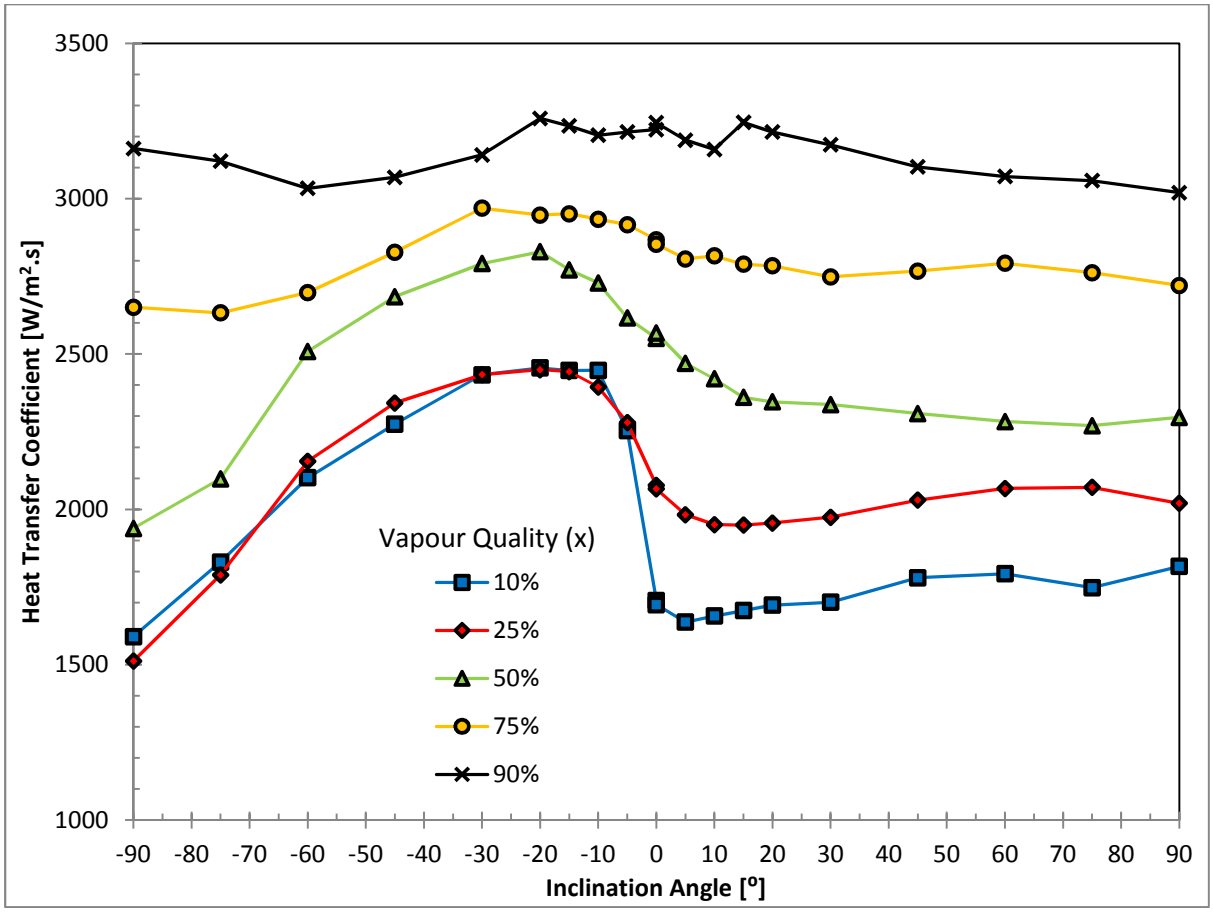

Figure 5.12: Heat transfer coefficients as a function of inclination angle for a mass flux of G = 200 kg/m^2.s and average vapour qualities of x = 10%, x = 25%, x = 50%, x = 75% and x = 90%

Despite the fact that the void fractions were observed to remain fairly constant over all ranges of inclination angles for the vapour qualities currently under consideration, significant variations in the heat transfer coefficients were observed (Figure 5.12). For downward inclinations, the heat transfer coefficients were again observed to increase with downward inclinations. For the 50% vapour quality case, the heat transfer coefficients increased by 11% at an inclination of -20° compared with horizontal flow. Similarly, for the 75% vapour quality case, the heat transfer coefficients increased by 4% at an inclination of -30°. The effect of downward inclinations was observed to diminish with an increase in vapour quality as expected. Further increases in the downward inclination resulted in reductions of the heat transfer coefficients with minimums observed at near-vertical downward flow for both 50% and 75% vapour qualities. The reason could be that the transition to annular-type flow resulted in a net increase in thermal resistance at the current flow conditions with the liquid layer thickness increasing with its distribution around the periphery of the tube. The heat transfer coefficients for 90% vapour quality were more erratic than those of the 50% and 75% vapour quality, but broadly similar trends were noticed, i.e. maximum value in the region of -20° inclination angle followed by reductions in the heat transfer coefficients with further increases in downward

inclination angles. The relative increase compared with horizontal flow was, however, not significant (less than 1%).

For upward inclinations, the heat transfer coefficients for 50% and 75% vapour qualities exhibited broadly similar trends. The heat transfer coefficients were observed to decrease by 11% and 5% for 50% and 75% vapour qualities respectively with increasing upward inclination angle up to vertical upward flow. The 90% vapour quality case was an exception where a slight increase in heat transfer coefficient was observed at 15° of upward inclination angle. No explanation for the aforementioned increase in heat transfer coefficient could be provided apart from possible experimental uncertainties resulting in unexpected deviations.

5.3.3 Mass flux of 300 kg/m^2.s

Vapour quality of 10%

The 10% vapour quality case will be discussed separately for the current mass flux since the observations were significantly different from the other vapour qualities. The measured void fractions were again observed to increase with increasing downward inclination angle (Figure 5.13). However, a maximum (28% increase compared with horizontal flow) was observed at vertical downward flow instead of the -20° downward inclination region as with previous flow conditions discussed in this chapter. Also, the measured void fractions were observed to increase more gradually with increases in downward inclinations than for previously considered mass fluxes. Both the aforementioned could be attributed to the higher mass flux suppressing the effect of gravity on the liquid-vapour distribution. Similarly, the effect of increasing upward inclination angle on the measured void fractions were more subdued than for lower mass fluxes with the expected decrease in measured void fractions occurring more gradually. The measured void fractions decreased (24% compared with horizontal flow) up to a minimum at 60° of upward inclination angle, which did not correlate with the observations at lower mass fluxes (i.e. 30° upward inclination). Again, it appeared that the higher mass flux and the accompanying higher vapour shear velocity resulted in the effect of inclination angle on the void fraction being suppressed to more extreme inclination angles.

As before, significant deviations were observed between the measured void fractions and the predicted values of the Rouhani and Axelsson (1970) correlation for downward inclinations (Figure 5.14a and Figure 5.14b) at 10% vapour quality. The Rouhani and Axelsson (1970) correlation under-predicted the measured void fraction at a downward inclination of -60° by 20%. The prediction accuracy improved for the -30° downward inclination angle with the measured void fractions under-

predicted by 8%. The modified Wojtan *et al*. (2005) flow pattern map predicted the observed flow patterns well with slug flow being predicted and stratified-wavy-dominant-type flow being observed.

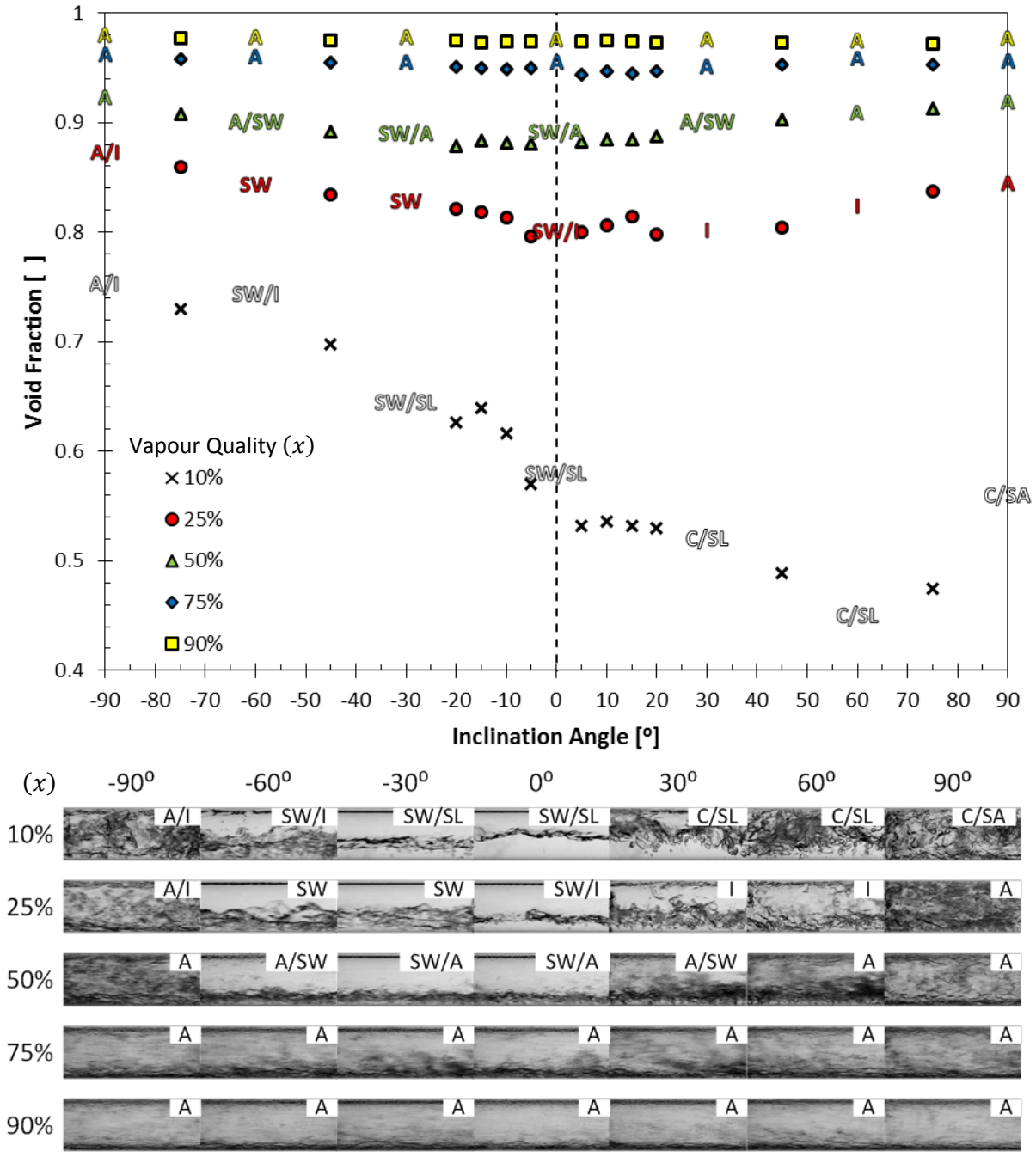

Figure 5.13: Void fractions as function of test section inclination angle for a mass flux of G = 300 kg/m^2.s and average vapour qualities of 10%, 25%, 50%, 75% and 90%. The flow pattern abbreviations are A=annular; SW=stratified-wavy; C=churn; I=intermittent; SL=slug; SA=semi-annular

Although the observed flow patterns were strictly speaking stratified-wavy dominant at -30° inclination, slug-type flow phenomena were also present in the flow in accordance with the predictions of the modified Wojtan *et al*. (2005) flow pattern map. At -60° downward inclination, a

stratified-wavy-type flow was dominant with secondary flashing between stratified-wavy- and slug-type flows, i.e. intermittent flow.

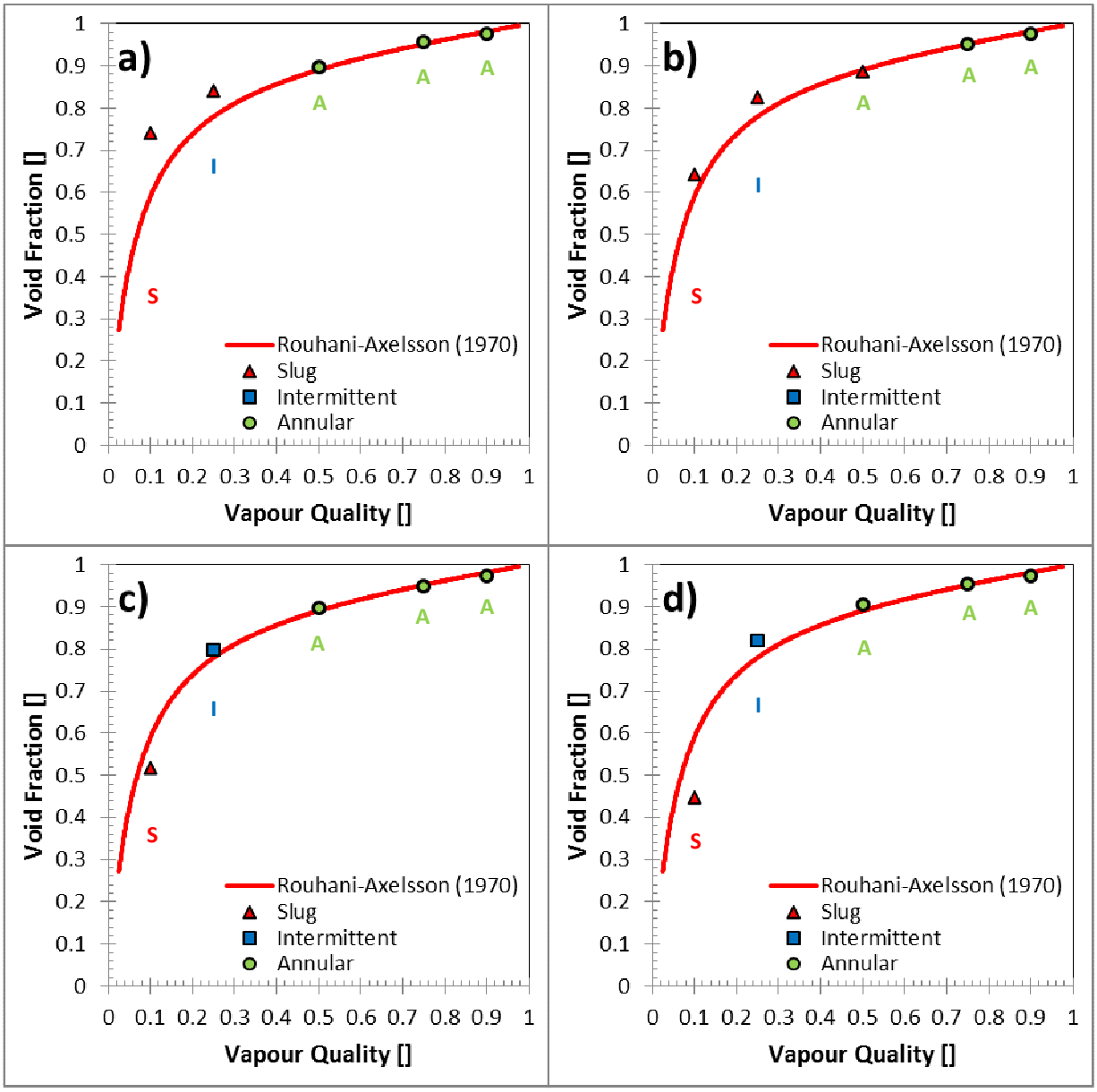

Figure 5.14: Experimental void fraction measurements as a function of average vapour quality compared with the predictions of the Rouhani and Axelsson (1970) void fraction correlation for the case of 300 kg/m^2.s mass flux and tube inclinations of a) -60°, b) -30°, c) 30° and d) 60°. The prevailing flow pattern as observed is indicated by the symbols in the legend. At each data point, the flow pattern predicted by the modified Wojtan *et al.* (2005) flow pattern map is indicated using the following abbreviations: Slug (S), stratified-wavy (SW), slug and stratified-wavy (SSW), intermittent (I) and annular (A). The colour-coding of the abbreviations also correlates with the flow classification of De Kerpel *et al.* (2013) in the legend.

The Rouhani and Axelsson (1970) correlation over-predicted the measured void fractions by 14% and 32% for 30° and 60° upward inclinations respectively (Figure 5.14c and Figure 5.14d). This

represented quite a significant difference between the measured and predicted void fractions for the 10% vapour quality case at upward inclinations. The flow patterns for upward flows did not correlate well with the predictions of the modified Wojtan *et al*. (2005) since the aforementioned flow pattern map did not account for churn-type flows with the accompanying recirculation of the liquid phase. The recirculation of the liquid slugs was, however, less profound than for the lower mass flux cases discussed earlier as a result of greater vapour shear velocity being able to carry the liquid slugs against gravity.

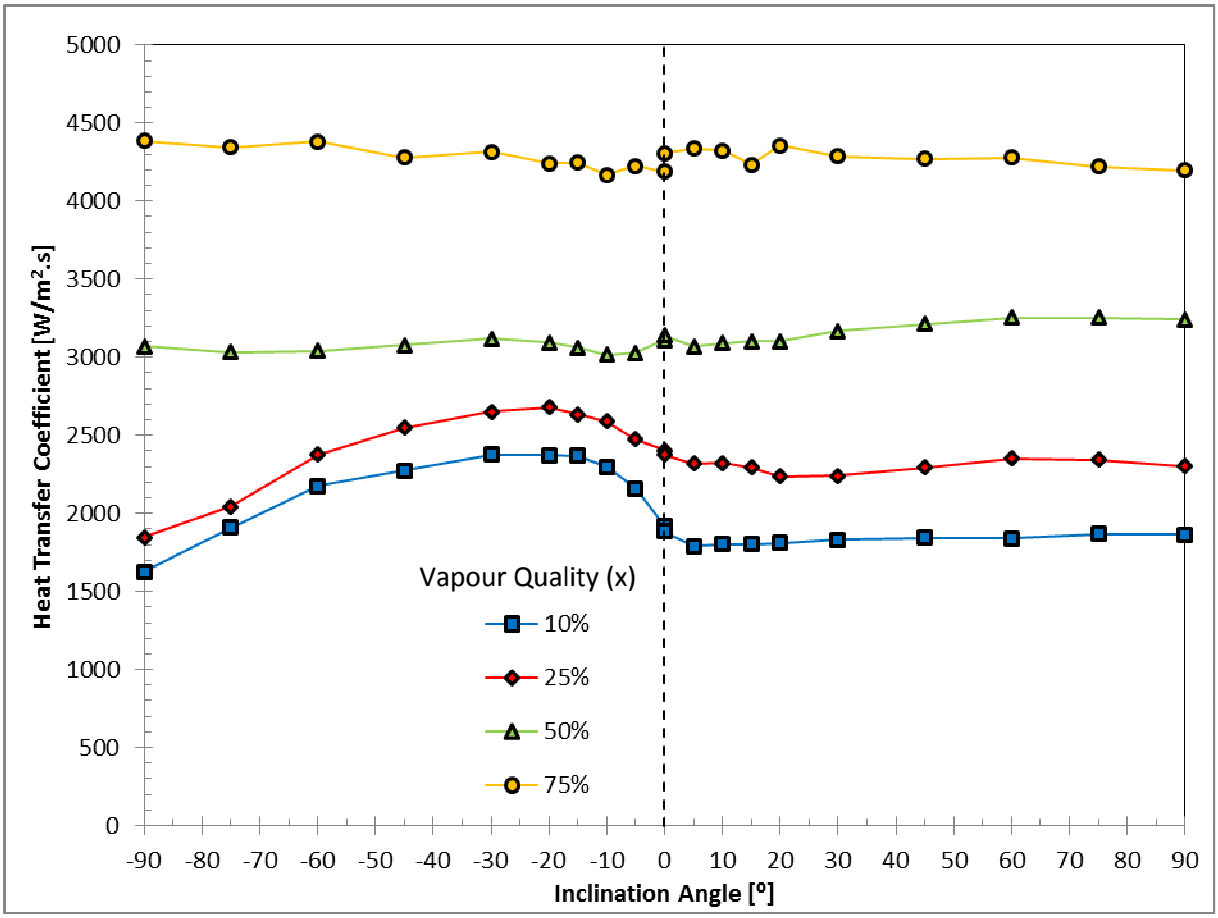

Figure 5.15: Heat transfer coefficients as a function of inclination angle for a mass flux of G = 300 kg/m^2.s and average vapour qualities of x = 10%, x = 25%, x = 50% and x = 75%

The 10% vapour quality case also exhibited significant variations in heat transfer coefficients with increasing downward inclination angles similar to prior mass flux cases (Figure 5.15). The heat transfer coefficients increased (25% compared with that of the horizontal case) up to a maximum in the region of -20° to -30° downward inclination angle. The inclination angle at which the maximum was observed correlated well with observations made earlier in this chapter. Further increases in the downward inclination angle resulted in decreased heat transfer coefficients up to a minimum at vertical downward flow where a 15% reduction in heat transfer coefficient was observed compared

with that of the horizontal flow case. The effect of upward inclination angle on the heat transfer coefficients was subdued compared with the effect downward inclinations. At near-horizontal flow, the heat transfer coefficients decreased to a minimum (6% reduction compared with horizontal flow) at 5° of upward inclination angle. Further increases in upward inclination angle did not drastically change the observed heat transfer coefficients with a slight increase from the aforementioned minimum (4% increase) being observed at near-vertical upward flow. As before, the slight increase in heat transfer coefficient may be due to the greater degree of liquid mixing.

Vapour quality of 25% and 50%

The measured void fractions for vapour quality cases of 25% and 50% are presented in Figure 5.13. For both 25% and 50% vapour qualities, the measured void fractions decreased with increasing downward inclination angle as expected. The increases were, however, not as profound compared with those of the horizontal flow case as for the 10% vapour quality case. The maximum increase in measured void fraction compared with that of horizontal flow was 8% and 4% for 25% and 50% vapour qualities respectively and was observed at vertical downward flow for both vapour qualities. The increase in measured void fractions could be explained by considering the observed flow patterns. With increasing downward inclination angle, the stratified-wavy- and slug-type flows were suppressed for both vapour qualities, i.e. the liquid film diminished along with the height of passing waves, as well as the frequency with which passing waves occurred. This phenomenon continued with increasing downward inclination angle until purely annular-type flows were observed at vertical downward flow, which coincided with the maximum measured void fraction values. The measured void fractions tended to be independent of upward inclination angle at near-horizontal flow with only small deviations (less than 1%) from the values observed for horizontal flow. Interestingly, for both 25% and 50% vapour quality, the measured void fractions were observed to increase with upward inclination angle from the region of 60° to vertical upward flow where increases of 5% and 3% relative to horizontal flow were observed for 25% and 50% vapour quality respectively. Again, the increase in measured void fraction could be correlated with the prevalence of annular-type flows at near-vertical flows. This, in turn, could be the result of the vapour shear velocity at the current mass flux and vapour qualities being sufficient to redistribute the liquid phase into a thin annular ring with a high velocity vapour core flowing against gravity.

For the 25% vapour quality case, the measured void fractions were under-predicted by the Rouhani and Axelsson (1970) correlation for both -60° and -30° downward inclinations by 7% and 6% respectively (Figure 5.14a and Figure 5.14b). The measured void fractions were predicted with greater accuracy than those of the 10% vapour quality case. At 25% vapour quality, the flows were

observed to be purely of the stratified-wavy type. This was observed against the backdrop of intermittent-type flow predictions of the modified Wojtan *et al*. (2005) flow pattern map. The downward inclinations seemed to suppress the formation of liquid slugs, which resulted in intermittent-type flows being diminished in favour of stratified-type flows. The predictions for the 50% vapour quality case were more accurate with the measured void fractions predicted within 1%. For both -60° and -30° downward inclinations, the small amount of liquid phase present meant that the flow exhibited strong annular-type tendencies. For the case of -30° downward inclination, the flow was adjudged to be stratified-wavy dominant with secondary annular effects while the -60° downward inclination was adjudged to be annular dominant with secondary stratified effects. The modified Wojtan *et al*. (2005) flow pattern map predicted annular flow, which correlated quite well with the observed flow patterns since annular tendencies were observed.

For upward inclinations, the predictions of the Rouhani and Axelsson (1970) correlation resembled the measured void fractions more closely (Figure 5.14c and Figure 5.14d). For the 25% vapour quality, the 30° and 60° upward inclination angles were under-predicted by 2% and 5% respectively. Intermittent flashing between annular- and slug-type flows were observed for the aforementioned inclinations, but a tendency towards annular flow was still observed, which may explain the good correlation between the void fraction predictions and measurements. For the 50% vapour quality case, the measured void fractions were slightly under-predicted by 1% and 2% for 30° and 60° upward inclinations respectively. This represented quite a good correlation between the void fraction measurements and the predictions of the Rouhani and Axelsson (1970) correlation. The observed flow patterns also correlated well with the predictions of the modified Wojtan *et al*. (2005) flow pattern map, i.e. annular flow.

The effect of inclination angle on the heat transfer coefficients was more profound for the 25% vapour quality case than for the 50% vapour quality case (Figure 5.14). As expected, the heat transfer coefficients increased with increasing downward inclination angle for the 25% vapour quality with a 12% increase in heat transfer coefficient relative to horizontal flow at -20°. Further increases in downward inclination led to a decrease in heat transfer coefficient with a minimum observed at vertical downward flow (23% reduction compared with horizontal flow). The maximum heat transfer coefficient was not observed at the same downward inclination as the maximum measured void fraction. Instead, the maximum heat transfer was observed for conditions where stratified-type flow prevailed. For the conditions currently under consideration, the conclusion can be made that the heat transfer is more dependent on the prevailing flow pattern than the inclination angle with stratified-type flow exhibiting lower thermal resistance than annular-type flows.

The heat transfer coefficients were not affected by changes in upward inclinations to the same extent as in downward inclinations. A slight reduction (6% compared with horizontal flow) in heat transfer coefficient was observed in the region of 20° upward inclination angle. Further increases in the upward inclination angle led to a slight reduction in the heat transfer coefficients compared with the maximum, but in general the heat transfer was not significantly affected by changes in the upward inclination angle. From the flow pattern observations, mainly annular-type flows were observed in accordance with the predictions of the modified Wojtan *et al*. (2005) flow pattern map. This might account for the independence of the heat transfer coefficients with upward inclination angles since the liquid film- and, in turn, the thermal resistance, remained mostly constant.

Vapour quality of 75% and 90%

The measured void fractions for the 75% and 90% vapour qualities were observed to exhibit independence towards the inclination angle in general (Figure 5.13). For both the 75% and 90% vapour qualities, the maximum deviation from the horizontal flow case was less than 1%.

The measured void fractions for upward and downward inclinations were predicted with good accuracy by the Rouhani and Axelsson (1970) correlation (Figure 5.14a to Figure 5.14d). Both 75% and 90% vapour qualities were predicted within ±1% for upward and downward inclination angles. The observed flow patterns also correlated well with the modified Wojtan *et al*. (2005) flow pattern map, i.e. only annular-type flow was observed for all inclination angles.

For the 75% vapour quality case, the heat transfer coefficients were observed to be independent of inclination angle (Figure 5.15) with a maximum deviation of 3% compared with horizontal flow. Unlike previous flow conditions, a clear trend in increases and decreases of heat transfer coefficient with upward and downward inclinations could not be observed. The accuracy of the measurements may not be enough to observe the changes in heat transfer coefficients at the current combination of higher vapour quality and mass flux. As mentioned earlier, the heat transfer results for the 90% vapour quality case were omitted due to issues with accuracy.

5.3.4 Mass flux of 400 kg/m^2.s

Vapour quality of 10%

For the 400 kg/m^2.s mass flux case, the 10% vapour quality case is discussed separately because the experimental results were observed to differ significantly from other vapour qualities. As before, significant changes in measured void fractions were observed with changes in inclination angle (Figure 5.16). The measured void fractions were observed to increase with increased downward

inclination angles similar to previously discussed mass fluxes. The maximum void fraction was measured at near-vertical flow (-75° downward inclination), which was similar to the 300 kg/m^2.s mass flux case and exhibited an increase of 16% compared with horizontal flow. The increase relative to horizontal flow was significantly less (by approximately 10%) than for the 300 kg/m^2.s mass flux case. At near-horizontal downward flows, the increase in measured void fractions were observed to exhibit some scatter, which might be a result of the intermittent liquid slugs which were observed at the aforementioned flow conditions.

For near-horizontal upward flows, the measured void fractions were observed to reduce with increased upward inclination angles. The reduction in measured void fraction could be explained by noting the prevalence of stratified-type flow at the current flow conditions. The results exhibited some scatter, especially for the 5° and 60° upward inclinations. No explanation for the aforementioned scatter could be provided other than the prevalence of intermittent-type flows, which due to its chaotic nature, might result in discrepancies in the measured results. The minimum measured void fraction was observed at a 60° upward inclination angle (18% reduction compared with horizontal flow), however, the aforementioned observation regarding scatter should be taken into account with this observation. The measured void fractions were observed to increase again at near-vertical upward flows relative to the aforementioned minimum. The increase in measured void fraction could be corroborated with the prevalence of more annular-type flows. At vertical upward flow, the flow pattern was adjudged to be of the churn semi-annular type due to thick liquid layer being formed by the high vapour shear velocity at the current mass flux. In general, the inclination effect on measured void fractions was subdued compared with lower mass flux cases.

The prediction accuracy of the Rouhani and Axelsson (1970) correlation improved for the 10% vapour quality case compared with the lower mass flux cases for both upward and downward inclination angles. For downward inclination angles (Figure 5.17a and Figure 5.17b), the measured void fractions were under-predicted by 13% and 5% for -60° and -30° downward inclination angles respectively. Only slug-type flows were observed for downward inclination angles, which meant that the predictions of the modified Wojtan *et al*. (2005) flow pattern map (i.e. intermittent-type) flow were not accurate.

For upward flow (Figure 5.17c and Figure 5.17d) the Rouhani and Axelsson (1970) correlation over-predicted the measured void fractions by 8% and 23% for 30° and 60° upward inclination angles respectively. The latter upward inclination angle represented an outlier to a degree which may have been due to experimental and/or flow uncertainties. For both upward inclination angles the observed flow patterns correlated well with the predictions of the modified Wojtan *et al*. (2005) flow

pattern map with intermittent-type flow being observed. At 60° upward inclination angle a secondary slug-type flow was observed along with the intermittent flashing between stratified- and annular flow.

The effect of inclination angle on the heat transfer coefficients was observed to diminish compared with lower mass flux cases (Figure 5.18). The heat transfer coefficients were observed to increase with increased downward inclination as expected up to a maximum at -15° downward inclination. However, the increase relative to horizontal flow (16%) was reduced compared with the 10% vapour quality case of lower mass fluxes. Further increases in downward inclination angle resulted in the heat transfer coefficients reducing gradually up to vertical downward flow (9% reduction compared with horizontal flow). The minimum heat transfer at vertical downward flow could be corroborated with the annular-intermittent flow that was observed. The greater amount of liquid phase present coupled with the annular-type flow could have resulted in a net increase in liquid layer thickness (i.e. thermal resistance), despite the fact that annular-type flows generally tend to reduce thermal resistance.

The heat transfer coefficients were observed to decrease with increasing upward inclination angle as expected. However, the minimum heat transfer coefficient (6% reduction) was not vastly different from that of horizontal flow. The aforementioned minimum heat transfer coefficient was observed at an upward inclination angle of 15°. Further increases in upward inclination angle resulted in the heat transfer coefficients increasing from the minimum value up to the point where the heat transfer coefficients were nearly identical to the horizontal flow case at vertical upward flow. The increase in the heat transfer coefficients from the minimum value for upward flow could be corroborated with the flow pattern observations by noting that the flow patterns tended away from slug-type flow to churn semi-annular flow at near-vertical flow. This change in flow pattern can be considered to account for the reduction in thermal resistance, i.e. annular-type flows tend to provide less thermal resistance than slug-type flows in general.

Vapour quality of 25%, 50%, 75% and 90%

The remaining vapour quality cases are presented together as a result of the diminished effect of inclination angle on the flow for the current mass flux. For both the 25% and 50% vapour qualities, slight increases in measured void fractions were observed for increasing downward inclination angles. The measured void fractions were observed to reach a maximum at vertical downward flow for both vapour qualities with a 6% and 3% increase relative to horizontal flow respectively. For the 75% and 90% vapour qualities, the measured void fractions remained practically unchanged, i.e. no

deviation greater than ±1% compared with horizontal flow was observed. The small deviations in measured void fractions at downward inclinations could be corroborated with the flow pattern observations. No significant changes in liquid-vapour distribution could be observed for the majority of downward flow inclinations. An exception was for the 25% vapour quality case where the stratified-type flow transitioned to annular-type flow with increasing downward inclination angle.

Slight increases in the measured void fractions were observed for the 25% and 50% vapour quality cases with increasing upward inclination angle. Maximum increases of 5% and 3% relative to horizontal flow were observed at 25% and 50% vapour quality respectively for vertical upward flow. The slight increases in measured void fractions could be put down to the stronger prevalence of annular-type flow, especially for the 25% vapour quality case. For 75% and 90% vapour quality conditions, no appreciable changes in measured void fractions could be observed for upward flows. Again, this corresponded to the flow pattern observations which remained unchanged with increasing upward inclination angle.

For 25% vapour quality and -60° downward inclination angle (Figure 5.17a), the measured void fraction was under-predicted by 3% which represented the greatest deviation between predictions and measurements for the vapour qualities and inclination angles currently under consideration. The predictions of the Rouhani and Axelsson (1970) correlation therefore matched the measured void fractions closely for both upward and downward inclinations for the current mass flux. The observed flow patterns also correlated well with the predictions of the modified Wojtan *et al*. (2005) flow pattern map for both upward and downward flows (Figure 5.17a-d). Exceptions were observed for the 25% vapour quality case at both -60° and -30° downward inclinations where slug-type flows were observed, but intermittent-type flow was predicted. As before, the tendency is for downward inclinations to suppress the occurrence of intermittent-type flows as a result of increased stratification of the liquid phase.

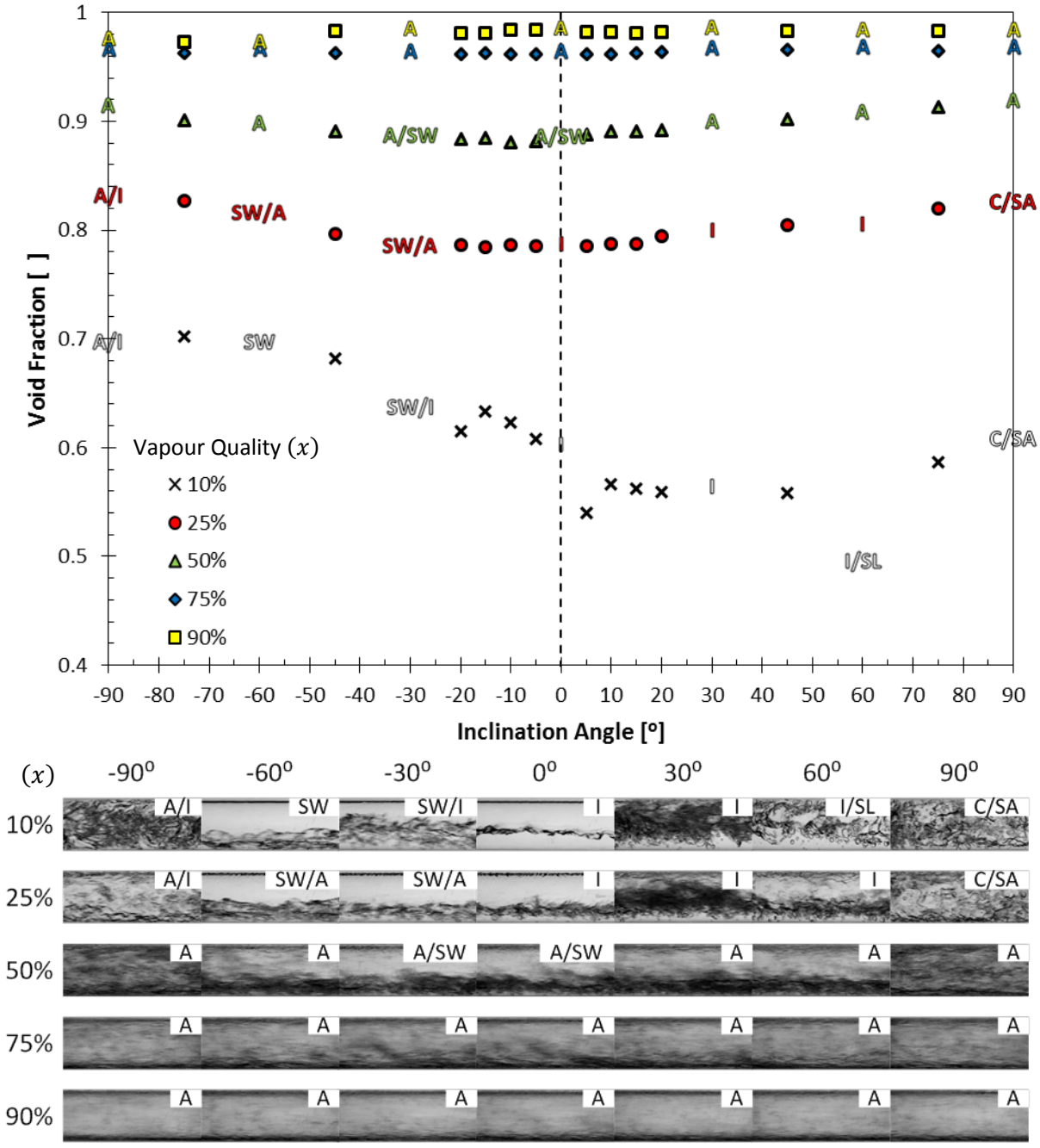

Figure 5.16: Void fractions as function of test section inclination angle for a mass flux of G = 400 kg/m^2.s and average vapour qualities of 10%, 25%, 50%, 75% and 90%. The flow pattern abbreviations are A=annular; SW=stratified-wavy; C=churn; I=intermittent; SL=slug; SA=semi-annular

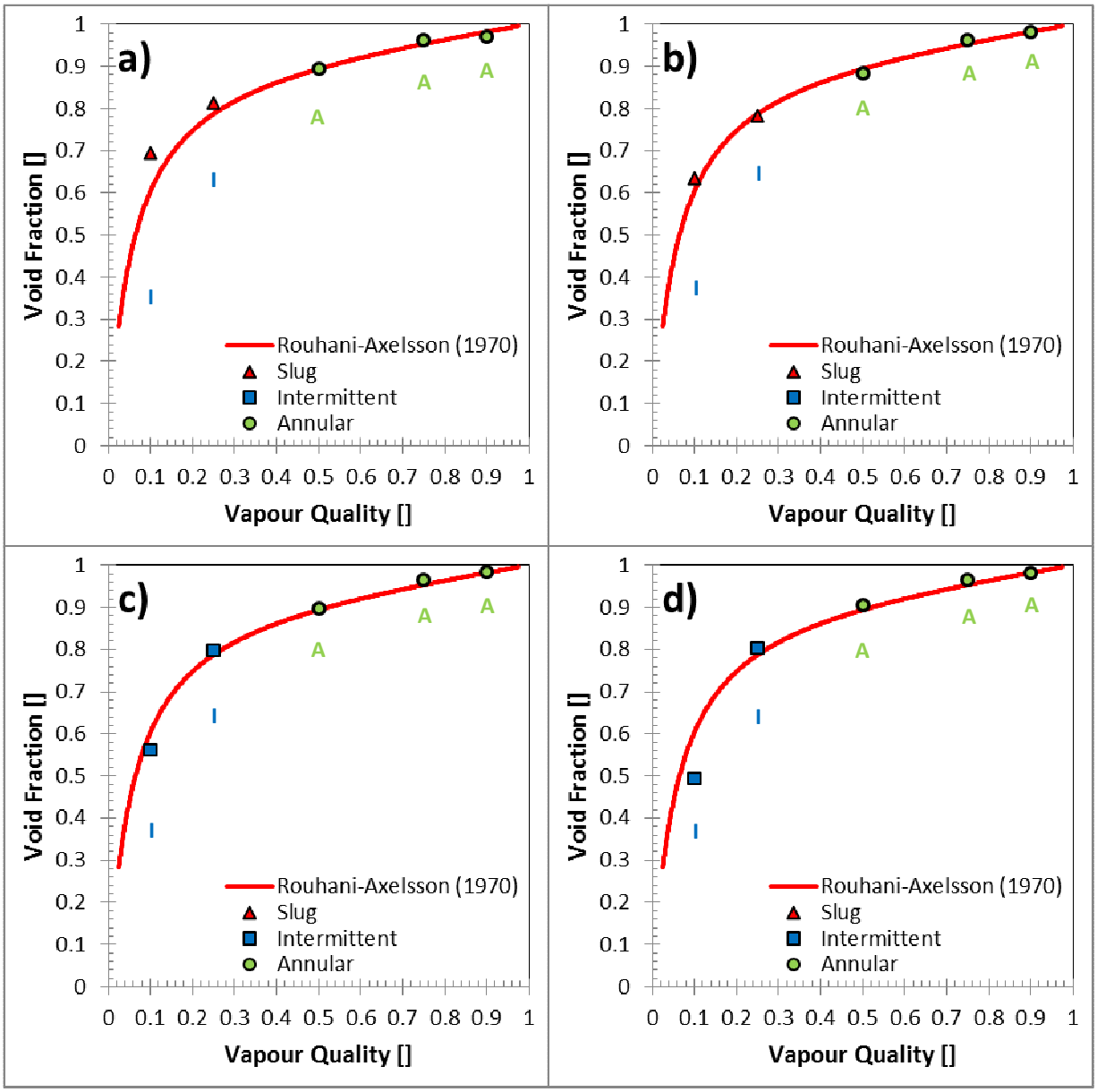

Figure 5.17: Experimental void fraction measurements as a function of average vapour quality compared with the predictions of the Rouhani and Axelsson (1970) void fraction correlation for the case of 400 kg/m^2.s mass flux and tube inclinations of a) -60°, b) -30°, c) 30° and d) 60°. The prevailing flow pattern as observed is indicated by the symbols in the legend. At each data point, the flow pattern predicted by the modified Wojtan *et al.* (2005) flow pattern map is indicated using the following abbreviations: Slug (S), stratified-wavy (SW), slug and stratified-wavy (SSW), intermittent (I) and annular (A). The colour-coding of the abbreviations also correlates with the flow classification of De Kerpel *et al.* (2013) in the legend.

The 25% vapour quality case exhibited a slight increase in heat transfer coefficient with increased downward inclination angle (Figure 5.18). A maximum increase of 10% relative to horizontal flow was observed at a -30° downward inclination angle, which correlates well with observations at lower mass fluxes. Further increases in downward inclination angle resulted in a reduction in heat transfer coefficient up to a minimum at near-vertical downward flow (9% reduction compared with

horizontal flow). As before, for lower vapour qualities, the reduction in heat transfer coefficient was accompanied by a transition to annular-type flow, i.e. the redistribution of the thicker liquid layer to the periphery of the tube resulted in a net increase in thermal resistance compared with the purely stratified-type flow where the thicker liquid layer is only distributed at the bottom of the tube.

The heat transfer coefficients were observed to increase with increasing upward inclinations up to a maximum (7% increase relative to horizontal flow) at 45° upward inclination. For the aforementioned inclination angle, the liquid-vapour distribution seemed to strike a balance between annular- and stratified-type flows with a pronounced annular liquid ring present, but also a relatively thick stratified liquid layer, which resulted in a net decrease in thermal resistance. For both 50% and 75% vapour quality cases, the heat transfer coefficients could be considered as independent of inclination angle with the majority of deviations from horizontal flow observed as less than 3%. At these conditions, the vapour shear velocity was great enough to keep the liquid-vapour distributions constant irrespective of inclination angle, as is evident from the flow pattern observations. As mentioned earlier, the heat transfer coefficients for the 90% vapour quality case were omitted as a result of issues with accuracy.

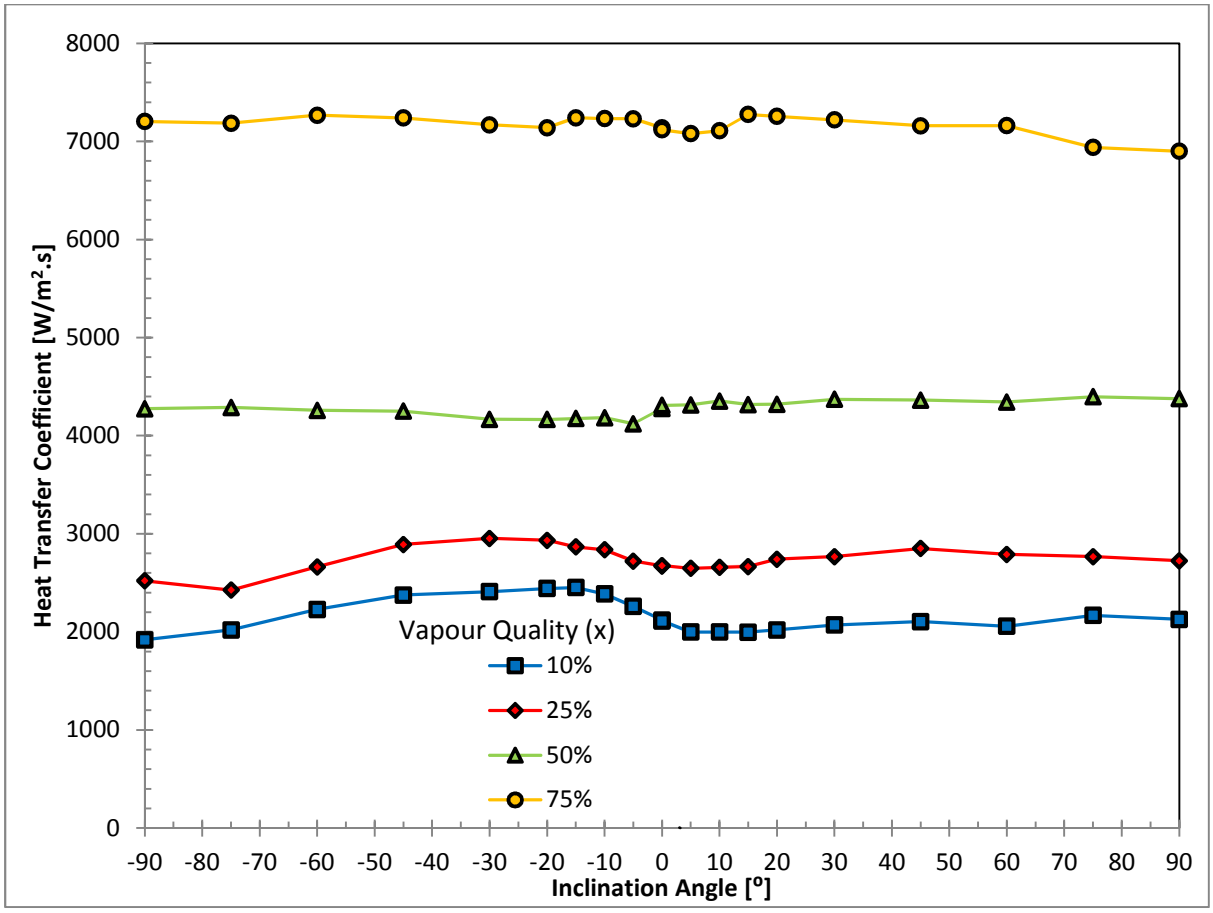

Figure 5.18: Heat transfer coefficients as a function of inclination angle for a mass flux of G = 400 kg/m^2.s and average vapour qualities of x = 10%, x = 25%, x = 50% and x = 75%

5.4 Sensitivity analysis

To determine the effect of possible errors in the void fraction measurements on the heat transfer coefficients, a sensitivity analysis was conducted. The heat transfer coefficients for horizontal flow were predicted with good accuracy by the Thome *et al*. (2003) correlation; thus the assumption could be made that the flow physics were adequately captured by the Thome *et al*. (2003) heat transfer model for horizontal flow. The sensitivity of the Thome *et al*. (2003) heat transfer predictions to changes in the void fraction would therefore serve to quantify the level of accuracy required from the void fraction sensors to be able to use their measurements in heat transfer correlations.

Figure 5.19 provides an illustration of the effect of a ±5% void fraction error on the heat transfer predictions of the Thome *et al*. (2003) correlation for a representative mass flux of 300 kg/m^2.s. Similar trends were observed for the other mass fluxes. For the lower vapour quality cases (10%, 25% and 50%), the changes in void fraction were observed to have a significantly smaller effect on

the heat transfer predictions of the Thome *et al*. (2003) correlation than for the higher vapour quality cases (75% and 90%).

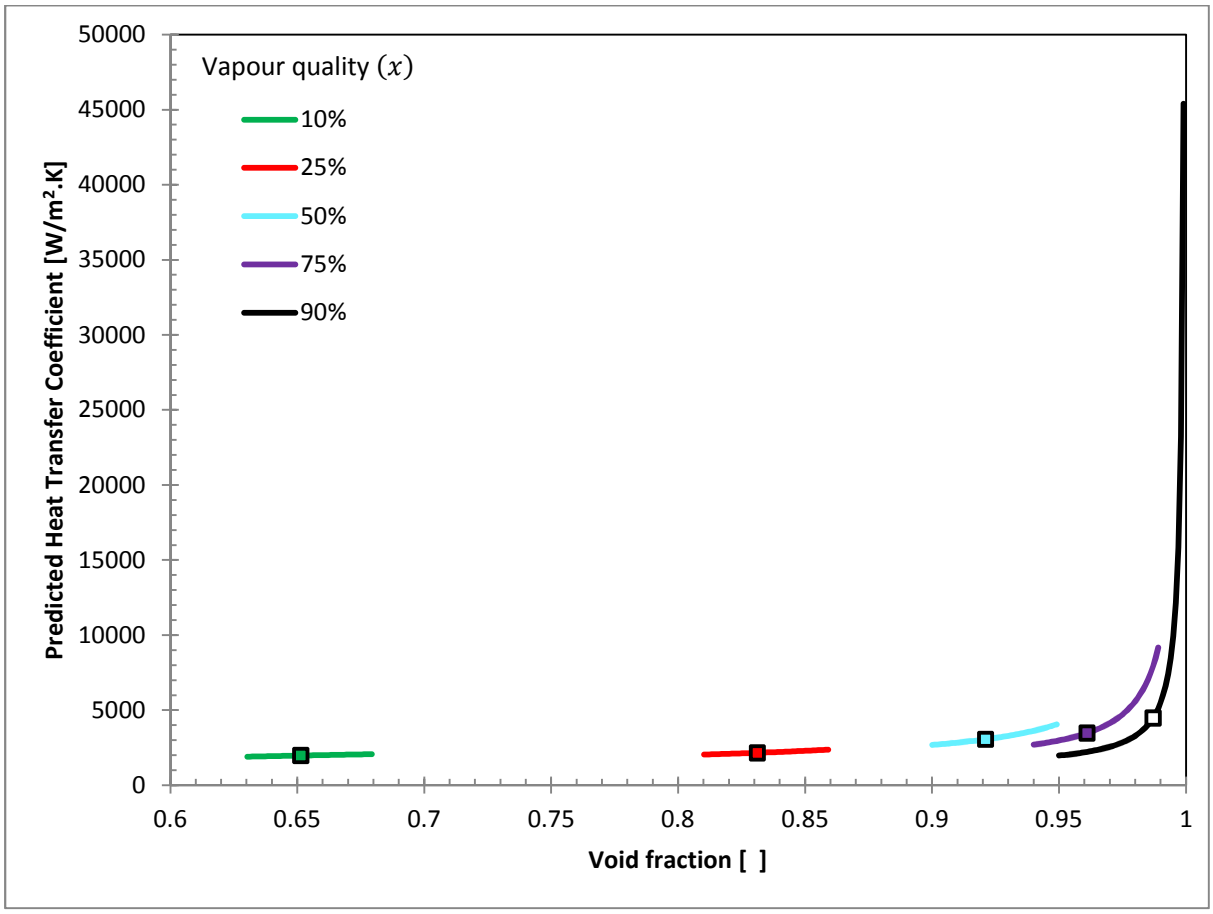

Figure 5.19: Graphical representation of the effect of a ±5% change in void fraction on the heat transfer predictions of the Thome *et al*. (2003) correlation for average vapour qualities of 10%, 25%, 50%, 75% and 90% at a 300 kg/m^2.s mass flux. The predictions of the Thome *et al*. (2003) correlation for each respective vapour quality is presented as a distinct data point in the range of calculated heat transfer coefficients.

To further quantify the sensitivity, the void fractions which would result in a ±10% change in the heat transfer predictions of the Thome *et al*. (2003) correlation were calculated for each respective vapour quality case. The percentage difference between the void fractions resulting from the aforementioned calculations was then determined. The aforementioned values are presented in Table 5.1.

Table 5.1: Sensitivity of Thome *et al.* (2003) heat transfer predictions to void fraction for 300 kg/m^2.s mass flux

Vapour quality (x)	Void fraction value at 90% of heat transfer predicted by Thome *et al.* (2003) correlation	Void fraction value at 110% of heat transfer predicted by Thome *et al.* (2003) correlation	Difference
10%	0.60	0.71	11 %
25%	0.79	0.86	7 %
50%	0.91	0.94	3 %
75%	0.96	0.97	1 %
90%	0.99	0.99	0 %

From Table 5.1 the percentage difference in void fraction which would result in a ±10% change in the heat transfer predictions of the Thome *et al.* (2003) correlation became significantly smaller with increasing vapour quality. With a vapour quality of 10%, a change of approximately 11% in the void fraction covers the span of ±10% in the heat transfer predictions. This could be compared with the case of 90% vapour quality where a 0.002% change in void fraction covered the ±10% band in heat transfer predictions.

The implications of the aforementioned observations were that the void fraction measurements at high vapour quality conditions needed to be very accurate to be used in heat transfer correlations at these flow conditions.

5.5 Summary and conclusions

Void fraction and heat transfer measurements were taken for a full spectrum of tube inclinations ranging from vertical downward to vertical upward flow with condensation heat transfer in a smooth tube. A range of vapour quality and mass flux conditions were considered. The goal was to determine the effect of varying tube inclinations on the void fraction and heat transfer behaviour of condensation flow.

The measured heat transfer coefficients generally correlated well with the predictions of two correlations from literature for horizontal flows with the majority of predictions within ±20% of the measured values. The measured void fraction results correlated well with the predictions of literature for horizontal flows as expected. The majority of the observed flow patterns corresponded with the predictions of the modified flow pattern map from literature. Substituting measured and predicted void fraction values into the heat transfer correlation from literature deteriorated its prediction accuracy.

For vertical upward flow, the void fraction correlation from literature generally performed well, barring the lowest vapour qualities, the predictions were within ±5% of the measured values. Flow patterns were observed to be either annular- or churn-type flows with liquid recirculation; no intermittent-type flows were observed for vertical upward flow. The prediction performance of the heat transfer correlations from literature suffered when compared with horizontal flows, but the majority of predictions were still within ±30% of the measured values. The heat transfer coefficients were over-predicted to a lesser degree at low heat transfer conditions and under-predicted at high heat transfer conditions. Substitution of measured and predicted void fractions did not improve heat transfer predictions from literature significantly.

For vertical downward conditions, only annular-type flow patterns were observed, albeit with significantly thicker and chaotic liquid layers at low vapour quality conditions. The measured void fractions were generally under-predicted; only high vapour quality conditions were predicted well by literature. The lower heat transfer coefficients were again over-predicted by the correlations, but more so than for the vertical upward flow case. The higher heat transfer coefficients were under-predicted by literature, but not to the degree of vertical upward flow. Substituting the void fraction parameter in the correlation from literature with measured and predicted values did not improve the predictions for the vertical downward case.

Significant departures from the horizontal results were observed for combinations of low vapour quality and mass flux at the various tube inclinations. Void fraction results for downward flows tended to be under-predicted and upward flows tended to be over-predicted by literature for the aforementioned conditions. The void fraction measurements tended to remain constant at downward inclinations (approximately -90° to -30°) at low mass fluxes up to a critical point where a decrease in the void fraction was observed. Maximum measured heat transfer coefficients tended to coincide with the point at which the measured void fraction values started to decrease at downward inclinations. On the contrary, minimum measured heat transfer coefficients tended to coincide with the inflection points of the measured void fractions at upward flow inclinations (approximately 5° to 10°). At some intermediate conditions of mass flux and vapour quality (i.e. 300 kg/m^2.s mass flux and 25% vapour quality), the void fraction and/or heat transfer coefficients were observed to remain relatively unaffected by changes to the inclination angle while the flow patterns were altered significantly from upward to downward flows. At higher mass fluxes and vapour qualities, the void fractions were observed to be independent of the tube inclination. At some of the lower mass fluxes and vapour quality conditions, the heat transfer coefficients were observed to deviate with inclination angle while the void fraction remained relatively unaffected.

A sensitivity analysis investigated the effect of an error in the void fraction measurements on the predictions of a prominent heat transfer correlation from literature, which predicted the measured horizontal heat transfer coefficients well. For a representative mass flux of 300 kg/m^2.s, it was observed that at high vapour qualities (i.e. 75% and 90%), a very small error (less than 1%) in void fraction would lead to a ±10% change in the heat transfer predictions of the correlation.

6. Summary, conclusions and recommendations

6.1 Summary

Two-phase condensation flow is an important phenomenon as it extensively occurs in various industries. Improved designs of heat transfer equipment resulting from a better understanding of the flow behaviour may result in significant reductions in energy usage and construction materials. In the past, studies have focused on horizontal and vertical flow conditions, which resulted in a relative scarcity of data for the case of inclined flows. An important flow parameter that is affected by the tube inclination is the void fraction. Studies considering the void fraction at various tube inclinations were even rarer than those considering pressure and heat transfer measurements.

It was the purpose of this study to measure void fractions with a capacitive void fraction sensor for a full spectrum of inclination angles ranging from vertical upward to vertical downward flow. Condensation measurements with refrigerant R134a were also conducted in a smooth tube with an internal diameter of 8.38 mm. Various mass fluxes ranging from 100–400 kg/m^2.s were considered at vapour qualities ranging from 10–90% with 200 ± 5 W of condensation heat transfer.

6.2 Conclusions

The predictions of both the heat transfer and void fraction correlations from literature for horizontal flow tended to match the measured results closely. The predictions of the correlations from literature both predicted the heat transfer coefficients well with the majority of data points predicted within ±20% of the measured values. The void fraction correlation from literature closely predicted the void fraction measurements for horizontal flows. The good correlation was not unexpected following a calibration procedure in which the inlet and outlet void fraction sensor measurements were adjusted to more closely resemble the predictions from literature for adiabatic horizontal flows. Measured and predicted void fraction values were substituted into a prominent heat transfer correlation from literature, but the prediction accuracy was observed to deteriorate compared with those of the original correlation for horizontal flows. The flow patterns were also predicted with reasonable accuracy by the modified flow pattern map from literature.

The prediction performance of the void fraction correlation from literature deteriorated for vertical downward flow at low to intermediate vapour qualities with the measured values tending to be under-predicted. However, for vertical upward flow, the void fraction prediction accuracy remained mostly intact – some of the data points were under-predicted, but not to the same extent as for downward flow. The prediction performance of both the heat transfer correlations from literature

was observed to deteriorate compared with that of the horizontal flow case. At low heat transfer conditions, the results tended to be over-predicted; for the vertical downward cases more so than for the vertical upward cases. At higher heat transfer conditions, the results tended to be under-predicted with the vertical upward flows exhibiting a greater degree of under-prediction. The observed flow patterns deviated from those observed for horizontal flow; annular-type flow dominated vertical downward inclinations while churn-type flow with liquid recirculation was most prevalent for vertical upward flows. Substituting the void fraction parameter in the heat transfer correlation from literature with the measured and predicted values did not improve the prediction accuracy.

Heat transfer coefficients were observed to increase significantly at downward inclinations for lower mass flux and vapour quality conditions. Maximum values tended to be observed for inclinations in the region of -30° to -15° of downward inclination. The maximum heat transfer values were observed to mostly coincide with the inclinations where the measured void fractions were observed to start decreasing. At inclinations in the region of -30°, the heat transfer conditions were therefore most favourable for lower mass flux and vapour quality conditions, i.e. assistance in the form of gravity as well as a thin stratified liquid layer providing minimal thermal resistance. Stratified flows dominated for downward inclinations and lower mass flux and vapour quality conditions.

With a transition from downward to upward inclinations, the heat transfer coefficients were observed to exhibit a minimum at approximately 5° to 15° of upward inclination for lower mass fluxes and vapour qualities. The minimum was observed to coincide with the inflection point of the void fraction measurements; the increase in the amount of liquid phase resulted in greater thermal resistance at these conditions. With further increases in upward inclination, the heat transfer and void fraction measurements were observed to remain fairly constant. For lower mass flux and vapour quality conditions at upward inclinations, churn-type flow was observed; for the lowest mass flux and vapour quality combinations, the flow exhibited recirculating behaviour. The highly chaotic liquid-vapour phase interactions could be the reason for the observed constant heat transfer; the liquid-vapour phase turbulence could dominate the effect of inclination for upward flows.

At high mass flux and vapour quality conditions, the flows exhibited independence towards the inclination angle as expected. For some intermediate mass flux and vapour quality conditions, the void fraction and heat transfer coefficients were observed to remain relatively constant, even though the flow patterns changed considerably. For these conditions, the heat transfer and void fraction results were observed to be independent of the flow pattern.

A sensitivity analysis was conducted into the effect of void fraction errors on the heat transfer predictions of a prominent correlation from literature. It was determined that for a representative mass flux of 300 kg/m^2.s, the void fraction sensors needed to measure with errors smaller than ±1% to enable their use in heat transfer correlations with a prediction accuracy of ±10%. This could mean that the use of the current design of capacitive void fraction sensor should be limited to lower vapour quality conditions if the absolute level of accuracy is determined to be unacceptable at higher vapour qualities.

6.3 Recommendations

It was not possible to investigate all aspects that influence void fractions for flows in inclined flows. The following is a list of suggestions for future work:

- Differential pressure drop measurements were not taken during the current study. Incorporating differential pressure drop measurements and relating them to void fraction measurements may improve the understanding of two-phase flow at various inclination angles. Combining pressure drop and void fraction measurements will also enable an investigation into assumptions made that the momentum pressure drop is always less than 10% of the frictional pressure drop (Lips and Meyer 2012b; Lips and Meyer 2012c).
- According to Ousaka *et al*. (2010), surface tension has an effect on the flooding behaviour of two-phase flows. Studies of void fraction at varying inclination angles which consider the effect of surface tension on the flooding behaviour of the two-phase flow may therefore be beneficial to the greater body of knowledge of the subject.
- Challenges were experienced with the measurements of the void fraction sensors in which they did not produce the expected absolute void fraction values. Their response to differences in fluid phase are, however, acceptable for investigating the slugging frequency of inclined flows similar to the work of Hernandez-Perez (2010) for refrigerant flows.
- Similar work can be conducted for other refrigerants and/or steam to increase the body of knowledge of the subject of two-phase flow at inclined flow conditions.

7. References

Adelaja, A.O., Dirker, J. & Meyer, J.P. 2014. Effects of the Thick Walled Pipes with Convective Boundaries on Laminar Flow Heat Transfer. *Applied Energy*. 130:838–845.

Akhavan-Behabadi, M.A., Kumar, R. & Mohseni, S.G. 2007. Condensation Heat Transfer of R-134a Inside a Microfin Tube with Different Tube Inclinations. *International Journal of Heat and Mass Transfer*. 50(23-24):4864–4871.

Ali, M.I., Sadatomi, M. & Kawaji, M. 1993. Adiabatic Two-Phase Flow in Narrow Channels Between Two Flat Plates. *Canadian Journal of Chemical Engineering*. 71:657–666.

Barbieri, P.E.L., Jabardo, J.M.S. & Bandarra Filho, E.P. 2008. Flow Patterns in Convective Boiling of Refrigerant R-134a in Smooth Tubes of Several Diameters. In *5th European Thermal-Sciences Conference*. The Netherlands.

Bertola, V. 2003. Two-phase Flow Measurement Techniques. In *Modelling and Experimentation in Two-phase Flow*. 5th ed. New York: Springer, Wien. 281–323.

Canière, H., T'Joen, C., Willockx, A., De Paepe, M., Christians, M., Van Rooyen, E., Liebenberg, L. & Meyer, J.P. 2007. Horizontal Two-Phase Flow Characterization for Small Diameter Tubes with a Capacitance Sensor. *Measurement Science and Technology*. 18(9):2898–2906.

Canière, H., T'Joen, C., Willockx, A. & De Paepe, M. 2008. Capacitance Signal Analysis of Horizontal Two-Phase Flow in a Small Diameter Tube. *Experimental Thermal and Fluid Science*. 32(3):892–904.

Canière, H., Bauwens, B., T'Joen, C. & De Paepe, M. 2009. Probabilistic Mapping of Adiabatic Horizontal Two-Phase Flow by Capacitance Signal Feature Clustering. *International Journal of Multiphase Flow*. 35(7):650–660.

Canière, H., Bauwens, B., T'Joen, C. & De Paepe, M. 2010. Mapping of Horizontal Refrigerant Two-Phase Flow Patterns Based on Clustering of Capacitive Sensor Signals. *International Journal of Heat and Mass Transfer*. 53(23-24):5298–5307.

Cavallini, A., Del Col, D., Doretti, L., Matkovic, M., Rossetto, L., Zilio, C. & Censi, G. 2006. Condensation in Horizontal Smooth Tubes: A New Heat Transfer Model for Heat Exchanger Design. *Heat Transfer Engineering*. 27(8):31–38.

Chato, J.C. 1960. Laminar Condensation Inside Horizontal and Inclined Tubes. Massachusetts Institure of Technology.

Chexal, B., Lellouche, G., Horowitz, J. & Healzer, J. 1992. A Void Fraction Correlation for Generalized Applications. *Progress in Nuclear Engineering*. 27(4):255–295.

Cioncolini, A. & Thome, J.R. 2012. Void Fraction Prediction in Annular Two-Phase Flow. *International Journal of Multiphase Flow*. 43:72–84.

Coddington, P. & Macian, R. 2002. A Study of the Performance of Void Fraction Correlations Used in the Context of Drift-Flux Two-Phase Flow Models. *Nuclear Engineering and Design*. 215(3):199–216.

Dalkilic, A.S. & Wongwises, S. 2009. Intensive Literature Review of Condensation Inside Smooth and Enhanced Tubes. *International Journal of Heat and Mass Transfer*. 52(15-16):3409–3426.

Demori, M., Ferrari, V., Strazza, D. & Poesio, P. 2010. A Capacitive Sensor System for the Analysis of Two-Phase Flows of Oil and Conductive Water. *Sensors and Actuators A: Physical*. 163(1):172–179.

Doretti, L., Zilio, C., Mancin, S. & Cavallini, A. 2013. Condensation flow patterns inside plain and microfin tubes: A review. *International Journal of Refrigeration*. 36(2):567–587.

Elkow, K.J. & Rezkallah, K.S. 1996. Void Fraction Measurements in Gas – Liquid Flows Using Capacitance Sensors. *Measurement Science and Technology*. 7:1153–1163.

Fuangworawong, N., Kikura, H., Aritomi, M. & Komeno, T. 2007. Tomographic Imaging of Counter-Current Bubbly Flow by Wire Mesh Tomography. *Chemical Engineering Journal*. 130(2-3):111–118.

El Hajal, J., Thome, J.R. & Cavallini, A. 2003. Condensation in Horizontal Tubes, Part1: Two-phase Flow Pattern Map. *International Journal of Heat and Mass Transfer*. 46:3349–3363.

Hernandez-Perez, V. 2010. Slugging Frequency Correlation for Inclined Gas–Liquid Flow. *World Acad. Sci. Eng.* 2(5).

Hibiki, T. & Ishii, M. 2003a. One-Dimensional Drift-Flux Model and Constitutive Equations for Relative Motion Between Phases in Various Two-Phase Flow Regimes. *International Journal of Heat and Mass Transfer*. 46:4935–4948.

Hibiki, T. & Ishii, M. 2003b. One-Dimensional Drift – Flux Model for Two-Phase Flow in a Large Diameter Pipe. *International Journal of Heat and Mass Transfer*. 46:1773–1790.

Jones, O.C. & Zuber, N. 1975. The Interrelation Between Void Fraction Fluctuations and Flow Patterns in Two-Phase Flow. *International Journal of Multiphase Flow*. 2(1971):273–306.

Kattan, N., Thome, J.R. & Favrat, D. 1998. Flow Boiling in Horizontal Tubes. Part 3: Development of a New Heat Transfer Model Based on Flow Patterns. *Journal of Heat Transfer*. 120(1):156–165.

Kawahara, A., Sadatomi, M., Okayama, K., Kawaji, M. & Chung, P.M.-Y. 2005. Effects of Channel Diameter and Liquid Properties on Void Fraction in Adiabatic Two-Phase Flow Through Microchannels. *Heat Transfer Engineering*. 26(3):13–19.

De Kerpel, K., Ameel, B., T'Joen, C., Canière, H. & De Paepe, M. 2013. Flow Regime Based Calibration of a Capacitive Void Fraction Sensor for Small Diameter Tubes. *International Journal of Refrigeration*. 36(2):390–401.

De Kerpel, K., Ameel, B., De Schampheleire, S., T'Joen, C., Canière, H. & De Paepe, M. 2014. Calibration of a capacitive void fraction sensor for small diameter tubes based on capacitive signal features. *Applied Thermal Engineering*. 63(1):77–83.

Keska, J.K., Smith, M.D. & Williams, B.E. 1999. Comparison Study of a Cluster of Four Dynamic Flow Pattern Discrimination Techniques for Multi-Phase Flow. *Flow Measurement and Instrumentation*. 10(2):65–77.

Koyama, S., Lee, J. & Yonemoto, R. 2004. An Investigation on Void Fraction of Vapor–Liquid Two-Phase Flow for Smooth and Microfin Tubes with R134a at Adiabatic Condition. *International Journal of Multiphase Flow*. 30(3):291–310.

Lienhard, J. & Lienhard, J. 2005. *A Heat Transfer Textbook*. 3rd ed. Cambridge, Massachusetts, U.S.A.: Phlogiston Press.

Lips, S. & Meyer, J. 2012a. Stratified Flow Model for Convective Condensation in an Inclined Tube. *International Journal of Heat and Fluid Flow*. 36:83–91.

Lips, S. & Meyer, J.P. 2011. Two-Phase Flow in Inclined Tubes with Specific Reference to Condensation: A Review. *International Journal of Multiphase Flow*. 37(8):845–859.

Lips, S. & Meyer, J.P. 2012b. Experimental Study of Convective Condensation in an Inclined Smooth Tube. Part I: Inclination Effect on Flow Pattern and Heat Transfer Coefficient. *International Journal of Heat and Mass Transfer*. 55(1-3):395–404.

Lips, S. & Meyer, J.P. 2012c. Experimental Study of Convective Condensation in an Inclined Smooth Tube. Part II: Inclination Effect on Pressure Drops and Void Fractions. *International Journal of Heat and Mass Transfer*. 55(1-3):405–412.

Lockhart, R. & Martinelli, R. 1949. Proposed Correlation of Data for Isothermal Two-Phase, Two-Component Flow in Pipes. *Chem. Eng. Prog*. 45(1):39–48.

Ma, Y.-P., Chung, M.-M., Pei, B.-S., Lin, W.-K. & Hsu, Y.-Y. 1991. Two Simplified Methods to Determine Void Fractions for Two-Phase Flow. *Nuclear Technology*. 94:124.

Meyer, J.P., Dirker, J. & Adelaja, A.O. 2014. Condensation Heat Transfer in Smooth Inclined Tubes for R134a at Different Saturation Temperatures. *International Journal of Heat and Mass Transfer*. 70:515–525.

Mishima, K. & Hibiki, T. 1996. Quantitative Limits of Thermal and Fluid Phenomena Measurements Using the Neutron Attenuation Characteristics of Materials. *Experimental Thermal and Fluid Science*. 12(4):461–472.

Mishima, K. & Hibiki, T. 1998. Development of High-Frame-Rate Neutron Radiography and Quantitative Measurement Method for Multiphase Flow Research. *Nuclear Engineering and Design*. 184(0029):183–201.

Mishima, K., Hibiki, T. & Nishihara, H. 1997. Visualization and Measurement of Two-Phase Flow by Using Neutron Radiography. *Nuclear Engineering and design*. 175:25–35.

Moreno Quibén, J. & Thome, J.R. 2007. Flow pattern based two-phase frictional pressure drop model for horizontal tubes, Part II: New phenomenological model. *International Journal of Heat and Fluid Flow*. 28(5):1060–1072.

Nebuloni, S. & Thome, J.R. 2013. Numerical Modeling of the Effects of Oil on Annular Laminar Film Condensation in Minichannels. *International Journal of Refrigeration*. 36(5):1545–1556.

Noie, S.H., Sarmasti Emami, M.R. & Khoshnoodi, M. 2007. Effect of Inclination Angle and Filling Ratio on Thermal Performance of a Two-Phase Closed Thermosyphon under Normal Operating Conditions. *Heat Transfer Engineering*. 28(January 2015):365–371.

Ousaka, A., Kariyasaki, A., Lucas, D., Vierow, K., Vallee, C. & Hogan, K. 2010. The Effects of Surface Tension on Flooding in Counter-Current Two-Phase Flow in an Inclined Tube. *Experimental Thermal and Fluid Science*. 34(7):813–826.

REFPROP. 2005. *NIST Thermodynamic Properties of Refrigerants and Refrigerant Mixtures, Version 8.0, NIST Standard Reference Database 23. National Institute of Standards and Technology. Gaithersburg, MD*. Gaithersburg, MD: National Institute of Standards and Technology.

Dos Reis, E. & Goldstein, L. 2005. A Procedure for Correcting for the Effect of Fluid Flow Temperature Variation on the Response of Capacitive Void Fraction Meters. *Flow Measurement and Instrumentation*. 16:267–274.

Rezkallah, K.S. & Clarke, N.N. 1995. Void Fraction Measurements in Gas-Liquid Flows Using Image Processing. In *Proceedings of the 1995 ASME/JSME Fluids Engineering and Laser Anemometry Conference and Exhibition*. New York: ASME. 31–35.

Da Riva, E., Del Col, D., Garimella, S. V. & Cavallini, A. 2012. The Importance of Turbulence During Condensation in a Horizontal Circular Minichannel. *International Journal of Heat and Mass Transfer*. 55(13-14):3470–3481.

Van Rooyen, E. & Christians, M. 2007. Time Fractional Analysis of Flow Patterns During Refrigerant Condensation. University of Pretoria.

Van Rooyen, E., Christians, M., Liebenberg, L. & Meyer, J.P. 2010. Probabilistic Flow Pattern-Based Heat Transfer Correlation for Condensing Intermittent Flow of Refrigerants in Smooth Horizontal Tubes. *International Journal of Heat and Mass Transfer*. 53:1446–1460.

Rouhani, S.Z. & Axelsson, E. 1970. Calculation of Void Volume Fraction in the Subcooled and Quality Boiling Regions. *International Journal of Heat and Mass Transfer*. 13:383–393.

Saito, Y., Mishima, K., Tobita, Y., Suzuki, T. & Matsubayashi, M. 2005. Measurements of Liquid–Metal Two-Phase Flow by Using Neutron Radiography and Electrical Conductivity Probe. *Experimental Thermal and Fluid Science*. 29(3):323–330.

Shao, D.W. & Granryd, E. 1995. Heat Transfer and Pressure Drop of HFC134a-Oil Mixtures in a Horizontal Condensing Tube. *International Journal of Refrigeration*. 18(8):524–533.

Da Silva, M.J., Thiele, S., Abdulkareem, L., Azzopardi, B.J. & Hampel, U. 2010. High-Resolution Gas–Oil Two-Phase Flow Visualization with a Capacitance Wire-Mesh Sensor. *Flow Measurement and Instrumentation*. 21(3):191–197.

Steiner, D. 1993. Verein Deutscher Ingenieure, VDI-Gesellschaft Verfahrenstechnik und Chenieingenieurswesen (GCV). In *VDI Wärmteatlas*. Düsseldorf.

Suliman, R., Liebenberg, L. & Meyer, J.P. 2009. Improved Flow Pattern Map for Accurate Prediction of the Heat Transfer Coefficients During Condensation of R-134a in Smooth Horizontal Tubes and

Within the Low-Mass Flux Range. *International Journal of Heat and Mass Transfer*. 52(25-26):5701–5711.

Thome, J.R. 2006a. Condensation Inside Tubes. In *Engineering Data Book III*. Wolverine Tube Inc. 1–27.

Thome, J.R. 2006b. Void Fractions in Two-Phase Flow. In *Engineering Data Book III*. V. 5. Wolverine Tube Inc. 1–33.

Thome, J.R., El Hajal, J. & Cavallini, A. 2003. Condensation in Horizontal Tubes, Part 2: New Heat Transfer Model Based on Flow Regimes. *International Journal of Heat and Mass Transfer*. 46(18):3365–3387.

Thome, J.R., Bar-Cohen, A., Revellin, R. & Zun, I. 2013. Unified Mechanistic Multiscale Mapping of Two-Phase Flow Patterns in Microchannels. *Experimental Thermal and Fluid Science*. 44:1–22.

Ursenbacher, T., Wojtan, L. & Thome, J.R. 2004. Interfacial Measurements in Stratified Types of Flow. Part I: New Optical Measurement Technique and Dry Angle Measurements. *International Journal of Multiphase Flow*. 30(2):107–124.

Winkler, J., Killion, J., Garimella, S. & Fronk, B.M. 2012. Void Fractions for Condensing Refrigerant Flow in Small Channels: Part I Literature Review. *International Journal of Refrigeration*. 35(2):219–245.

Wojtan, L., Ursenbacher, T. & Thome, J.R. 2004. Interfacial Measurements in Stratified Types of Flow. Part II: Measurements for R-22 and R-410A. *International Journal of Multiphase Flow*. 30(2):125–137.

Wojtan, L., Ursenbacher, T. & Thome, J.R. 2005. Investigation of Flow Boiling in Horizontal Tubes: Part I—A New Diabatic Two-Phase Flow Pattern Map. *International Journal of Heat and Mass Transfer*. 48(14):2955–2969.

Woldesemayat, M.A. & Ghajar, A.J. 2007. Comparison of Void Fraction Correlations for Different Flow Patterns in Horizontal and Upward Inclined Pipes. *International Journal of Multiphase Flow*. 33(4):347–370.

Yashar, D.A., Wilson, M.J., Kopke, H.R., Graham, D.M., Chato, J.C. & Newell, T.A. 2001. An Investigation of Refrigerant Void Fraction in Horizontal , Microfin Tubes. *HVAC&R Research*. 7:67–82.

Zuber, N. & Findlay, J.A. 1965. Average Volumetric Concentration in Two-Phase Flow Systems. *Journal of Heat Transfer*. 87:453–468.

Appendix A: In-situ calibration of thermocouples

Initial measurements with the void fraction sensors installed revealed discrepancies in the heat transfer coefficients when compared with past results obtained using the same experimental set-up. The heat transfer measurements were repeated with the void fraction sensors removed and the discrepancies remained similar; the void fraction sensors did not have a noticeable effect on the heat transfer. By extension, the assumption could then be made that the void fraction sensors did not affect the flow significantly.

An investigation of the thermocouple measurements at a quiescent, constant temperature state revealed that the thermocouple readings were not as expected. For a constant temperature condition, it was discovered that the thermocouple measurements differed from each other, some by as much as 0.6 ^{o}C from the mean of the other measurements. This difference was significant as the thermocouples were rated with an accuracy of 0.5 ^{o}C and initially calibrated to an accuracy of 0.1 ^{o}C; the thermocouples were therefore not measuring with the desired level of accuracy.

The decision was made to conduct an in-situ calibration of the thermocouples, i.e. the thermocouples were calibrated while installed on the test section. The test section was fixed in the horizontal position for the entire calibration procedure. The refrigerant side of the test section was isolated and placed under vacuum conditions; this reduced heat transfer through the test section tube wall. The annular section was then connected to a cooling thermostat equipped with pumping capabilities.

Two four-wire PT100 resistance temperature detectors (RTDs) were installed inline up- and downstream of the inlet and outlet of the annulus respectively. These were calibrated to within 0.1 ^{o}C accuracy and would more accurately represent the actual water temperature within the annulus which was used to do the calibration.

The on-board pump of the cooling thermostat was set at its maximum flow rate and water at a set temperature was continuously pumped through the annulus. The calibration was conducted by linearly interpolating between each thermocouple measuring station along the test section using the temperatures measured by the PT100 RTDs. The assumption was made that the thermocouple measuring station closest to each respective PT100 thermocouple was equal to the PT100 measurement. The two PT100 thermocouples were mounted close to the inlet and outlet of the annulus respectively and the setup was insulated to improve the validity of this assumption.

Assuming linear behaviour for each thermocouple, new calibration correlations were developed for each thermocouple individually. The new sets of calibration correlations for each individual thermocouple were incorporated into the data acquisition software. Subsequent validation revealed that the in-situ calibration procedure was successful; the thermocouples measured nearly identical to each other.

Appendix B: Nitrogen flushing and leak testing

Before any measurements were taken, the refrigerant in the system was replaced. Once evacuated, the entire system was placed under vacuum conditions for an extended period of time and this subsequently ensured that the system was entirely free of old refrigerant. To remove any remaining moisture and impurities from the system, it was flushed numerous times with pure nitrogen at 1 000 kPa of pressure for approximately 15 minutes and the system was kept under vacuum conditions for an extended period of time between each flush to completely remove any nitrogen. The nitrogen flushing procedure was also used to check the system for any leaks.

After the final nitrogen flush, the system was again maintained under vacuum conditions for an extended period of time to remove all traces of nitrogen – non-condensable gases like nitrogen could have a detrimental effect on the heat transfer coefficients if not removed completely. Once all the nitrogen was evacuated from the system, it was charged with new refrigerant. Heat transfer coefficients taken after the system had been charged with new refrigerant compared well with expected values.